Biosensing of dissolved analytes with AFM-based single-molecule force spectroscopy

Dem Fachbereich Produktionstechnik

der

Universität Bremen

zur Erlangung des Grades

Doktor-Ingenieurin

genehmigte

Dissertation

von

M. Sc. Qing Li

Gutachter:

Prof. Dr.–Ing. Lucio Colombi Ciacchi (Universität Bremen)

Prof. Dr.–Ing. Jorg Thöming (Universität Bremen)

Tag der mündlichen Prüfung: 10 August, 2016

Abstract

Atomic force microscopy-based single-molecule force spectroscopy is an important tool for directly investigating the interactions between synthetically engineered biomolecules and different materials interfaces. Based on this technique, biosensors for the detection of adenosine, mercury ions, and thrombin are developed in the thesis. The biosensors based on specific aptamers for the detection of adenosine and mercury ions show extremely high sensitivity and selectivity. A novel method based on single-molecule force mapping method is also developed and applied for the detection of mercury ions. The method is simple, quick, and also shows excellent sensitivity and selectivity. In addition, the interactions of avidin-biotin and streptavdin-biotin are investigated by single-molecule force spectroscopy in combination with a specific oligopeptide sequence, with the aim to detecting thrombin in aqueous solution. This system and the underlying sensing principle are relatively complex, so more efforts are needed to improve this biosensor's performance. In summary, it is believed the AFM-based single-molecule force spectroscopy sensing technique developed in the present thesis will be useful and promising also for many other analytes. It has the potential to be exploited in commercial devices especially because of the low detection limit, if a sufficient degree of automatization and reproducibility are achieved.

Zusammenfassung

Rasterkraftmikroskopbasierte Kraftspektroskopie einzelner Moleküle ist ein wichtiges Werkzeug zur direkten Untersuchung der Wechselwirkungen zwischen synthetisch erzeugten Biomolekülen und verschiedenen Liganden wie auch ihrer Wechselwirkung mit Materialgrenzflächen.

Ausgehend von dieser Technik sind im Rahmen dieser Doktorarbeit Biosensoren zur Detektion von Adenosin, Quecksilberionen und Thrombin entwickelt worden. Die Sensoren für die ersten beiden Moleküle basieren auf spezifischen DNA-Aptameren, die über eine ausgeprägten Sensitivität und Selektivität gegenüber diesen Stoffen verfügen. Zudem ist hinsichtlich der Detektion von Quecksilberionen ein neues, einfaches und schnelles Verfahren etabliert worden, welches ebenfalls eine ausgeprägten Sensitivität und Selektivität aufweist und Einzelmolekülkraftspektoskopiebasierte Kraftkartenerstellung genannt wird.

Des Weiteren sind die Wechselwirkungen zwischen Biotin und Avidin wie auch Biotin und Streptavidin herangezogen worden, um mit ihrer Hilfe und einer spezifischen Peptidsequenz mittels Einzelmolekülkraftspektroskopie Thrombin zu detektieren. Diese zuletzt vorgestellten Systeme sind im Vergleich komplizierter hinsichtlich der involvierten Wechselwirkungen, weshalb weitere Anstrengungen unternommen werden müssen, um die Eignung dieses Biosensors auf verifizieren.

Es konnte im Rahmen dieser Ausarbeitung bestätigt werden, dass rasterkraftmikroskopbasierte Einzelmolekülkraftspektroskopie einen vielversprechender Ansatz zur Entwicklung und Verwendung von Biosensoren darstellt und die Möglichkeit einer kommerziellen Nutzung besteht, da die erreichten Nachweisgrenzen unter denen andere etablierter Techniken liegen.

Contents

1 Introduction

1.1 From synthetic biology to biosensing

"What I cannot create, I do not understand."

Richard P. Feynman

Synthetic biology is a new interdisciplinary branch of bridging biology and engineering. It can be utilized to design and build novel biomolecular components, networks and pathways, and these constructs can be exploited to rewire and reprogram organisms.[1] Based on studies of complex artificial biological systems, synthetic biology is used to investigate natural biological phenomena and for a variety of applications.[2]

The sequencing of the first human genome was started in 1995, completed already and published in 2004, and has undergone further rapid development in the recent years.[3, 4] For instance, DNA testing once required months to process in a major laboratory, but now it can be done in hours at almost any local police precinct.[5]

The increased options arising from high-throughput sequencing and the ability of synthesizing arbitrary DNA or peptide oligomers caused a paradigm shift in biology allowing the usage of specific sequences for technical solutions. Thus, we expected our lives to be changed in the future by development of re-engineered organisms.[1]

Based on a specific biological recognition element in combination with a transducer for signal processing, also biosensing techniques has developed rapidly together with the development of synthetic biology.[6] Biosensor is an abbreviation for "biological sensor"; it is generally defined as an analytical device which converts a biological response into a quantifiable and processable signal.[7] It is made up of a transducer and a biological element (e.g. a nucleic acid, an enzyme, an antibody or a microorganism) which can react with an analyte. Biosensors are widely used in different applications, including medicine, industry, environment, society and biology.

Most commercialized biosensors are applied in medicine applications. In this field, biosensors are not new, as they have been used in blood tests, glucose monitoring and pregnancy tests for decades. Figure 1.1 shows several a few well-developed commercialized biosensors. With the help of a pregnancy test, it is possible to tell “yes or no” in just a few minutes; and with the help of a blood glucose meter, quantitative measurements of sugar levels can be read within seconds, which is helpful for people with diabetes mellitus. Hospitals and research centers do also benefit from glucose and lactate analyzers with high precision. So it is possible now to use biosensors to detect compounds at small concentrations within short time in the clinical and pharmaceutical markets.

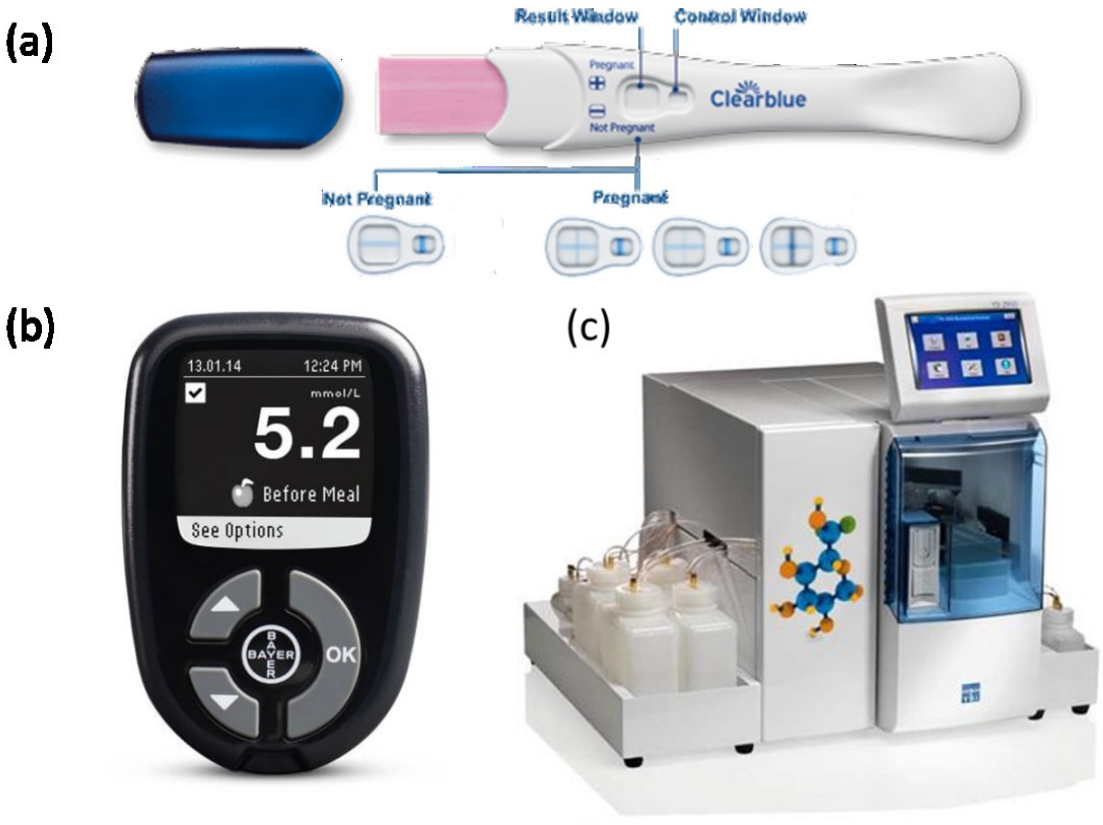

Figure 1.1 Commercialized biosensors of (a) a pregnancy test from Clearblue. Retrieved 21 April, 2016, from http://cdn.clearblue.com/sites/default/files/pictures/cb11ht04.png?1; (b) a blood glucose meter from Bayer. Retrieved 21 April, 2016, from http://www.bayer-shop.co.uk/res/shop/product/2588/thumbnail/Contour%20NEXT%20high%20res%20web%20ready.jpg; (c) a glucose and lactate analyzer from Yellow Springs Instruments. Retrieved 21 April, 2016, from https://www.ysi.com/ProductImages/37711787-aff0-4497-a6ef-e00543e3ba77/images/prev_YSI-2950-Biochemistry-Analyzer.jpg.

Biosensors are also used in industry, especially in the food industry for the detection of contaminants, and the verification of product freshness. For example, biosensors have already been used in the beer industry for improving and controlling the products.[8]

Due to the fast development of industry, a great amount of toxic chemical wastes are released to the environment, which make public health and ecosystem under huge risk. So it is important to develop biosensors to detect trace levels of heavy metals and other environmental contaminants. Over the last 4 years, a very large number of publications about biosensors for environmental monitoring have appeared.[9-12] Generally speaking, biosensors have already been developed for monitoring pesticides in soil, heavy metals in water, polluting gases in air.[13]

Biosensors play an important role in society applications. With airport security purposes, it is significant to detect illegal drugs and explosives. For instance, biosensors are already applied to detect the presence of cocaine and heroin.[14, 15] In addition, biosensors also exhibit good performance on detecting 2,4,6-trinitrotoluene (TNT).[16-18]

Investigations of the interactions between biomolecules, such as DNA-protein, protein-protein, and protein-drug are significant to understand protein functionality and many disease mechanisms.[19-21] Biosensors are also employed to study DNA, RNA, proteins, peptides, which opens the door for life science applications.[22-25]

Many techniques have already been used to develop biosensors, including fluorescence,[26] colorimetry,[27] electrochemistry,[28] and raman-scattering.[29]

In the fluorescence-based detection, either target molecules or biorecognition molecules are labeled with fluorescent tags, such as dyes. The intensity of the fluorescence indicates the presence of the target molecule and the interaction strength between the target and biorecognition molecules. The fluorescence-based detection is quite sensitive, with a detection limit down to 200 pM for DNA.[30] But it also has some disadvantages. For example, the labelling process in the lab may interfere with the function of biomolecules, and as the number of fluorophores on each molecule cannot be precisely controlled, quantitative analyses are challenging.[31]

Introduction

Colorimetry-based detection attracted much attention because the change of the color in the measurements can be easily read out with the naked eye.[32] The extremely high extinction coefficients (2.7×10^8 M^{-1} cm^{-1} for 13 nm diameter gold nanoparticles) and the strongly distance-dependent optical properties of gold nanoparticles make it possible for nanoparticles to be used as ideal colorimetric sensor elements.[33] This kind of biosensor is based on DNA/nanoparticle conjugates, for example, DNA-functionalized gold nanoparticles have been used in many forms to detect proteins, oligonucleotides, metal ions and some small molecules.[34-37] But as nanoparticles are always required to make the oligonucleotide-nanoparticle conjugate, and the detection limits for these kinds of biosensors are not very low, developing a new kind of biosensors with an easily handled system and small detection limit is still in need.

Electrochemical biosensors are also widely used because they are cost-effective and field portable. They are mostly based on immobilized DNA and its parts integrate sensitivity of detection with a high specificity of biomolecules.[38] Change of peak current can be obtained by switching structures of aptamers from DNA/DNA duplex to DNA/target complex, and the detection limit can be enhanced by using gold nanoparticles (Au NPs).[39] With the Au NPs amplification, 0.5 nM (100 ppt) mercury ions can be detected.[28] But the sensitivity of the electrochemical biosensors still needs to be improved.

Compared with the methods above, surface-enhanced Raman-scattering (SERS) can be used to obtain a better detection limit, as the enhancement factor can reach 10^{10} to 10^{11}.[40] SERS is a surface-sensitive technique which enhances Raman scattering by molecules adsorbed on rough metal surfaces or by nanostructures such as plasmonic-magnetic silica nanotubes or nanoporous gold.[29, 41] By using dealloyed nanoporous gold (NPG) as a plasmonic substrate and Cy5-labeled aptamers as optical tags, the NPG/aptamer based hybrid SERS sensor shows different Raman intensities after adding different concentrations of mercury ions, thus this sensor reaches the detection limit of 1 pM (0.2ppt) for mercury ions detection.[29] Even if this method shows very good sensitivity, the aptamer needs to be the labelled, which may be a

complicated process.

All the methods above have some limitations, such as complicated labeling or nanoparticles conjugation procedures, high detection limit, long detection times, or inconvenient purification procedures. Therefore, developing more effective and economic biosensors remains an important goal. In label-free detection, target molecules are not labelled, which means that they can be detected in the natural forms, and the quantitative and time-resolved measurement of molecular interactions is possible.[42]

Atomic force microscopy (AFM) is a rapidly developing technique in biological applications. It is a powerful surface analytical technique with high vertical and lateral resolutions, and it can be operated under a variety of environmental conditions, especially for biomolecular investigation.[43] It provides three-dimensional images of the surface ultrastructure with atomic or molecular resolution in air, vacuum or liquids.[44] Besides its well-known imaging ability, another significant application of AFM is to detect the interactions between biomolecules and materials interfaces (including organic and inorganic interfaces) at the single-molecule level by using it in spectroscopy mode (AFM-FS or AFM-SMFS).[45, 46] Compared with other techniques, AFM represents a promising method to investigate biological systems, which can detect the intra- and intermolecular forces with high sensitivity without labelling. For example, it can be used to study the interactions between single pairs of molecules in the 10 pN force resolution range.[47] Besides, modified probes with biomolecules can be exactly controlled with the substrates due to the precise x, y, and z positioning of the piezoelectric scanners of the AFM. In addition, the forces applied on the tip and the rate of retracting the tip away from the surface can also be exactly controlled, which makes it possible to investigate the interactions in a dynamic way. As AFM can be used to do force measurements in real time, under physiological conditions, and with minimal sample preparation, the physical properties of the specimen can be probed, such as molecular interactions, surface hydrophobicity, surface charges, and mechanical properties.[48]

AFM measurements provide new insight into the biomolecular interactions, which

will lead to deeper understanding of many biological and physical phenomena at the single-molecule level. Many researches have been conducted with AFM-based single-molecule force spectroscopy because it allows for the measurements of tiny forces associated with formation and breaking of single hydrogen bonds. It has therefore been widely used to study the specific molecular recognition interactions in antigen-antibody, ligand-receptor, and complementary ssDNA pairs.[49-52] Single-molecule force spectroscopy is also powerful for studying any function and property of biomolecules associated with force changes, and especially for measuring the adsorption force between biomolecules and functional nanomaterials.[53-55]

Understanding the interactions between biomolecules and material interfaces is an important step in the design of new functional hybrid biomaterials and developing novel biosensing technologies.[56, 57] Combining biomolecules with nanomaterial substrates can lead to hybrid materials with improved properties of multi-functions and biocompatibility and have wider applications in nanotechnology and biomedicine.[58] For example, carbon nanotubes modified with biomolecules have been used in biomedical applications, such as gene transfer,[59] drug delivery,[60] biosensing,[61] and early detection of diseases.[62]

Aptamers are folded single-stranded DNA or RNA oligonucleotide sequences with the capacity to recognize target molecules or analytes. They are generated by means of the so-called systematic evolution of ligands exponential-enrichment (SELEX) process.[63, 64] Peptides are also found in biology to impart selectivity for a wide variety of analytes.[65] Combining aptamers or peptides with AFM is a current trend for developing biosensors.[50, 66]

We thus hypothesize that AFM-based SMFS employing specific aptamers or peptides can be used in the biosensing of drugs, metallic pollutants, or enzymes. It is expected to possess the advantages of testing in physiological environments, relatively short testing time and low detection limit.

Figure 1.2 shows overview of the work in this thesis. Based on the rapid development of aptamers and peptides in synthetic biology, we will develop and apply SMFS-based biosensing techniques to detect the presence of adenosine,

mercury ions and thrombin in water solutions at ultralow concentrations. The main questions that we aim to answer are the following. Are the engineering DNA and peptide sequences highly selective and specific? Can the aimed-for analytes be detected using AFM-based SMFS? How should AFM probes and substrates be functionalized to develop biosensors? What are the key limiting factors for the performance of the biosensors?

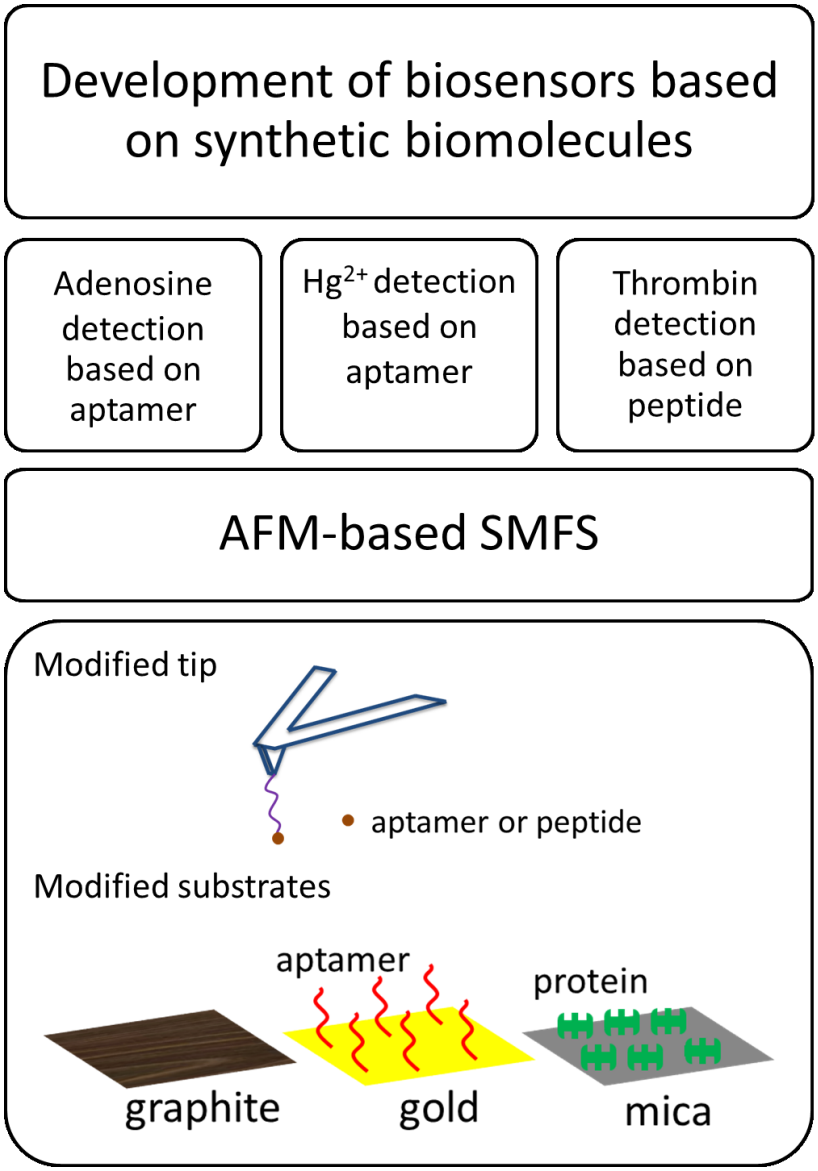

Figure 1.2 Overview of the work in this thesis.

1.2 Structure of the thesis

In this thesis, Chapter 2 is introducing what atomic force microscopy (AFM) is, how it works, and its applications on both imaging and force spectroscopy. Chapter 3

summarizes literatures of AFM-based SMFS applications for biomolecules-materials interface interactions and biosensing. Chapter 4 describes how to detect adenosine using single-molecule force spectroscopy. Chapter 5 extends the single-molecule force spectroscopy method to detect mercury ions, and develops a method called single-molecule force mapping. Chapter 6 discusses the interactions of avidin-biotin and streptavidin-biotin, with the aim of detecting thrombin. Chapter 7 summarizes the whole thesis and addresses the limits and drawbacks of the AFM method, and then discusses outlook of the future research interest to develop AFM methods combined with other techniques, and also the potential to be exploited in commercial devices.

2 Atomic force microscopy-based imaging and force spectroscopy

This chapter will introduce the technique of atomic force microscopy. Starting with what an atomic force microscope is and how it works, it will continue with applications of imaging and force spectroscopy. The last section will give an example of single-molecule force spectroscopy.

2.1 Background and experimental setup

Atomic force microscope (AFM) was invented by Binnig in 1986, is one kind of scanning probe microscopes (SPM).[67] Unlike the traditional microscopes, AFM gets information by "touching" instead of "seeing" the surface. Compared with electron beam techniques, such as scanning electron microscope (SEM) or transmission electron microscope (TEM), AFM allows the sample to be imaged without prior treatment, which means imaging of the topography of both conducting and insulating surfaces can be obtained directly with atomic resolution.[68] And AFM can be used in an ambient atmosphere or even the liquid, which makes it possible to investigate biological samples in a physiological-like environment.[69] In general, AFM can be used to get the image of surfaces and to measure adhesion forces between biological samples and substrates.

Figure 2.1a shows one kind of AFM from JPK Company. The whole system is consisted by the head which has the laser and cantilever inside, charge-coupled device (CCD) camera and also computer screens are used to read the signal.

Figure 2.1b shows schematics of an AFM. AFM consists of three main parts: piezoelectric scanners, force sensors and feedback control. The heart of the system is the cantilever; at the end of the cantilever is a very sharp tip. The cantilever can be regarded as springs, which can sensitively detect the change of tiny forces. The primary idea of AFM is that the interactions between tip and sample, either attractive or repulsive, will let the cantilever bend or deflect. This deflection of the cantilever

towards or away from the surface will change the angle of the reflected laser beam change; as a result, the spot on the quadrant photodiode will be on a different position, thus measuring the deflection signal.

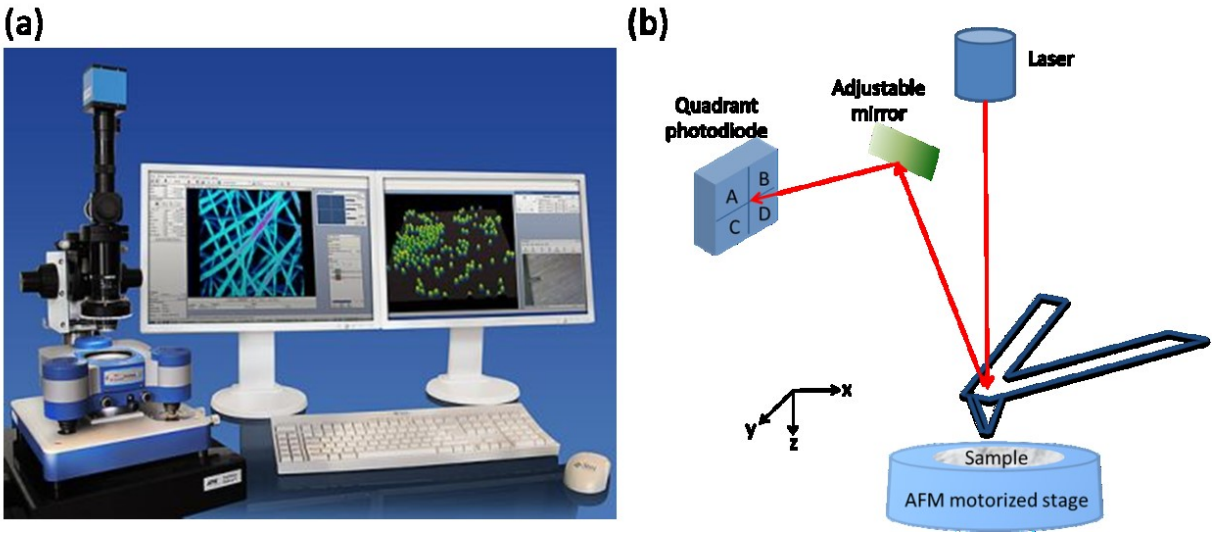

Figure 2.1 (a) JPK's NanoWizard 3 NanoScience AFM. Retrieved 21 April, 2016, from http://usa.jpk.com/index.media.8fc0435d2b83f3361a1026408da1b44dv2.jpg; (b) Schematics of an Atomic force microscope.

2.2 Imaging

There are some general modes for AFM imaging, the most commonly used modes are contact mode and tapping mode, and different cantilevers are used for either mode.

2.2.1 Contact mode

Contact mode was the first and also the simplest mode developed in AFM measurements.[70] In contact mode, the tip stays always on the surface, so it is good at obtaining very high-resolution images. In addition, as the deflection of the cantilever leads directly to the topography of the sample, it is the fastest of all the topographic modes.[70] However, contact mode also has some disadvantages: as the tip is always sliding on the surface of the sample, both the tip and the sample could be damaged. Except the normal force between the tip and the sample, lateral forces are also experienced by both probe and sample which could be a problem in some situations,

but also can give information about the friction force between the tip and the sample.[71]

One important factor to get high resolution images is the sample preparation, which means that the sample should be very clean and firmly adsorbed on the substrate. Figure 2.2 shows an exemplary AFM image of a gold substrate with adsorbed streptavidin using contact mode. The contact image was obtained with non-conductive silicon nitride AFM probes (DNP-S10) coated on the back side with a 45±10 nm thick Ti/Au layer from Bruker Corporation (France) on a NanoScience atomic force microscope (JPK Instruments AG, Berlin, Germany). As we can see from the image, particles lie on the surface. Using the section analysis of the JPK data processing software, we can measure the height of the particles, which is about 12 nm.

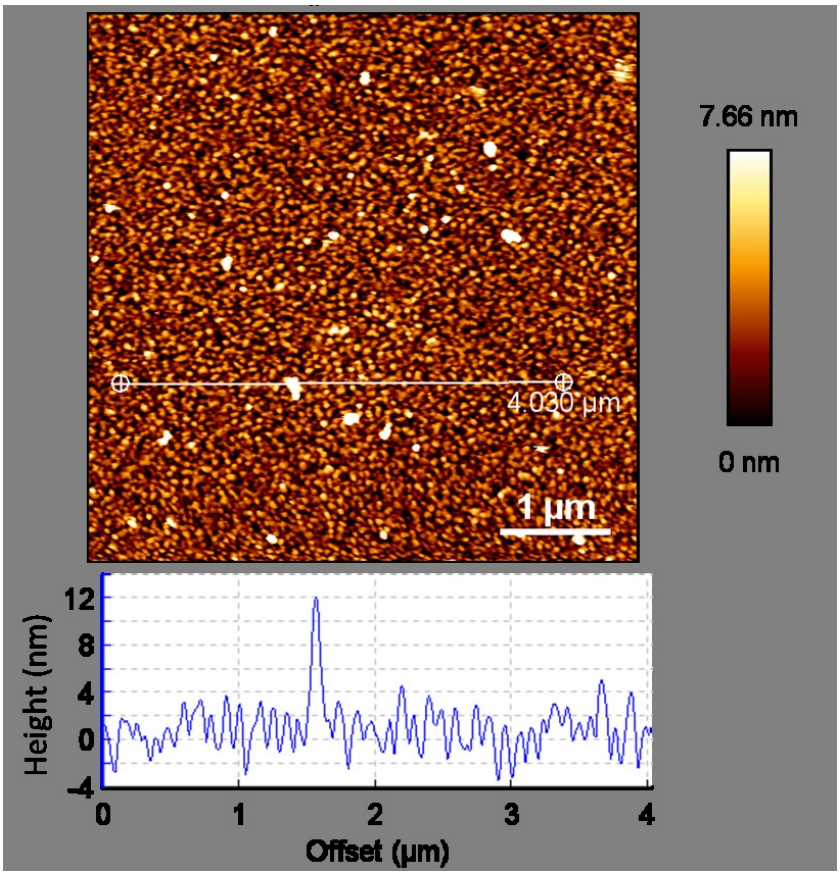

Figure 2.2 Exemplary AFM image and section analysis of gold substrate adsorbed with streptavidin using contact mode. A non-conductive silicon nitride AFM probe (DNP-S10) from Bruker Corporation (France) was used as the cantilever.

Contact mode in liquid is also an important application. For instance, it is an important tool to study direct interactions between biomolecules and surfaces in realistic environment, and the solution can be changed easily during the experiment. Details will be introduced in Section 2.3.

2.2.2 Tapping mode

Tapping mode, also called intermittent contact mode or AC mode, is a commonly used mode for imaging in air.[72] In the tapping mode, the AFM cantilever oscillates with (or near) its resonance frequency close to the sample surface. A tapping mode AFM image is obtained by imaging the force of the intermittent contacts of the tip with the sample surface.[73] Since the AFM probe is not always contact with the surface, tapping mode allows for higher lateral resolution and also less sample damage than contact mode. But in the real experiments, it is not always easy to find the specific resonance frequency, so may take more time than contact mode.

Besides the topographic image, phase image can also be obtained from tapping mode at the same time, as the phase of the cantilever's oscillation with respect to the driving signal can be simultaneously recorded. Due to the conditions of the sample interaction, phase shift will occur between the drive amplitude which is applied to the piezo and the lock-in-amplitude which is measured from the detector. Phase image can show regions of varying stiffness or with different adhesion properties, which is not visible in the topographic image.

Figure 2.3 shows the AFM topographic and phase image of graphene oxide (GO) using tapping mode.[74] The topography image of the surfaces was obtained using silicon AFM probes (NCHV) from Bruker Corporation (France) with a resonant frequency of 320 kHz on a NanoScience atomic force microscope (JPK Instruments AG, Berlin, Germany). AFM was utilized as it is the most direct method to quantify the degree of the GO exfoliation. Figure 2.3a shows the presence of sheets with a uniform thickness of about 1 nm, which agrees well with the data reported for GO monolayer.[75] Figure 2.3b shows the phase change of the GO sheet. Since there are no different components except GO, so the phase change is not obvious.

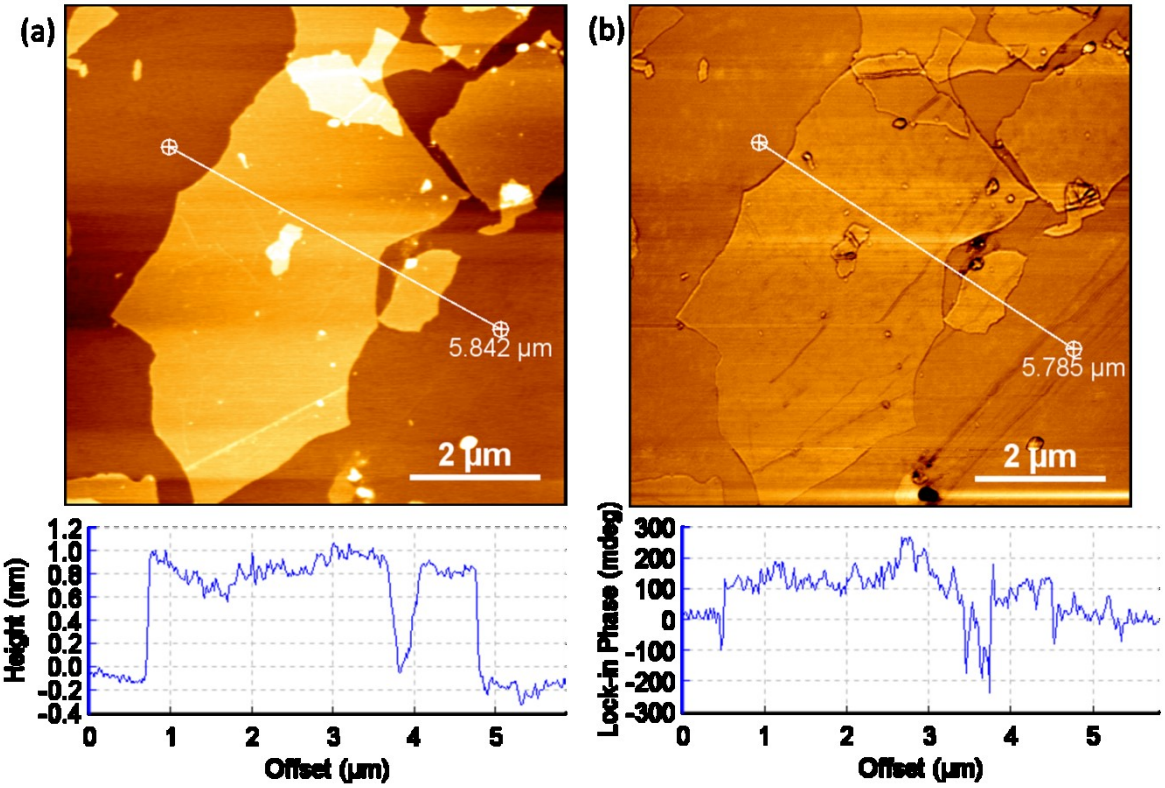

Figure 2.3 AFM topographic image and phase image section analysis of graphene oxide (GO) using tapping mode.[74] A silicon AFM probe (NCHV) with a resonant frequency of 320 kHz from Bruker Corporation (France) was used as the cantilever.

2.2.3 Cantilevers

Generally speaking, different kinds of AFM cantilevers are used in different modes.

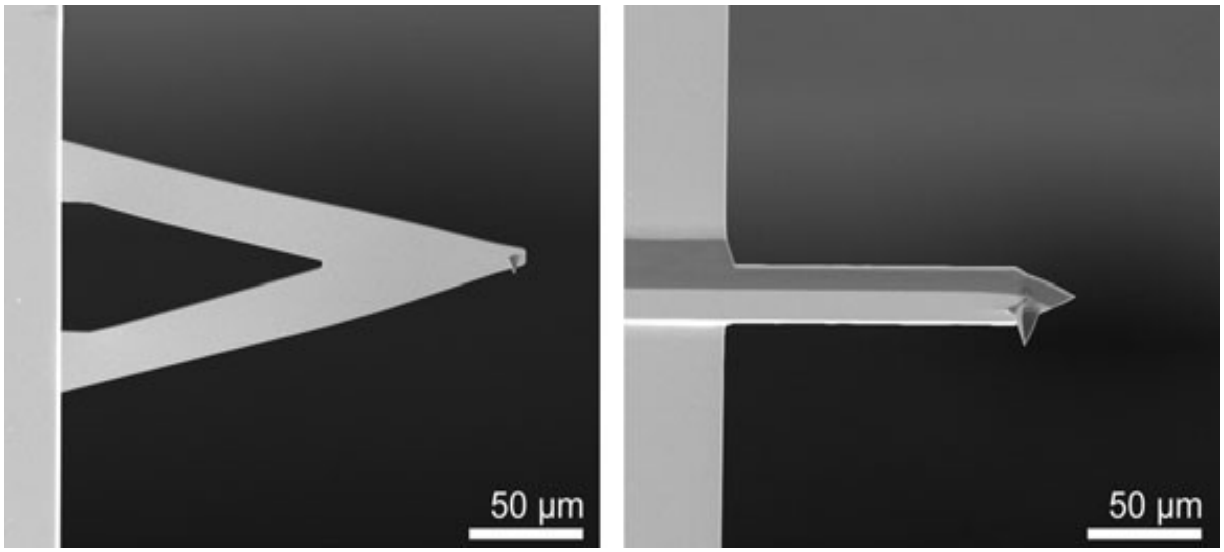

Figure 2.4 Examples of contact (left) and non-contact or tapping mode (right) probes. (Cited from ref. 76. © 2010, Peter Eaton and Paul West.)

Figure 2.4 shows examples of contact and non-contact or tapping mode probes.[76] The left cantilever is a typical v-shaped contact-mode cantilever, which is made from silicon nitride (Si_3N_4); at the end of the probe is an integrated square pyramidal probe tip. The right cantilever is a typical rectangular-shaped (in this case it is a modified-rectangular-shaped) probe, designed for oscillating modes, such as non-contact or tapping mode. It is made from silicon (Si), and is much stiffer and more brittle than the contact probe; at the end of the probe is a sharper tip.

In my work, non-conductive silicon nitride AFM probes (DNP-S10) coated on the back side with a 45±10 nm thick Ti/Au layer from Bruker Corporation (France) were used in contact mode for imaging and force spectroscopy; silicon AFM probes (NCHV) with a resonance of 320 kHz from Bruker Corporation (France) were used in tapping mode for imaging.

2.3 Force spectroscopy

Except for the high-resolution imaging capabilities in topographic fields by AFM, this technique also plays an important role in force measurements. Force spectroscopy is widely used to investigate the intra- and inter-molecular forces with picoNewton (pN) resolution.

In the force measurements, both the cantilever sensitivity and spring constant are needed for the calibration. As it is introduced in Section 2.1, the movement of the cantilever is measured by the vertical deflection of the reflected spot position on the quadrant photodiode, and this deflection value, in unit of Volts, is the difference in voltage between the different sections of the photodiode. The sensitivity is used to transfer vertical deflection of laser to the deflection of the cantilever, which can be measured by obtaining a force curve on a hard surface. After sensitivity calibration, the spring constant is used to transfer the deflection of the cantilever into a force. The spring constant is very sensitive to the thickness of the cantilever, and the most commonly used method for the calibration is the thermal noise method. This is based on measuring the thermal fluctuations in the deflection of the cantilever, and then using the equipartition theorem to extract the spring constant.[77]

Figure 2.5 shows an example of force-distance (F-D) curve, and this curve is actually a plot of the deflection of the cantilever versus the extension of the piezoelectric scanner.

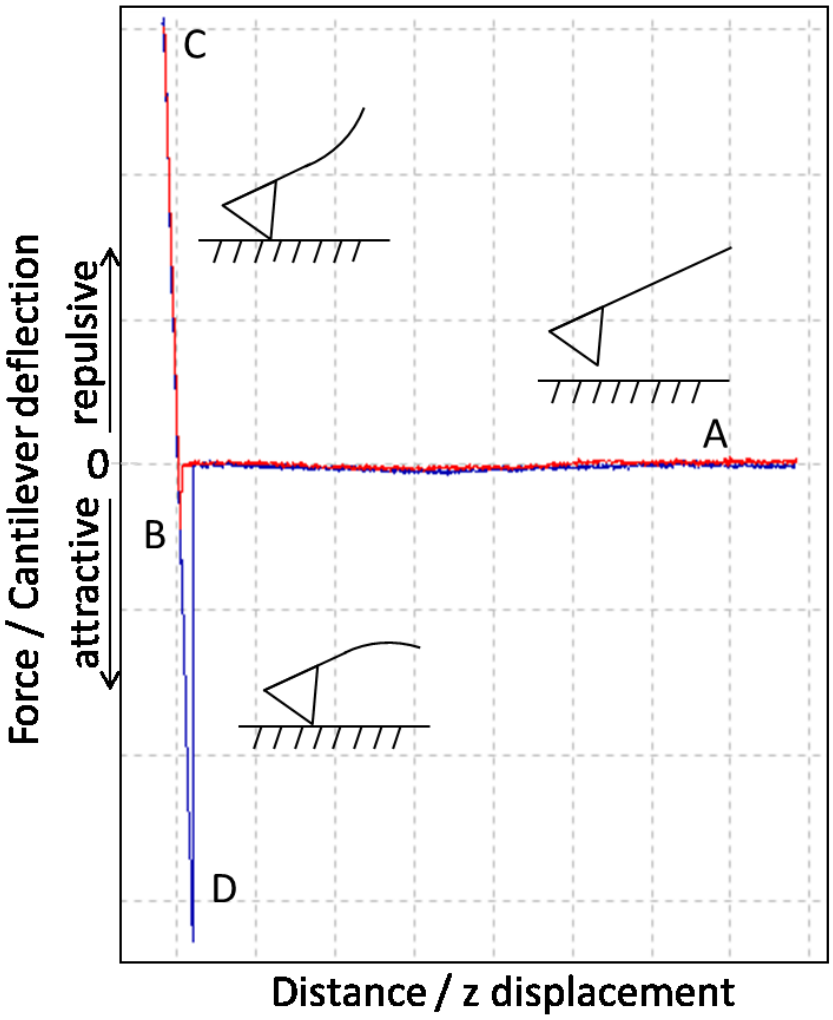

Figure 2.5 Exemplary force-distance curve from a blank probe on a bare gold surface.

In the approach and retract cycle, the approach curve (red curve) begins with the tip far away from the surface of the sample (position A), thus no interaction is detected. As the tip of the cantilever is moved towards the surface of the sample, the cantilever will initially deflect towards the surface because of van der Waals forces (position B), which cause a “snap-on” event. Then the tip is approached further to the surface, while the cantilever is positively deflected due to repulsive forces until the setpoint value is reached (position C). After that, the cantilever is moved away from

the surface of the sample (blue curve). At first, the cantilever follows back the approach curve. Later, however, the cantilever becomes negatively deflect (position D) until the adhesion force is overcome by the force applied on the cantilever. Afterwards, the tip is again away from the surface, and no more interactions are recorded on the way back to the position A. The value of the force needed to withdraw the probe from the surface can be obtained following Hooke's Law ($F= -kd$). It converts the cantilever deflection (d) into the force F with the coefficient of k, which is the spring constant of the cantilever.

2.3.1 Functionalization of AFM probes

How to suitably functionalize the AFM probes plays a vital role in force spectroscopy experiments. In general, there are four steps to functionalize AFM probes (Figure 2.6). (1) To start, the probes need to be activated to generate more surface hydroxyl groups by removing organic contaminants on the hydrophilic surface. There are some efficient ways to do that, for instance, the probes are washed with 10% nitric acid solution, or Piranha solution (H_2SO_4: 30% H_2O_2=7:3) or $CHCl_3$ solution.[78-80] Alternatively, they can be placed well as under the oxygen plasma or UV-ozone treatment.[81, 82] (2) After that, the probes are cleaned using ultrapure water, and then the dried probes are subjected to a silanization reaction with 3-aminopropyl triethoxysilane (APTES), which has amino terminal groups. (3) The next step is to introduce a linker or spacer group between the tip and biomolecules, which can prevent the biomolecule on the tip to be compressed during contact with the substrate. The most commonly used linkers or spacers are polyethylene glycol (PEG), glutaraldehyde (GA) and or nanotubes.[83, 84] PEG is preferred due to some advantages: as a flexible molecule, it allows the biomolecule attached on the tip to reorient freely; it is possible to distinguish the unspecific and specific binding because the soft PEG molecule extend according to well-known nonlinear elasticity; the tip can scan a large surface for target molecules during experiments.[85] The N-hydroxysuccinimide (NHS) ester function at one end of the PEG linker will be covalently coupled with the amino terminal groups in the second step, while the NHS ester function at the other end will

bind to biomolecules, such as DNA, proteins or peptides. (4) Finally, the biomolecules are attached on the probe.

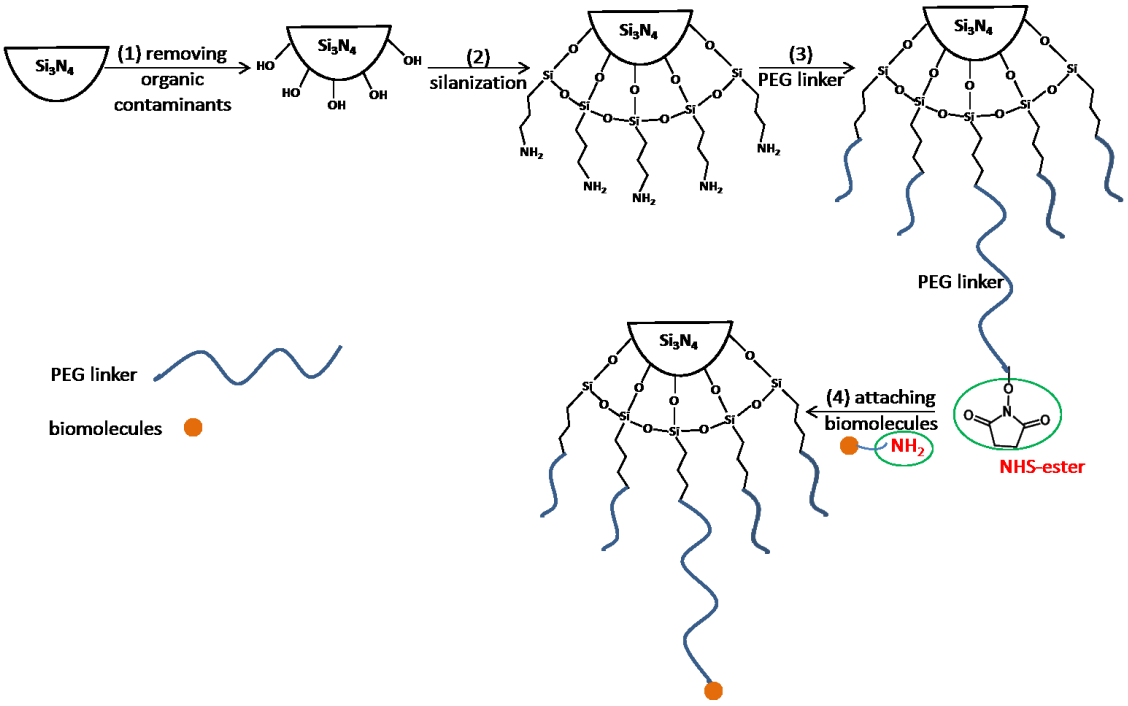

Figure 2.6 Scheme of functionalization of AFM probes in a general way.

To get clear force spectroscopy results between a functionalized probe and a surface, it is better to attach biomolecules at a low surface density to ensure single molecule detection, so we can limit the biomolecule concentration by mixing other silanes without amino terminal groups in the second step; or we can mix other linkers without NHS ester function in the third step. Detail processes of functionalization of AFM probes will be found in the method sections in each chapter.

2.3.2 Surface preparation

As AFM measures the interactions between a modified probe and a surface, so obtaining a uniform surface is also quite important. The most commonly used substrates for AFM experiments are glass, silicon wafer, highly oriented pyrolytic graphite (HOPG), mica and gold-coated silicon wafer.[55, 81, 86-88]

Glass is used as a substrate because it is relatively cheap and can be modified with biomolecules, such as DNA.[89] Silicon wafer is widely used as a substrate due to its flatness, uniform charge density, because the surface chemistry can be easily

controlled by silanization.[90] HOPG, which is hydrophobic, can also be used as a substrate because it can be freshly cleaved with adhesive tape to ensure a clean and atomically flat surface, and researches between HOPG and DNA are making progress.[55, 91] Mica is a commonly used substrate for AFM, due to its very smooth surface on which biomolecules can be easily adsorbed.[87] Gold-coated silicon wafer can be used as a substrate because it can anchor biomolecules, based on the capability of gold to form covalent bonds with sulphur atoms from exposed, native or engineered, thiol groups on the biomolecules.[92]

The details of the preparation of surfaces used in my work will be found in the following chapters: HOPG in Chapter 4 and 5, gold surfaces in Chapter 5, mica and gold surfaces in Chapter 6.

2.4 An example of single-molecule force spectroscopy

Parts of this chapter have been published in *Phys. Chem. Chem. Phys.*, 2014, **16**, 3995—4001 (DOI: 10.1039/c3cp54121e).

Single-molecule force spectroscopy (SMFS) can be used to detect the interactions between biomolecules and inorganic surfaces, antibody and antigen, ligand and receptor and so on.[54, 93, 94]

We used SMFS to detect the direct force on peeling two randomly-sequenced ssDNA oligomers (DNA1 and DNA2 in Table 2-1) from a graphite surface.

Table 2-1 DNA sequences for the SMFS experiments.

DNA	Sequences
DNA1	5'-NH_2-$(CH_2)_6$-AGT CAG TGT GGA AAA TCT CTA GC-3'
DNA2	5'-NH_2-$(CH_2)_6$-AGG TCG CCG CCC-3'

The AFM probes are first cleaned in newly prepared Piranha solution (H_2SO_4: 30% H_2O_2=7:3) for 30 min to remove the organic contaminants on the probes, then washed with large amount of ultrapure water and ethanol (98%) for several times. Then the following procedure for the modification of AFM probes for DNA binding is shown in Figure 2.7. In this strategy, the cleaned probes are silanized through

incubation with 3-aminopropyl triethoxysilane (APTES) and thiethoxychlorosilane (TTCS) at a total concentration of 1%. The addition of TTCS in this reaction greatly decreases the amount of $–NH_2$ groups bound to the AFM probe, effectively ensuring the subsequent binding of only very few ssDNA molecules.[95] Each created $–NH_2$ group on the AFM probe is then further modified with one N-succinimidyl ester of the PEG-NHS ester linker. The ssDNA molecules are finally connected onto the AFM probes through the binding of their terminal $–NH_2$ groups to the free N-succinimidyl ester ends of the linkers. It should be noted that the use of PEG-NHS as a bifunctional linker can greatly decrease the nonspecific interaction between AFM probe and graphite. The flexible linker structure allows the DNA molecules to interact with the graphite surface with a large conformational freedom.[96] Freshly cleaved HOPG was chosen as substrate in the experiment.

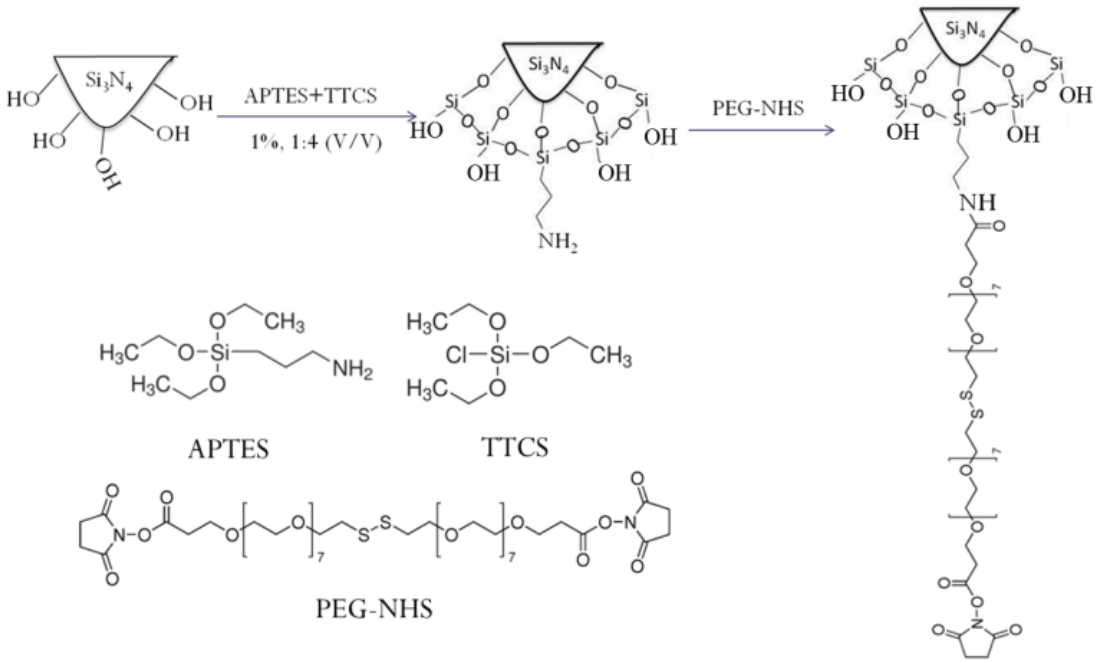

Figure 2.7 Modification of AFM probes for DNA binding.

When the ssDNA-modified AFM probe approaches and gets in contact with the graphite surface, non-covalent interactions lead to the formation of a molecular bridge between the probe and the surface.[80] Upon retraction, the molecular bridge is progressively peeled off the surface, leading to a characteristic force-distance (FD) signal.

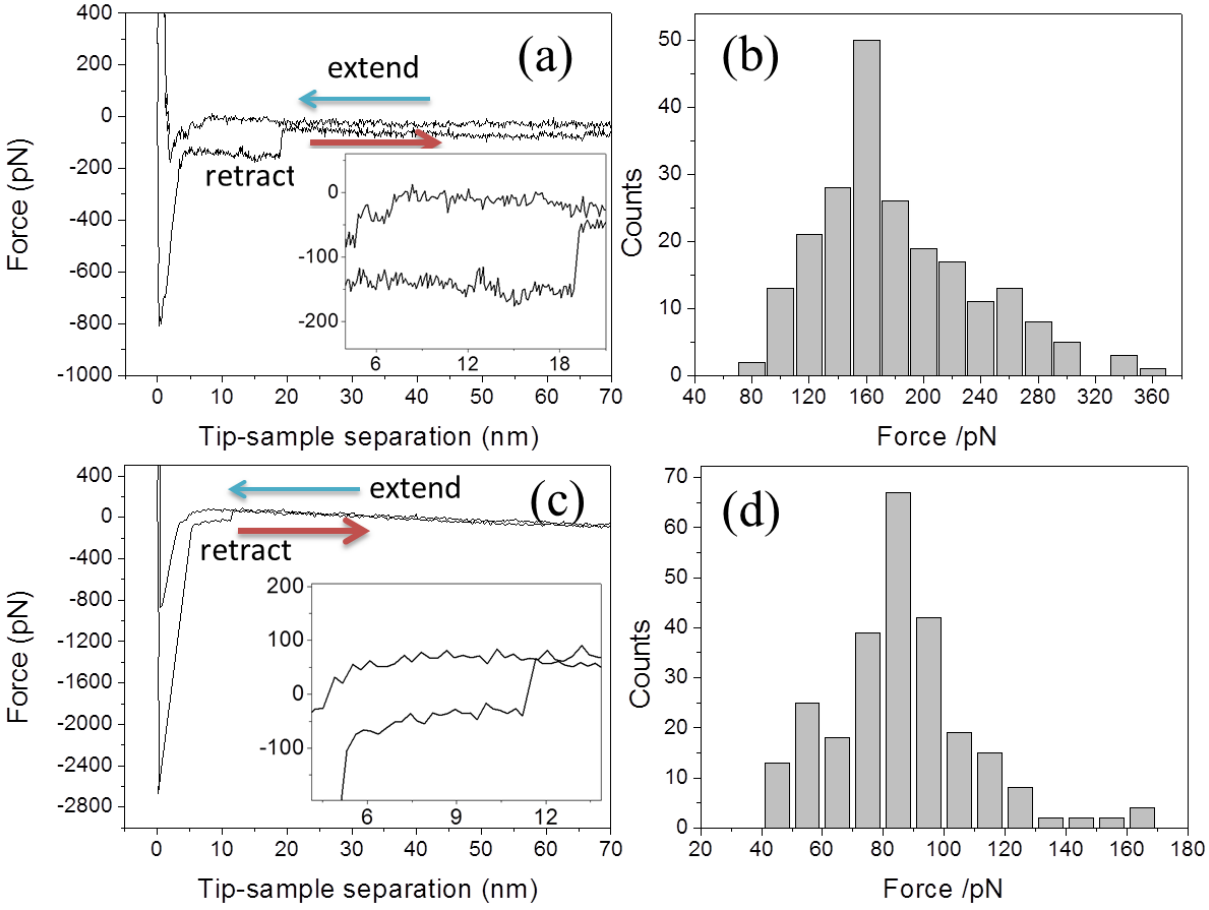

Figure 2.8 Exemplary FD curves and distribution histograms of the peeling force of DNA1 (a, b) and DNA2 (c, d) with a loading rate of 1.6×10^5 pN/s. The average force was 176.8±50.7 and 99.0±43.7 pN for DNA1 and DNA2, respectively.

Typical FD curves measured for DNA1- and DNA2-modified AFM probes using a loading rate of 1.6×10^5 pN/s are presented in Figure 2.8. The retract trace of both FD curves (Figure 2.8a and c) shows first an initial sharp peak and then a plateau where the tip-sample separation increases at a roughly constant force. The first sharp pull-off event corresponds to the breaking of the nonspecific adhesive junction between the monolayer-coated AFM probe and the hydrophobic surface.[54, 55, 97, 98] The plateau force is caused by peeling the ssDNA molecules off the graphite surface, with progressive breaking of the DNA/graphite molecular interactions.[54, 55, 97] A statistical analysis of the plateau forces from many FD curves gives average peeling forces of 176.8±50.7 and 99.0±43.7 pN (±SD, n>200) for DNA1 and DNA2, respectively, as shown in Figure 2.8b and d.

Therefore, the interactions between heteropolymer ssDNA oligomers and the surface of graphite can be directly measured with SMFS, and adhesion forces can be obtained from the FD curves. As different forces are obtained from the specific interactions, this accurate force change can be used to develop biosensors, by using specific sequence of DNA aptamers or other biomolecules. Following this idea, the following chapters will introduce the use of SMFS to detect adenosine (Chapter 4), mercury ions (Chapter 5) and thrombin (Chapter 6).

3 Atomic force microscopy based single-molecule force spectroscopy applications for biomolecules-materials interfaces interactions and biosensing

This chapter reviews the literature in the fields of biomolecule interactions and biosensing using AFM-based SMFS. Parts of this chapter have been published in *RSC Advances*, 2016, **6**, 12893—12912 (DOI: 10.1039/c5ra22841g).

3.1 Atomic force microscopy based single-molecule force spectroscopy for biomolecules-materials interfaces interactions

Understanding the interactions between biomolecules and materials interfaces (MI) is very important for the development of materials science, nanotechnology, biophysics, biomedicine, and analytical science.[56, 99]

Biomolecules, such as proteins, peptides, DNA and polysaccharides play important roles in the metabolism, control, sensing, communication, growth, and reproduction of living cells. More and more studies with various methods have been performed, in which a very important part is to study the interactions between biomolecules and MI. Here we would like to present representative cases of interactions of biomolecules with MI using SMFS.

3.1.1 Proteins

Since it allows to detect the interactions between protein-functional tips and selected MI, SMFS becomes a very useful tool to study the folding and unfolding of proteins.[100-102] As the aggregation and misfolding of the proteins may lead to diseases or even cancers, SMFS may also have promising application in the biomedical field.[101, 102]

Botello et al. investigated the mechanical unfolding of the I27 domain from human cardiac titin under thermal and chemical denaturing conditions.[100] By connecting one

end of the individual titin molecule to a gold substrate, the other end to a silicon nitride cantilever (Figure 3.1a), they used force as a physical parameter to alter the protein folding energy landscape and compared the change in the unfolding free-energy barrier of the I27 domain of human cardiac titin. They found that the trends in protein unfolding free-energy barriers are consistent for single-molecule force measurements and bulk chemical and temperature studies. The results suggest that the information from single-molecule pulling experiments are meaningful and useful for understanding the mechanism of folding *o*f titin I27.

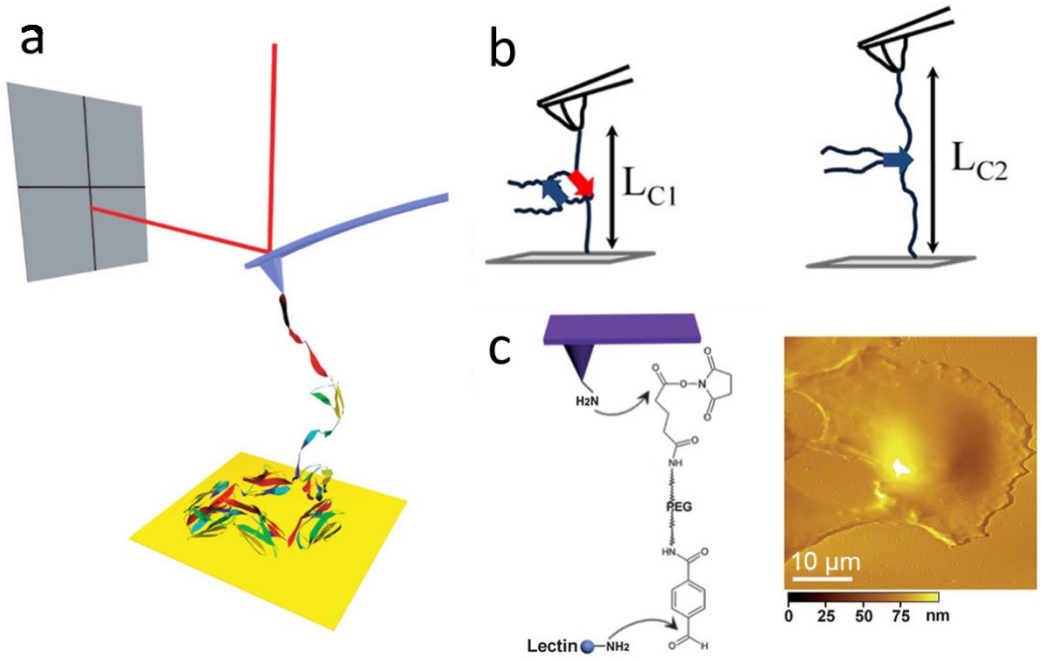

Figure 3.1 AFM-SMFS studying for (a) unfolding of the I27 domain from human cardiac titin (Reprinted with permission from ref. 100. © 2009, American Chemical Society); (b) formation of a dimer (Reprinted with permission from ref. 101. © 2013, American Chemical Society); (c) the scheme of the tip modified with lectin and the AFM amplitude image of Hela cell (Reprinted with permission from ref. 103. © 2013, Royal Society of Chemistry).

In another case, Krasnoslobodtsev *et al.* used AFM-SMFS to study the formation of a dimer by measuring the interactions between alpha-synuclein (*α*-Syn) proteins.[101] In their study, one end of the *α*-Syn was attached onto AFM probe and the other end was fixed onto the mica surface via maleimide-cysteine coupling, as shown in Figure 3.1b. They investigated the formation of a dimer by analyzing the rupture force values and distribution of contour length of force-distance curves, and proved the

pathogenic mutations A30P, E46K, and A53T do not increase the propensity of α-Syn to misfold but rather change conformational preferences of α-Syn. This SMFS method was used to study the formation of a dimer, which can be extended for understanding the aggregation process of proteins.

Protein-ligand interactions

Protein-ligand interactions play essential biological roles in every aspect of living systems and show important applications in biomedicine and nanotechnology.[102] The development of AFM-based SMFS made it possible to directly probe the ligand binding with proteins. Recently, Hu and Li provided an overview of protein-ligand interactions as studied by AFM-based SMFS,[103] in which many recent examples on how to apply SMFS to investigate the mechanical stability and protein folding/unfolding dynamics that modulated by protein-ligand interactions have been introduced. A particularly interesting work on protein-protein interactions is the study by Schoeler et al.,[104] who measured the interactions between X-modules (XMod) protein and binding modules dockerins:cohesins (Doc:Coh) with AFM-based SMFS and steered molecular dynamics simulations. They found that the XMod-Doc:Coh complex withstands forces of 600-700 pN, making it one of the strongest bimolecular interactions reported. This work on the cellulosomal network components may help in the development of biocatalysts for production of fuels and chemicals form renewable plant-derived biomass.

Protein-RNA interactions

Protein-RNA interactions are fundamental for understanding aspects of molecular biology such as gene expression, assembly of biomolecular complexes and macromolecular transport. Andreev *et al.* for the first time investigated the molecular interactions between a plant virus movement protein (MP) and RNA molecules with AFM.[105] They found that the minimal unbinding forces determined for individual interactions of the MP-MP and MP-RNA were estimated to be 70 and 90 pN, respectively. This work provides the physical ideas for further study to understand the

formation mechanism of movement-specific RNA complexed by MPs. In another case, Liu and co-worker reported the pulling of genetic RNA molecules out of the tobacco mosaic virus (TMV) protein by using AFM-based SMFS.[106] In this study, RNA molecules were bound onto the AFM tip and the TMV particles were immobilized onto a gold substrate via cysteine bridges. In the SMFS experiments, they found that the interaction between RNA and TMV is approximately 400±50 pN. The presented results demonstrate the possibility to study the nucleic acid-protein interactions in more complicated systems using AFM-based SMFS technique. In a further study, they studied the mechanism of RNA disassembly in TMV by using AFM-based SMFS under different pH and Ca^{2+} concentrations.[107]

Protein-cell interactions

Using SMFS to study the interactions between proteins and cells, especially cancer cells, gained more and more attention.[108-112] By comparing the forces between proteins and special cells, it could be possible to develop potential anti-tumor drugs. In a typical example, Zhao *et al.* investigated the interactions between lectins and carbohydrates on cancer and normal cells using SMFS.[109] Lectins were tethered on AFM tips, while Hela and MDCK cells were selected as the typical cancer and normal cells (Figure 3.1c), and attached onto glass cover slips. They found that the carbohydrate-lectin complex on cancer cells is less stable than that on normal cells. This SMFS method opens a way to study the specific interactions of receptor-ligand systems and metastasis, progression and invasion of tumor.

In another study, Zhang *et al.* used AFM to real-time and in-situ detect epidermal growth factor receptor (EGFR) expression levels on living MCF-7 cells for evaluating the anticancer activity of resveratrol.[108] The inhibition effect of resveratrol on the expression of EGFR on MCF-7 cells was probed by AFM tips functionalized with epidermal growth factor (EGF). Unbinding forces between the EGF-functionalized tip and cell surface decreased after adding the proper concentrations of resveratrol, which proved the inhibition effect of resveratrol. Thus, SMFS techniques are expected to become a promising tool for screening of drugs.

3.1.2 Peptides

Peptides are biologically occurring short chains of amino acid monomers linked by peptide (amide) bonds. Peptides can specifically bind to many materials, for example polymers, cell membranes, and inorganic materials.[113-115] The study of the interactions between peptide and materials interfaces will help to understand the specificity of peptide binding to the surfaces, thus possibly lead to a better design of composite nanomaterials and nanodevices.

Amino acid-inorganic surfaces

Because of the high complexity concealed in the interactions between peptides and inorganic surfaces, the interactions between individual amino acids and inorganic surfaces have been previously studied by means of AFM-based SMFS.[81, 116-118] Recently, one review paper on the insights into the interactions of amino acids and peptides with inorganic materials with AFM-SMFS has been presented,[116] and therefore we will only provide a few typical examples here.

Razvag *et al.* measured the interaction of individual amino acid with inorganic surfaces using SMFS.[81] Five different kinds of amino acid residues (lysine, glutamate, phenylalanine, leucine, and glutamine) were bound to the AFM tips. The interaction between the tips and a silica substrate in aqueous solution were recorded and analyzed. The results showed that hydrophobic forces and electrostatic interactions dominate the adhesion between the amino acids and the inorganic substrate. These results might help to understand the interactions between biomolecules and inorganic surfaces, which will improve the design of biosensors and composite materials of new organic-inorganic interfaces.

In another study, Li and co-workers studied the interactions between 3,4-dihydroxyphenylalanine (DOPA) and wet surfaces by means of AFM-based SMFS.[117] In their approach, multiple DOPA molecules were attached onto a single polymer chain, hyaluronan (HA), and the stretching of each HA-DOPA molecule resulted in many rupture events of single DOPA-surface bridges. This is similar to the stretching of polyproteins shown in the part of Section 3.1.1. This method could

increase the efficiency of obtaining high-quality SMFS data and reduce the nonspecific interactions and multiple unbinding events.

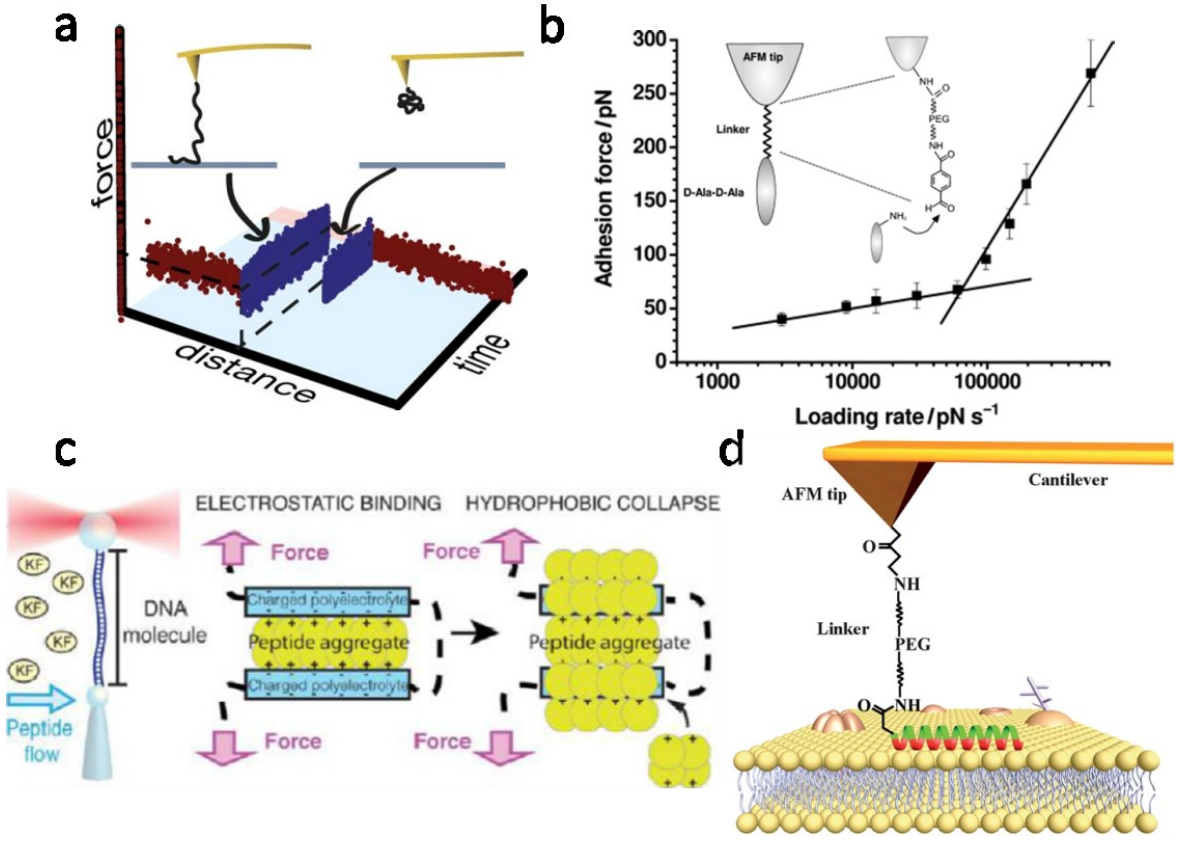

Figure 3.2 AFM-SMFS for measuring the interactions between (a) peptide-SAM (Reprinted with permission from ref. 86. © 2014, American Chemical Society); (b) peptide-SS (Reprinted with permission from ref. 120. © 2011, Wiley); (c) peptide-DNA (Reprinted with permission from ref. 124. © 2013, American Chemical Society); and (d) peptide-Hela cell membrane (Reprinted with permission from ref. 114. © 2012, Royal Society of Chemistry).

Peptide-inorganic surface

AFM-SMFS has been extensively used to investigate the single molecular interactions between polypeptides and inorganic materials.[86, 119-121] For instance, Krysiak *et al.* combined SMFS and the equilibrium theory of polymer desorption under terminal pulling to study the intrinsic monomeric desorption rate k_0 of polytyrosine and polylysine homopeptides that were covalently attached to an AFM probe from hydrophobic self-assembled monolayers on glass slides (Figure 3.2a).[86] By fitting the results from the experiments in the constant-pulling and waiting-time protocols with simple two-state kinetic polymer theory, they were able to interpret

the model parameters corresponding to polymer contour length *L*, Kuhn length *a*, adsorption free energy λ, and intrinsic monomeric desorption rate k_0, which was about 10^5 Hz, in terms of a cooperativity in the desorption process of single polymers.

In another case, Landoulsi *et al.* investigated the interaction between D-Ala-D-Ala peptides and a stainless steel surface by SMFS.[119] Force-distance curves were recorded between D-Ala-D-Ala modified tip and the surface in a $NaHCO_3$-enriched medium (Figure 3.2b). Based on the dynamic force measurements of unbinding forces, which linearly increased with the logarithm of the loading rate in two regimes, they revealed the presence of multiple energy barriers in the energy landscape. The results from SMFS showed a new way to study the adsorption mechanism of peptide on inorganic oxide surfaces and to understand the origin of peptide-specific binding.

Our group combined metadynamics and steered molecular dynamics simulations to probe the selectivity of the binding motif RKLPDA peptide for Ti and Si surfaces, and the obtained adsorption free energies and adhesion forces were found to be in quantitative agreement with the corresponding AFM experiments.[121] Recently, our group further utilized molecular dynamics simulations and AFM-SMFS experiments to measure the interactions between GCRL peptide and amorphous SiO_2 surface.[120] By the obtained rupture force of the peptide from the surface, we estimated a free energy of adsorption value, which agreed well with the computer simulation data of adsorption free energy.

Peptide-nucleic acids interaction

Understanding the mechanisms of interaction between peptide and nucleic acids or other polyanions is very important to discover the aggregation process of protein correlated with several human diseases like Alzheimer and Parkinson. The interaction between peptides and DNA molecules can also be detected by means of AFM-based SMFS.[122-125]

In a typical case, Camunas-Soler *et al.* investigated the electrostatic binding and hydrophobic collapse of peptide-DNA aggregates by using AFM-based SMFS, as shown in Figure 3.2c.[124] In their work, the formation of peptide-DNA complexes can

be directly observed with AFM and dynamic light scattering measurements, and the riving thermodynamic forces within the binding process can be quantitatively determined with AFM-based SMFS. In another study, Chung *et al.* investigated the interactions between DNA and a miniature (39 residues) engineered peptide at the single-molecule level.[125] Direct force measurements between DNA-modified mica surfaces and peptide-functionalized AFM probes were performed in 10 mM PBS, the rupture force versus the logarithm of the loading rate was fitted with a single linear plot, indicating a single barrier between bound and unbound state. Using SMFS to study the sequence-specific peptide-DNA interaction has a potential to design well-defined peptide-DNA hybrid nanostructures for further applications in biomaterials and nanodevices.

Peptide-cell membrane interaction

Investigations on the interactions between membrane-active peptides and cell membranes are getting more and more attention, because certain antimicrobial peptides show anticancer activities and even strong specificity against cancer cells.[126] The high sensitivity of AFM-SMFS makes it possible to detect pN forces, therefore it is becoming a promising method to detect the interaction within cell binding peptide.[114, 127-130] For instance, Shan *et al.* studied the binding of single anticancer peptides with HeLa cell membranes by SMFS.[114] Interaction forces between the anticancer peptide-functionalized AFM tip and the lipid bilayer of HeLa cell membranes were successfully detected (the mechanism is shown in Figure 3.2d), and it was found that the interaction increased with the increase of peptide hydrophobicity, but the interaction force was dependent on the binding sites of the peptide on the cell membranes. This result implied that SMFS can be used to provide more insights into the interaction mechanism of anticancer peptides with biomembranes.

3.1.3 Polynucleotides

DNA, the molecule of life, has been a fascinating research subject since its

discovery. Understanding the interactions between DNA molecules with biomolecules and inorganic materials is very important for the developments of DNA chips, biosensors, nanodevices and functional biomaterials.[131] In this section, the interactions of DNA molecules with complementary DNA, peptide nucleic acid (PNA), antibodies, and various substrates detected with AFM-SMFS will be introduced.

ssDNA-ssDNA interaction

The specific interaction between ssDNA and its complementary sequence is important for the storage, retrieval and modification of information in biological systems. SMFS can directly measure the forces and loading rates, which can help to understand the DNA hybridization process.[89, 132, 133] For example, Strunz *et al.* measured the unbinding force between ssDNA and its complementary ssDNA strand with AFM-based SMFS by covalently immobilizing complementary oligonucleotides with a 5'-SH modification via a cross-linker on the tip of an AFM tip and a glass substrate, as shown in Figure 3.3a.[89] They studied the DNA duplexes with different base pairs (10, 20, and 30 bp) under different loading rates (16-4000 pN/s), and found that the cooperative unbinding of the base pairs in the DNA duplex leads to a scaling of the unbinding force with the logarithm of the loading rate, which can be explained as a single energy barrier along the mechanical separation path.

In another study, Sattin and co-workers presented a novel experimental design to observe the DNA hybridization at a single base-pair resolution by using AFM-based SMFS.[133] They were able to measure the interactions between different sequences under exactly the same conditions of cantilever, probe and solution by using a microarray of short oligodeoxynucleotides, which can achieve direct comparisons with minimal random errors. Their results indicated that base stacking contributed to a larger extent to the interactions within DNA hybridization than H-bonding.

ssDNA-PNA interaction

PNA is a DNA mimic in which the normal DNA phosphodiester backbone is replaced by a 2-aminoethyl-glycine linkage and the nucleotide bases are connected to

the backbone by a methylene bridge and a carbonyl group.[134] The interactions between ssDNA and PNA are stronger than between two ssDNA because of a lack of electrostatic repulsion from uncharged PNA. For example, Cao *et al.* studied the interaction between PNA and DNA by AFM-based SMFS.[135] The PNA sequence with only six thymine bases, $p(T)_6$ was tethered on the tip, while the complementary DNA sequence of $d(A)_6$ was attached to the silica surface, as shown in Figure 3.3b. Rupture forces of $p(T)_6$-$d(A)_6$ hybrids were around 148 pN, which was larger than the forces to unbind short DNA duplexes. The kinetic parameters were also obtained by the rupture force-loading rate function, which highlighted the stronger binding affinity between PNA and DNA than between DNA and DNA. Thus, it is believed that PNAs could be used as a tool for the single-molecule sequence detection and manipulation.

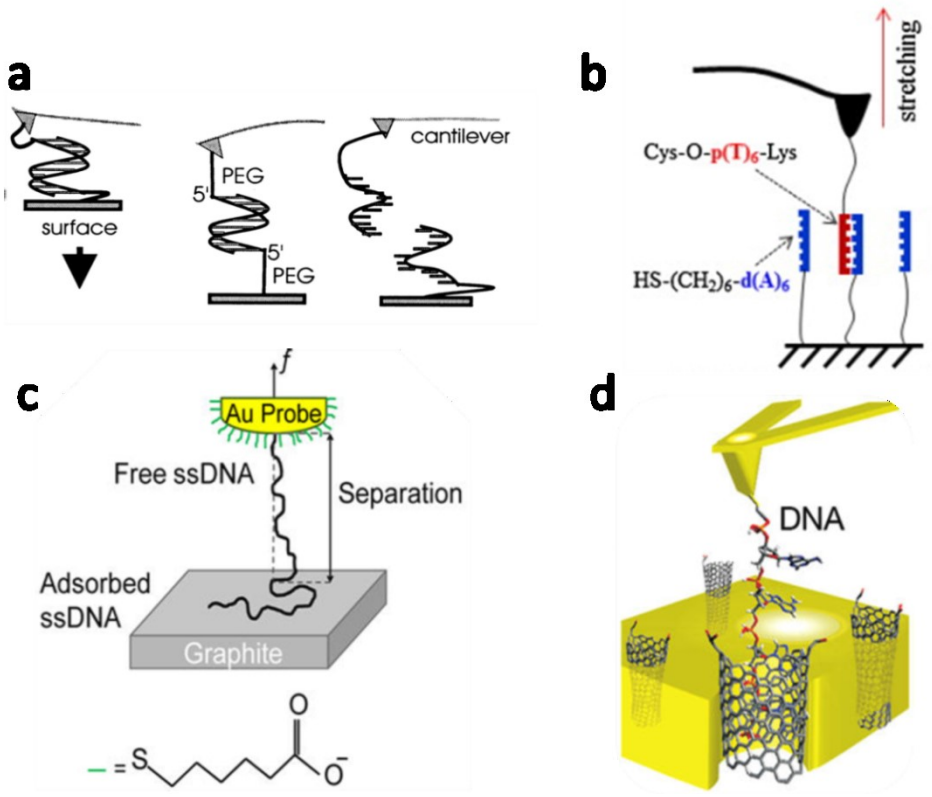

Figure 3.3 (a) Unbinding forces between complementary ssDNA strands (Reprinted with permission from ref. 89. © 1999, National Academy of Sciences); (b) interaction between antibody modified tip and ssDNA modified glass substrate (Reprinted with permission from ref. 135. © 2015, Elsevier B.V.); (c) frictionless peeling of a ssDNA from graphite surface (Reprinted with permission from ref. 55. © 2012, American Chemical Society); (d) scheme of pulling ssDNA from a carbon nanotube pore (Reprinted with permission from ref. 98. © 2011, American Chemical Society).

ssDNA-antibody interaction

An antibody is a Y-shape protein produced by plasma cells that is used by the immune system to identify and neutralize pathogens such as bacteria and viruses. Since some antibodies can bind two 5-methylcytidine bases of a surface-immobilized DNA strand, research of attaching antibody to the cantilever to study the DNA methylation pattern has been performed.[136, 137] In a typical case, Zhu *et al.* used SMFS to measure the distance between 5-methylcytosine bases in individual DNA strands and determine the methylation pattern.[136] A monoclonal antibody specific for 5-methylcytidine was conjugated via a flexible poly(ethylene) (PEG) cross-linker to an AFM cantilever, while a 5-methylcytidine-containing ssDNA was coupled via its 3'-terminus to a glass slide. The antibody is able to bind two 5-methylcytidine bases of a surface-immobilized DNA strand, thus there is a unique rupture signature reflecting the spacing between two tagged bases. Using SMFS in this system has the potential to allow related chemical patterns to be retrieved from biopolymers at the single-molecule level.

ssDNA-graphite interaction

As individual DNA bases are known to bind graphite surfaces through noncovalent π-π interaction, the ssDNA-graphite system will help to understand the interactions between polyelectrolytes and hydrophobic substrates.[138] SMFS can be directly used to measure the interaction forces between ssDNA molecules with flat solid surfaces. For example, Manohar *et al.* measured the force by peeling 50-mer ssDNA from graphite surface with AFM-based SMFS and they further determined the binding energy of the oligonucleotide with graphite.[54] With the same technique, Iliafar *et al.* investigated the interactions between DNA oligomers and graphite (Figure 3.3c).[55] Table 3-1 showed the peeling forces and binding affinity of pyrimidine and purine oligomers on a graphite surface. Their studies suggest that the DNA chain length and its direction of attachment to a gold-coated AFM tip have negligible effects on the peeling forces of homopolymers.

Table 3-1 Peeing force of different DNA on graphite surface

sequence	force (pN)	binding energy (k_BT)
3'-poly(dT_{50})	85.3±4.7	11.3±0.8
3'-poly(dC_{50})	60.8±5.5	8.3±0.7
5'-poly(dT_{50})	73.4±5.5	9.4±0.9
5'-poly(dT_{100})	78.5±5.0	10.2±0.8
3'-poly(dA_{50})	76.6±3.0	9.9±0.5
5'-poly(dG_{100})	66.4±1.4	8.3±0.2

Moreover, from the table above, we can see that the binding energy determined from the peeling force data did not scale with the size of the base. In a further study, the same authors used Brownian dynamics to study the peeling of a polymer molecule, represented by a freely jointed chain (FJC), from a frictionless surface in an implicit solvent with parameters representative of ssDNA adsorbed on graphite.[97] They found, in the limit of slow peeling, that the Brownian dynamics model replicates the results of an equilibrium statistical thermodynamic model under both force control and displacement control.

Recently, we studied the interactions between two heteropolymer ssDNA molecules and graphite using SMFS.[53] We found that the peeling forces of heteropolymer ssDNA were different from homopolymer ssDNA, and there was a direct influence of the precise DNA sequence on the interaction with graphite. In addition, the unbinding force decreased with the increase of the ionic strength of the liquid environment. The unbinding force increase d nonlinearly with the logarithm of the applied loading rate, which can be fitted with a newly developed single-barrier adsorption model.[139]

ssDNA-carbon nanotubes interaction

Carbon nanotubes (CNTs) are important in biomedical applications such as sensing and drug delivery due to their intriguing electrical, mechanical, and thermal properties. Hybrid ssDNA-CNT systems have also emerged as promising materials for practical exploitation.[140] SMFS is helpful to investigate the interactions when ssDNA is

encapsulated within CNTs bundles.

For instance, Iliafar *et al.* investigated the interaction of ssDNA with single-walled CNTs (SWCNTs).[141] They found that forces are required to remove each of the four ssDNA homopolymers from surface-adsorbed SWCNTs and methy-terminated SAMs. In addition, they found that the free energy of ssDNA binding to both substrates decreased in the order of poly(A)>poly(G)>poly(T)>poly(C), while the magnitude of the latter is significantly smaller than the formers. The binding strength of ssDNA to the curved SWCTs is 2-3 times higher than that to flat graphite. Combined with replica-exchange molecular dynamics, the enhancement is explained from the spontaneous curvature of ssDNA, or the preference of the ssDNA to adopt highly curved conformations when adsorbed on nonpolar surfaces.

In another very interesting work, Lulevich *et al.* investigated the interactions between ssDNA and CNT pores by pulling an ssDNA-modified AFM tip from a CNT membrane Figure 3.3d).[98] They found that the rupture forces decrease with an increase of salt concentration. This differs from the measurement on graphite by Manohar *et al.*,[54] which indicates that the interactions of ssDNA with the narrow CNT pore are significantly different from its interactions with a flat graphitic carbon surface. In a theoretical study, Roxbury *et al.* used replica exchange molecular dynamics (REMD) to study the equilibrium sequence-specific structures formed by single strands of 12-mer oligonucleotides adsorbed on a SWCNT.[142] They found that the actual structural motif of the adsorbed strand depends strongly on the sequence and composition of DNA molecules.

3.1.4 Polysaccharides

Polysaccharides are polymeric carbohydrate molecule composed of long chains of monosaccharide units bound together by glycosidic linkages, that release the monosaccharides or oligosaccharides constituents upon hydrolysis. They range in structure from linear to highly branched, and they are important in food technology to control structure, texture and stability. Some protein molecules may be attracted or repelled by the polysaccharide due to the formation of electrostatic complexes.

Dextran-substrate interaction

Dextran is one kind of polysaccharide, a polymer formed by glycosidic bonds linking the carbon atoms number 1 and 6 of consecutive α-D-glucopyranose rings. The elasticity of dextrans can be studied by SMFS; in particular due force-extension curves of single molecules can be obtained using this technique. In a typical case, Rief et al. used SMFS to probe the elastic properties by chemically binding dextran strands to a gold surface and letting them interact with an AFM tip through a streptavidin-biotin bond.[143] They found that at low forces the deformation of dextran was dominated by entropic forces, which can be described by the Langevin function with a 6 angstrom Kuhn length; at elevated forces the deformation was governed by a twist of bond angles, while and at higher forces it was determined by a distinct conformation change.

Components of mixtures of polysaccharides

SMFS is also helpful to identify the components of mixtures of polysaccharides because the force-extension curves can show the fingerprints of elasticity of linear polysaccharides. For example, Marszalek *et al.* investigated fingerprinting polysaccharides with SMFS.[144] They studied polysaccharides based on stretching single molecules in solution with AFM. This method recorded the molecular fingerprint of force-induced conformational transitions within the pyranose ring, and has the potential to identify specific polysaccharide molecules in the mixture solution.

Polysaccharides on living cells

SMFS can be also used to investigate the adhesive and conformational properties of polysaccharides on the membrane of living cells, which help to understand their functions. For instance, Francius *et al.* used SMFS to probe the adhesion and mechanics of polysaccharides and proteins on cells.[145] They developed a protocol to stretch single polysaccharide molecules on the surface of Lactobacillus rhamnosus GG (LGG) bacteria with lectin-modified tips. The protocol can be easily modified for other

cell types.

3.1.5 Antigen-antibody interaction

The interaction between antigens and antibodies is fundamental to many immunochemical techniques. AFM-SMFS has been widely used to investigate various specific interactions between antigens and antibodies.[78, 93, 146-148] For instance, Dammer *et al.* investigated specific interaction between immunopurified polyclonal goat IgG antibodies (anti-biotin antibodies) and biotinylated bovine serum albumin (BBSA).[93] Roy *et al.* studied the interaction between captured prostate-specific antigen (PSA) and its detection antibody (5A6) after cross-linking during force measurement.[78] From the result of the number of the captured antigens in a specific area, it is believed that the approach can be applicable to the quantitative analysis of the antigen in a sample, which can be extended to a sample of very low copy numbers as long as the size of the microarrayed spot is reduced.

3.2 Atomic force microscopy based single-molecule force spectroscopy for biosensing

Generally, biosensors are composed of three parts: a sensor device employing different physical and/or optical principles, a sample delivery system, and a sensor surface where one of the interaction partners is immobilized. SMFS can be used in molecule-recognition based biosensing of DNA, RNA, proteins, antibody-antigens, enzymes, drug molecules, and metallic ions.

3.2.1 Sensing of DNA

SMFS can be used as a DNA sensor because the DNA match and mismatch will change the rupture forces which can be obtained in the curves. In 2003, the Gaub group for the first time reported a novel approach to design a programmable force sensor based on AFM.[22] In their setup, the cantilever spring was replaced by a polymeric anchor and a known molecular bond carrying a fluorescence label. During the separation of two surfaces, the polymeric anchor was stretched and the bonds

were ruptured to elicit a fluorescence signal. This technique has very high sensitivity and can be used to detect single-base pair mismatch in a DNA sequence, as well as specific antibody-antigen interactions.

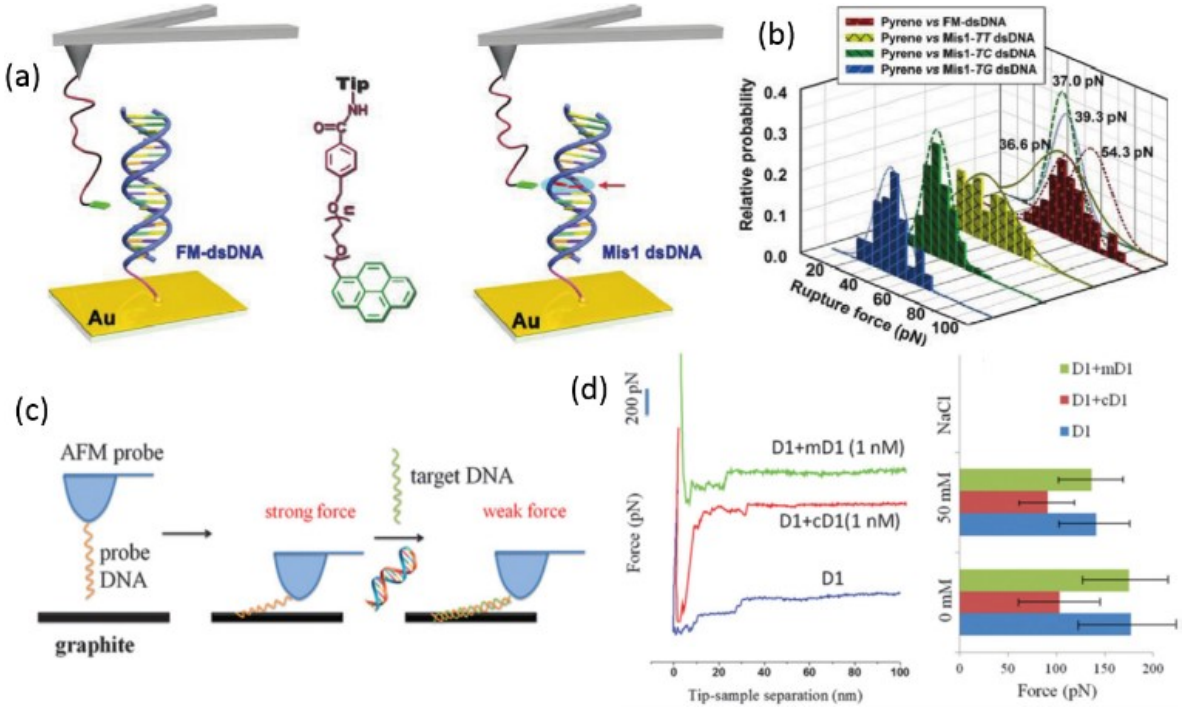

Figure 3.4 (a and b) AFM-SMFS sensing of DNA by the interaction between pyrene and DNA. (Reproduced with permission from ref. 80. © 2010, American Chemical Society), (c and d) AFM-SMFS sensing of DNA by the interaction between DNA and graphite surface. (Reprinted with permission from ref. 79. © 2013, Royal Society of Chemistry).

In the first label-free sensing study with AFM-based SMFS, Jiang *et al.* used SMFS to investigate the interaction between pyrene modified tips and fully matched or mismatched dsDNA which was immobilized onto a gold substrate via a thiol-Au bond (Figure 3.4a).[80] They found that the introduction of mismatched sites into dsDNA reduces the interaction of pyrene binding to dsDNA. This clear difference in rupture forces for pyrene to unbind from matched and mismatched dsDNA opens a new way to detect mismatches in dsDNA (Figure 3.4b).

Recently, our group has demonstrated a novel single-molecule, label-free bioanalytical system capable of sensing the presence of specific ssDNA oligomer sequences with high selectivity and sensitivity (Figure 3.4c).[79] As ssDNA has a strong interaction with graphite due to the π-π stacking, it is possible to compare the force

change when ssDNA hybridize with complementary DNA. A specific sequence of ssDNA (D1) was bound to an AFM probe, and the binding force was detected against a graphite surface in deionized water. The D1-modified AFM probe was then immersed in 1 nM complementary target ssDNA sequence (cD1), or in a mismatched ssDNA sequence (mD1) with one single base mismatch (Figure 3.4d). It was found that the mean plateau force of hybridized DNA (D1+cD1) decreased about 35.5% while the plateau force of mis-hybridized DNA (D1+mD1) did not change significantly compared to that of D1. In this study, an ssDNA concentration of 1 nM has been detected, and it opened a possibility to detect DNA using SMFS.

3.2.2 Sensing of RNA

RNA plays major roles in coding, decoding, regulation and expression of genes, so it is important to use proper methods to detect RNA.

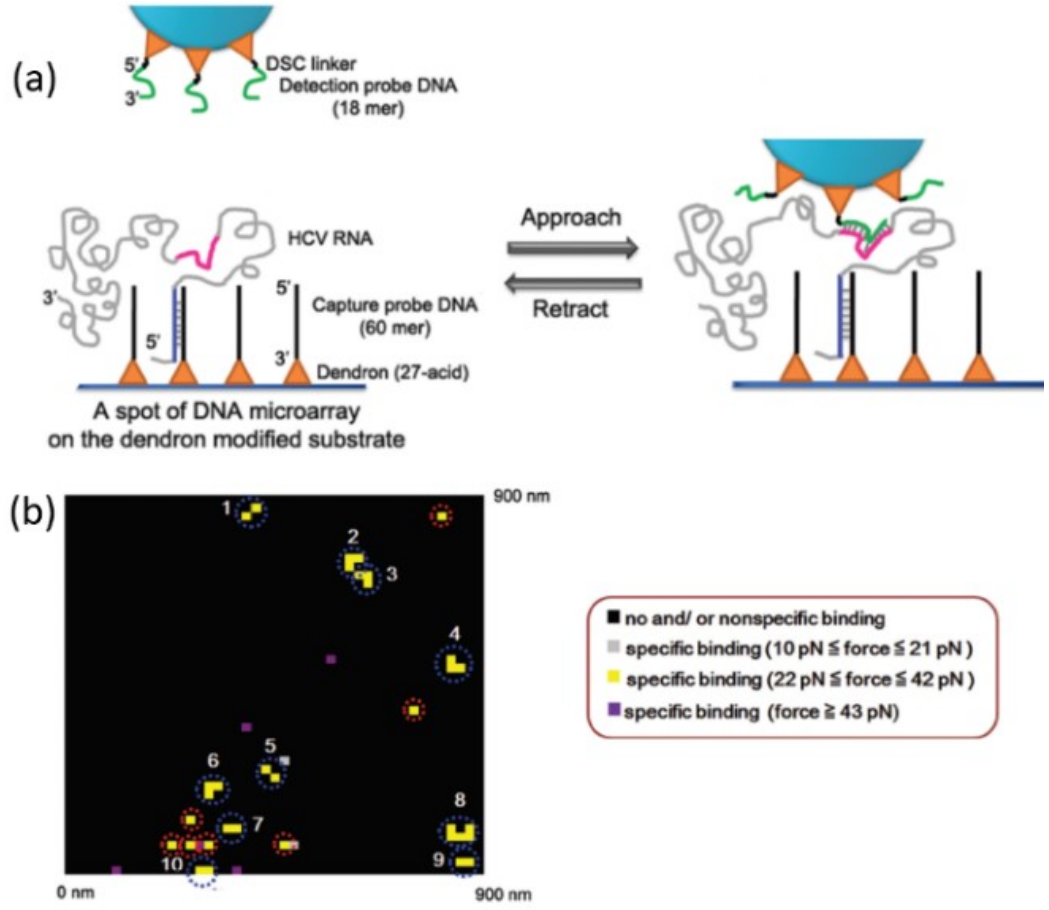

Figure 3.5 (a) Schematic presentation of AFM-SMFS sensing of RNA, (b) Force mapping detection of RNA. (Reprinted with permission from ref. 23. © 2012, Oxford University Press).

Jung *et al.* used AFM to detect hepatitis C virus (HCV) RNA directly without labelling or amplification.[23] The capture probe DNA was covalently linked to the apex of the Dendron immobilized on the slide, while the detection DNA was linked to the apex of the Dendron immobilized on the AFM tip (Figure 3.5a). After HCV RNAs were hybridized with the capture DNA on the slide, the interaction between the detection DNA on the AFM tip and captured RNAs was measured. By utilizing Dendron self-assembly on the surface, it could be find a mostly 1:1 interaction between the DNA on the AFM tip and the captured RNA on the surface. This SMFS method can direct detect RNA without labelling, modification, reverse transcription and amplification, which overcome the limitations of other approaches. With this AFM-SMFS based force mapping technique, RNA sample with very low concentration about 5 fM can be detected easily (Figure 3.5b).

3.2.3 Sensing of proteins

Protein detection is also an important aspect in AFM-based biosensing. Previously, Blank and co-workers reported the fabrication of a force-based protein biochip.[149] This assay for the quantification of single-molecule binding forces was developed based on differential unbinding force measurements where ligand-receptor interactions were compared with the unzipping forces of DNA hybrids. In their study, the DNA zippers enabled not only to distinguish the specific and non-specific interactions, but also allowed the highly sensitive detection of proteins and antibodies.

Recently, our group used AFM-based SMFS to detect lysozyme with high selectivity and sensitivity, and the detection limit of lysozyme was 0.65 nM.[79] By attaching an anti-lysozyme aptamer (D2) on an AFM tip, forces were detected and compared after adding lysozyme. The results showed that there was a very weak detachment force (about 70 pN) for a D2-modified AFM probe on an oxidized Si (SiO_2) surface, while there were four peaks with a detachment force of about 500 pN between a lysozyme-modified AFM probe and SiO_2. The interaction force between D2-modified AFM probes and SiO_2 in the presence of 0.65 nM lysozyme showed

lysozyme-characteristic features and a strong detachment force of about 700 pN. This method proved that an increase in the detachment force and the appearance of lysozyme-characteristic peaks can be used as force fingerprints to reveal the presence of lysozyme in the solution system.

3.2.4 Sensing of antibody-antigen interactions

Antibody-antigen recognition is the primary event at the basis of many biosensing platforms. Kienberger *et al.* combined high-resolution AFM-FS imaging with topographical imaging, which is called force-volume mode, to study the interaction between anti-lysozyme antibody-conjugated tips and lysozyme adsorbed mica substrates.[150] It was found that the imaging with the antibody-modified tip gave strikingly different images than with a bare silicon-nitride tip. The binding sites on the lysozyme layer were detected, and the unbinding forces were scaled in each pixel with gray values. After blocking with antibody in solution, the binding probability dropped significantly, which becomes quite clear in the force-volume data.

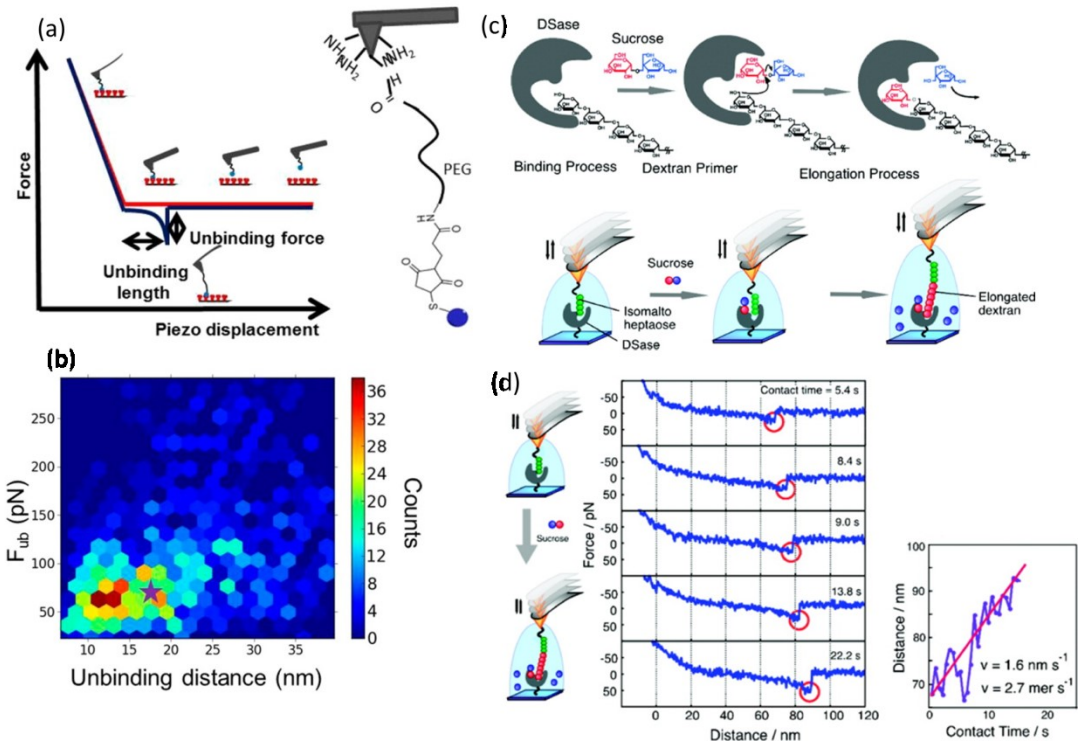

Figure 3.6 (a and b) AFM-SMFS for studying the antibody-antigen interaction. (Reproduced with permission from ref. 152. © 2015, American Chemical Society); (c and d) AFM-SMFS for measuring the enzymatic activity and kinetics. (Reprinted with permission from ref. 153. © 2011, American Chemical Society).

Recently, Casalini and co-workers reported the multiscale sensing of antibody-antigen interactions by combining organic transistors and AFM-SMFS technique.[151] In their work, they used an antigen (interleukin-4, IL4) to modify the AFM probe and an anti-IL4 to modify the substrate, as shown in Figure 3.6a. Figure 3.6b shows the 2D histograms containing the number of events with five unbinding force peaks and unbinding lengths. The statistical analysis of force-distance curves made it possible to quantify the probability, the characteristic length scales, the adhesion energy, and the time scale of the specific recognition. This work proves that the specific molecular recognition events in biosensors can be assessed, quantified, and optimized.

3.2.5 Sensing of enzymes and their activities

Enzymes catalyse various biochemical reactions and AFM-based SMFS can be used for studying the activity and catalysis mechanism of enzymes.[152-154] For instance, Ditzler *et al.* investigated the catalytic activity of enzymes by forming a stable monolayer of active Escherichia coli dihydrofolate reductase (ecDHFR) directly bound to an ultra-flat gold surface.[152] By detecting the rupture force between the enzyme-modified gold surface and a tip modified with a tight-binding inhibitor (methotrexate), they collected significant rupture forces upon dissociation of the inhibitor from the enzyme's active site and also showed the viability of a simple and direct enzymatic surface-functionalization without spacers. This method opens the door to further applications in the field of bio-macromolecular force spectroscopy.

In another interesting study, Mori *et al.* presented how to apply AFM-SMFS for studying the kinetics of enzymatic dextran elongations.[153] Dextransucrase (DSase) is a glucosyltransferase that catalyze the transfer of a D-glucose unit in sucrose to a D-glucose at the nonreducing end of a dextran acceptor (Figure 3.6c). The elongation process is visible from the shifts of rupture peaks between the dextran-immobilized probe and the DSase-modified mica surface in the presence of sucrose as a monomer (Figure 3.6c). In order to monitor the real-time enzymatic reaction dynamics, they further utilized the continuous FD scanning to measure each second on a particular

DSase molecule at the same point, as shown in Figure 3.6d. The obtained result indicated that the rupture force peak shifted by the order of 1 nm for every few seconds of contact time. By statistical analysis, a catalytic elongation rate constant (K_{cat}) of 2.7 s^{-1} was obtained.

3.2.6 Sensing of drug molecules

SMFS has also attracted much attention for the detection of drug molecules such as adenosine and cocaine, due to molecular recognition between ssDNA aptamers and drug molecules.

In a typical study, Nguyen *et al.* measured single small molecule binding via rupture forces of a split aptamer by AFM to detect adenosine monophosphate (AMP).[155] To prevent the target analyte interacting with the surface, they used a "split", namely a bipartite aptamer, in which one component was immobilized on the AFM probe, and the other on the sample surface (Figure 3.7a). They found that the rupture force between the two components increased in the presence AMP in comparison with the force measured in absence of AMP. With this SMFS technique, a detection limit of 3.7 μM was obtained for sensing AMP (Figure 3.7b). This method showed potential applications to develop other drug sensors.

Very recently, in our group we demonstrated a simple force-based label-free strategy for the highly sensitive sensing of adenosine.[156] This sensor took advantage of the specific molecular recognition between adenosine and an appropriate DNA aptamer, as well as of the intrinsic SMFS sensitivity (Figure 3.7c and d). We have reached a relatively low adenosine detection limit in the range of 0.1–1 nM and very good selectivity against uridine, guanosine and cytidine. This method without labelling makes the detection much easier, and can be used in similar chemical detections. In a further study, we utilized a SMFS-based force mapping technique to sense the presence of adenosine and cocaine with a concentration of 0.1 nM by visual observation of the color changes of force maps before and after adding analytes, these results belong to a paper which has been submitted to *Scientific Reports*.

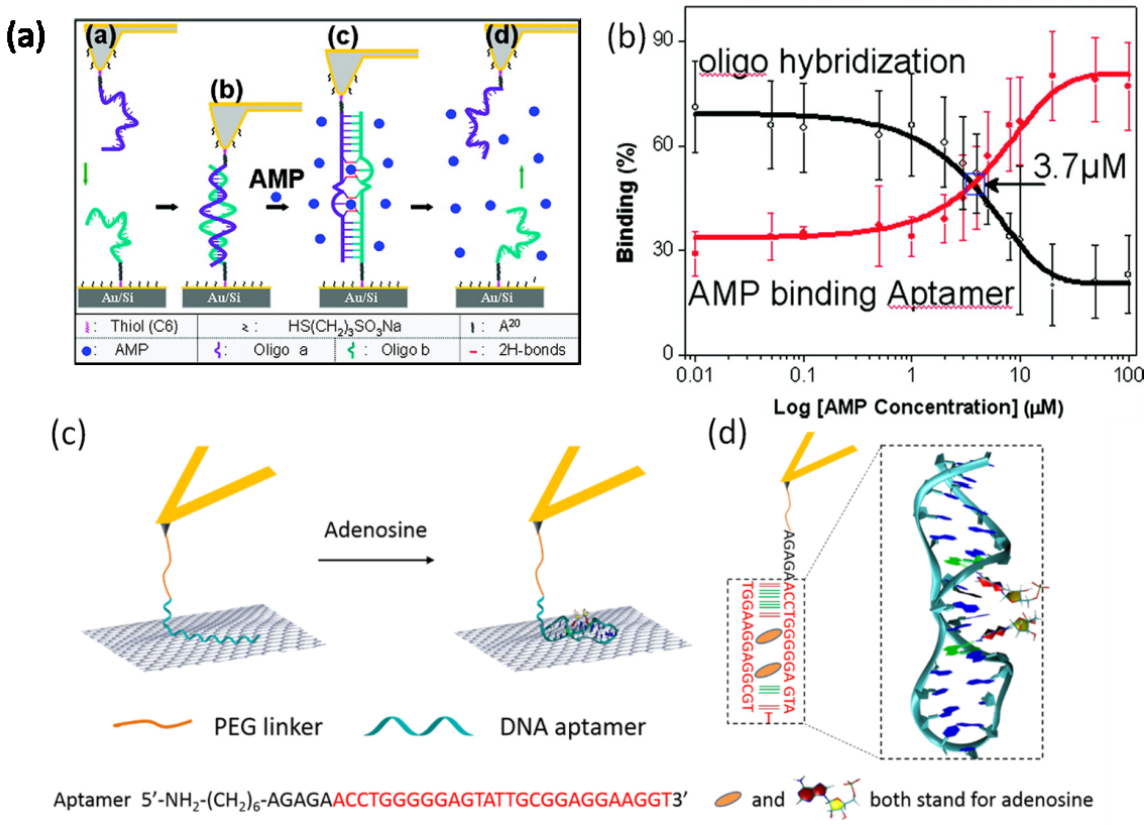

Figure 3.7 (a and b) AFM-SMFS sensing of AMP by the interaction between DNA aptamers. (Reproduced with permission from ref. 156. © 2011, American Chemical Society); (c and d) AFM-SMFS sensing of adenosine by the interaction between DNA aptamer and graphite surface. (Reprinted with permission from ref. 157. © 2015, MDPI).

3.2.7 Sensing of metallic ions

Some metallic ions pose a great threat to both the environment and human health, and SMFS is a newly developed method to detect them. Recently, we fabricated a novel aptasensor based on AFM-SMFS capable of detecting mercury ions (Hg^{2+}) with sub-nM sensitivity.[157] A specific aptamer sequence for Hg^{2+} was covalently attached on an AFM probe, and by detecting the force between the ssDNA aptamer and graphite in water solutions with different concentrations of Hg^{2+}, we found that the peeling force between aptamer and graphite surface increased obviously after adding Hg^{2+}. The detection limit was approximately 0.1-1 nM and the technique showed very high selectivity of Hg^{2+} over other metal cations. This novel technique will have wider applications for other polluting metal ions, and will be described in detail in Chapter 5.

In another recent work, Kuo *et al.* studied the metal-crown ether complexes by means of AFM-based SMFS.[158] In their work, a classical model of $M^{n+}[15C5]_2$, a metal cation hosted jointly by two 15-crown-5 moieties immobilized on both the AFM probes and substrates was investigated. The addition of metallic ions into the system could create a crown-metal-crown bridge and the SMFS peeling experiments could detect a clear unbinding force. Therefore, a good ionic selectivity could be achieved. In addition, by using the isotherms of binding probability and dynamic force spectroscopy, the free energy landscapes and kinetic parameters for the dissociation of complexations could be estimated via the Bell-Evans model.

4 Adenosine detection

This chapter demonstrates how to use single-molecule force spectroscopy to detect adenosine. Parts of this chapter have been published in *Biosensors* 2015, **5**, 85-97 (DOI: 10.3390/bios5010085).

4.1 Introduction

Adenosine is a nucleoside composed of adenine and d-ribose. Adenosine or adenosine derivatives play many important biological roles in addition to being components of DNA and RNA. For instance, adenosine is involved in cellular energy transfer and performs important signaling functions in both the peripheral and central nervous system.[159, 160] It is well known that adenosine is a product of ATP degradation and its release from cells is a possible sign of disease. Therefore, the direct detection and monitoring of adenosine under physiological conditions have gained increasing significance in analytical, environmental, and biomedical applications.[161-163]

Several traditional assays, such as high-performance liquid chromatography, UV-absorbance, Raman spectroscopy and fluorescence spectroscopy, have been applied for the detection of adenosine.[30, 164-168] These techniques present the main problems of high detection limit and low selectivity. With the development of biotechnology and nanotechnology, enzymes and aptamers with specific molecular recognition ability have been used to fabricate different biosensors for the highly sensitive and selective detection of adenosine.[39, 162, 163, 169-171] For example, Zhang *et al.* reported an electrochemical biosensor for detecting adenosine based on a structure-switching aptamer and the subsequent amplification with DNA-modified nanoparticles.[39] Li and co-workers demonstrated an aptamer biosensor based on surface-enhanced Raman scattering, and obtained a detection limit of 12.4 pM.[169] However, these biosensors suffer from drawbacks due to the complicated synthesis of DNA-modified nanoparticles and the labeling of probes and targets. Therefore,

developing simpler, label-free adenosine biosensors with high sensitivity and selectivity is desired.

Atomic force microscopy (AFM)-based single-molecule force spectroscopy (SMFS) allows for the measurements of tiny forces associated with formation and breaking of single hydrogen bonds. It has therefore been widely used to study the specific molecular recognition interactions in antigen-antibody, ligand-receptor, and complementary ssDNA pairs.[49-52] SMFS is also powerful for studying any function and property of biomolecules associated with force changes, and especially for measuring the adsorption force between biomolecules and functional nanomaterials.[53-55] AFM-based SMFS can also be employed as a promising label-free biosensing technique with high sensitivity. Until now, there are a few reports on the detection of biomolecules with SMFS. For example, Zhang and co-workers reported SMFS-based detection of DNA mismatched hybridization.[80] Nguyen *et al.* reported the detection of adenosine monophosphate, with a detection limit of 3.7 ± 2.5 μM.[155] Recently, our group presented an SMFS-based, label-free bioanalytical system capable of selectively sensing the presence of specific ssDNA oligomers and proteins with sub-nM sensitivity.[79]

In this chapter, we would like to explore the potential of AFM-based SMFS for the label-free detection of adenosine. To achieve this aim, an adenosine aptamer was bound onto the AFM tip, and the corresponding force-distance (FD) curves between the aptamer and a graphite surface were measured by SMFS until complete detachment, providing a reference desorption force. After that, low-concentrated adenosine was added into the liquid cell to bind to the aptamer. The formation of an adenosine-aptamer complex triggers a DNA conformational transition, which is associated with a change of the FD curve and in particular of the desorption force from graphite. Based on the obtained experiments, we have proven that our SMFS-based biosensor can be utilized to effectively detect adenosine in the range of 0.1 to 1 nM. In addition, our biosensor presents a very high selectivity for adenosine against uridine, guanosine, and cytidine. Our strategy is very simple but powerful, being mainly based on molecule-molecule and molecule-material recognitions. We

expect that similar SMFS-based sensing strategies will be developed in the near future to detect a wide range of other analytes at sub-nM concentrations.

4.2 Experimental section

4.2.1 Reagents and materials

A highly oriented pyrolytic graphite (HOPG) wafer with ZYB quality (10 × 10 mm^2) was purchased from NT-MDT Company (Moscow, Russia). Non-conductive silicon nitride AFM probes (DNP-S10) with a 45 ± 10 nm thick Ti/Au layer coated on the back side were obtained from Bruker Corporation (France). An adenosine-binding DNA aptamer (5'-NH_2-$(CH_2)_6$-AGAGAACCTGGGGGAGTATTGCGGAGGAAGGT-3') was synthesized by IBA company (Göttingen, Germany), aliquoted, and stored at -20 °C. All the chemicals used in this work were bought from Sigma-Aldrich (Germany). The water used in this work is ultrapure water after purification with a Mill-Q Integral system (18.0 MΩ).

4.2.2 Preparation and characterization of flat graphite surfaces

The preparation of flat graphite surfaces was performed by mechanical exfoliation of an HOPG wafer using Scotch® tape.[172] The topography images of the surfaces were obtained in AC (tapping) mode using silicon AFM probes (NCHV) with a resonant frequency of 320 kHz on a NanoScience atomic force microscope (JPK Instruments AG, Berlin, Germany). Topographical and deflection images were collected as 512 × 512 pixels with a lateral scan speed of 2.0 Hz.

Figure 4.1a presents a typical AFM height image of a flat graphite surface made by means of mechanical exfoliation of a HOPG wafer. From the cross-section analysis, a mean roughness of about 0.2 nm in the 2 µm × 2 µm area was found, as shown in Figure 4.1b. This is flat enough to ensure no effect of the surface roughness on the measured adhesion forces.

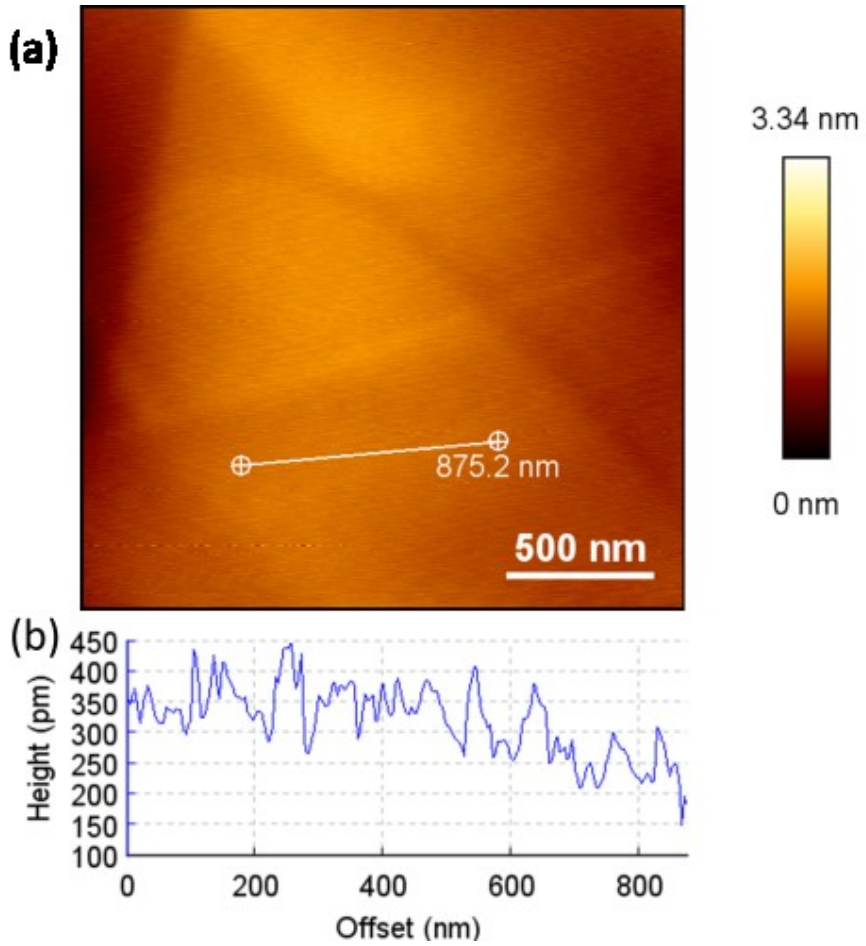

Figure 4.1 Typical (a) AFM image, and (b) cross-section analysis of the prepared graphite surface by mechanical exfoliation.

4.2.3 Functionalization of AFM probes

Figure 4.2 shows the procedure for AFM probe functionalization. All silicon nitride AFM probes were cleaned in newly prepared Piranha solution (H_2SO_4: 30% H_2O_2=7:3) for 30 min to remove the organic contaminants on the probes. All AFM probes were washed with large amount of ultrapure water and ethanol (98%) for several times. Then the cleaned probes were silanized by a mixed solution of 3-aminopropyl triethoxysilane (APTES) and triethoxy(ethyl)silane (TEES) (1% in toluene, APTES:TEES, 1:4, v/v) for 15 minutes to functionalize the probe with amino groups. After washing with ethanol and ultrapure water for several times, the AFM probes were transferred into 4,7,10,13,16,19,22,25,32,35,38,41,44,47,50,53-Hexadecaoxa-28,29-dithiahexapentacontanedioic acid di-N-succinimidyl ester (PEG-NHS ester disulfide (n=7)) (0.1 mg/ml) for 1 h to tether the PEG-NHS ester disulfide to the AFM probes by

covalent interaction between the NH_2 and NHS groups. Then the probes were washed with ultrapure water and then incubated with ssDNA (100 nM) solutions for 30 minutes to bind the aptamer to the probes. Finally, the aptamer-modified AFM probes were washed with a large amount of ultrapure water to remove non-covalently adsorbed DNA molecules prior to the experiments.

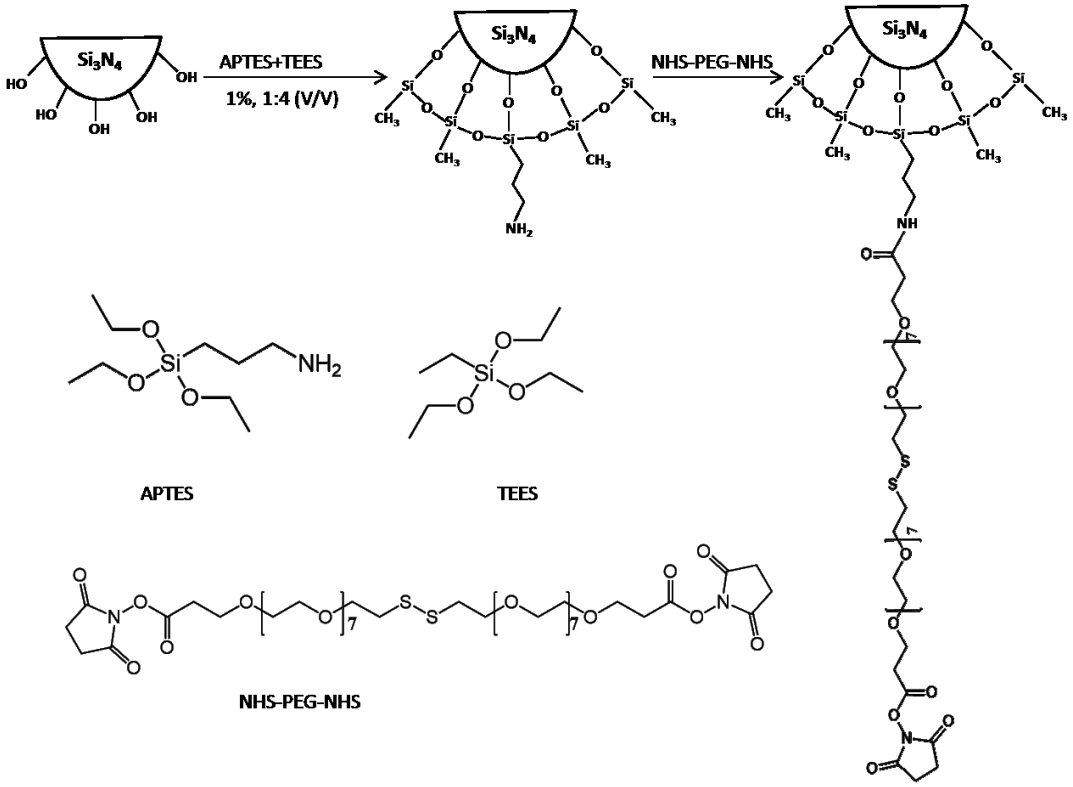

Figure 4.2 Functionalization of AFM probes.

4.2.4 Force measurements

The force measurements were carried out with a NanoScience atomic force microscope (JPK Instruments AG, Berlin, Germany) in liquid cells. Cantilevers with a spring constant ranging from 0.32 to 0.68 N/m (according to measurement of their thermal fluctuations) were used. Graphite surfaces were freshly cleaved with Scotch® tape prior to each experiment and immediately placed in a liquid cell, which was then filled with the binding buffer or other analyte solutions. The spring constant of each AFM cantilever was calibrated in buffer by the thermal fluctuations method. During the SMFS experiments, the AFM probe was brought into contact with graphite, settled at the surface for 1 s and then pulled away, while the deflection of the

cantilever and its displacement were measured at different locations on the graphite surface. For the detection of adenosine and the selectivity test against uridine, guanosine and cytidine, after filling the liquid cell with the analyte solution, the probe was kept submerged in the cell at a few hundred μm over the graphite surface for 1 h before starting the SMFS measurement. Typical parameters for the force measurements were: (1) Z-length: 0.4 μm; (2) moving speed of AFM probe: 0.5 $\mu m \cdot s^{-1}$; (3) extend time: 0.8 s; (4) delay time on substrate: 1 s. The 1 s delay ensures equilibrium interaction between the aptamer tethered to the AFM probe and the graphite surface.

4.2.5 Sensitivity test

The detection limit was tested by performing a series of SMFS experiments in liquid cells filled with adenosine binding buffer solutions at different concentrations (1 pM, 100 pM, 1 nM, 10 nM, 100 nM, and 1 μM).

4.2.6 Selectivity test

The selectivity of our SMFS-based sensor architecture towards adenosine was verified by performing SMFS successive experiments in uridine, guanosine, cytidine and adenosine solutions (1 μM in binding buffer). All the experiments were conducted under the same conditions.

4.2.7 Statistic analysis of force data

All the data were analyzed with the JPK SPM Data processing software (Version 4.3.11). For the statistical analysis, all data were expressed as means ± standard deviation (SD) for n>50 (n represents the number of data being analyzed). The statistical analysis was conducted with the software Origin 8 (version 8.0724; OriginLab Corp., Northampton, USA, 2007) at a confidence level of 95%.

4.3 Results and discussion

4.3.1 Sensing principle

Figure 4.3 demonstrates the construction and detection principle of our SMFS-based sensing architecture. A 32-mer ssDNA aptamer with the sequence showed in the picture (Figure 4.3a) was tethered onto the AFM probe through a PEG-NHS linker. The effective adenosine binding motif is highlighted in red color. Then the probe was brought into contact with a freshly cleaved HOPG surface. In the absence of adenosine, the ssDNA molecule lays on the graphite surface in a flexible manner and interacts with the graphite surface through the π- π stacking.[54, 55, 98] Upon retraction of the AFM probe, the adsorbed bases of the ssDNA can slide freely on the flat graphite surface, resulting in a steady-state peeling force.[54, 55]

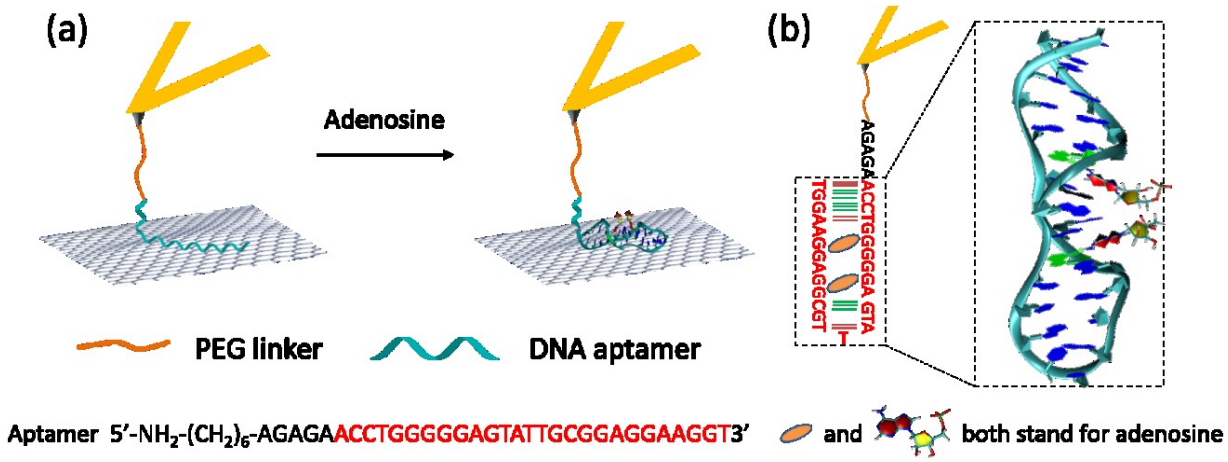

Figure 4.3 (a) Schematic representation of our AFM-based SMFS detection of adenosine, (b) scheme and 3D structure of the adenosine/aptamer complex (PDB ID: 1AW4).[173]

In the presence of adenosine, the aptamer will undergo a conformation transition after formation of a DNA/adenosine complex. Figure 4.3b shows the schematic structure of the aptamer after binding with adenosine. A 3D structure of the binding motif is also reported, based on its determined atomistic structure (PDB-ID: 1AW4).[173] The strength of the interaction between the adenosine-bound, folded aptamer and the graphite surface will differ from that without adenosine. Therefore, different FD curves and desorption forces will be recorded in SMFS experiments in the absence

and presence of adenosine, allowing for detection of adenosine above a certain concentration. The detection limit is set by both the binding kinetics, or, under equilibrium conditions, by the binding affinity of adenosine for its aptamer.

4.3.2 Force changes induced by adenosine

SMFS measurements were then performed between the aptamer-tethered AFM probe and the graphite surface in binding buffer and adenosine solution (1 µM in binding buffer), respectively. Before the SMFS measurement in the presence of adenosine, the AFM probe was kept submerged in the solution (a few hundred µm above the graphite surface) for 1 h to allow enough time for the molecular recognition between aptamer and adenosine to take place. Typical FD curves obtained for both systems under a loading rate of 3.29×10^5 pN·s^{-1} are presented in Figure 4.4a,b, respectively. The approaching traces of both FD curves display a small jump-to-contact force at about 5 nm separation, probably due to the initial contact between the hanging ssDNA strand and the graphite surface.[54] On retraction, an initial large adhesive force is observed in both FD curves, which is associated to the nonspecific adhesive junction between the monolayer coating of the AFM probe and the hydrophobic surface.[54, 55, 98] After the initial pull-off, there is a large drop in force, but a roughly constant force persists with increasing tip-sample separation in both curves. This stable force plateau is interpreted as the progressive desorption of a single ssDNA strand from the graphite surface.[55, 79, 98] Importantly, for long enough PEG linkers and DNA aptamers, the non-specific interaction between probe and surface will not affect the value of the plateau force. In the absence of adenosine, in many cases the length of the plateau is up to the contour length of the fully extended 32-m ssDNA (approximately 18 nm). In some of the curves, the force decreases in characteristic discrete steps (not shown here), which we interpret as resulting from the successive detachment of a small number of ssDNA strands.

To analyze the force data, for each FD curve we measure the magnitude of the plateau steps as the difference between the average force value estimated over a distance of 1 nm just before and after the force jump. Figure 4.4c shows the distribution of the plateau force values before adding adenosine, which is

characterized by a mean desorption force of 117.8 ± 29.5 pN (±SD, *n* = 75). This value increased to 164.3 ± 25.4 pN (*n* = 79) after adding 1 µM adenosine (Figure 4.4e). This ~40% increase of the peeling force is obviously associated to the conformational transition of the aptamer after molecular recognition with adenosine.

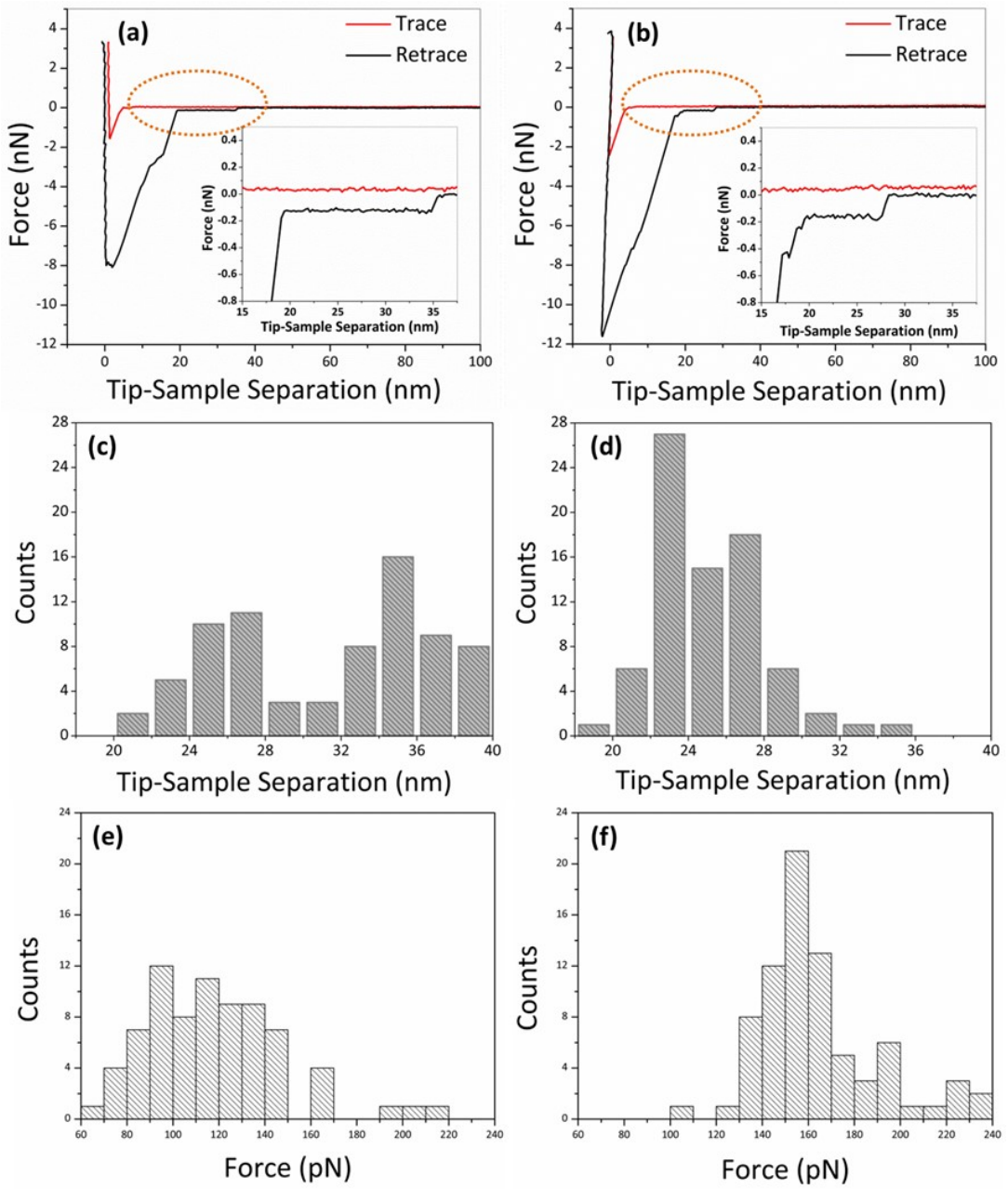

Figure 4.4 SMFS experiments and statistical analysis: (a,b) Typical FD curves by peeling aptamer from graphite surface (a) before and (b) after adding 1 µM adenosine, (c, d) tip-sample separation analysis of the FD curves of (c) before, and (d) after adding 1 µM adenosine. (e, f) corresponding rupture force (e) before, and (f) after adding 1 µM adenosine. After the adding of adenosine, the mean rupture force by peeling aptamer from graphite surface increased from 117.8 ± 29.5 to 164.3 ± 25.4 pN, and the mean tip-sample separation decreased from about 36.1 ± 2.0 to 25.2 ± 3.4 nm.

Besides the force enhancement, also a significant reduction of the tip-sample separation is observed after the addition of adenosine. Namely, in the absence of adenosine the distribution of tip-sample separation presents a first peak centered at about 26 nm and a second, slightly larger peak between 32 and 40 nm with a mean value is 36.1 ± 2.0 nm (Figure 4.4d). The latter corresponds to a plateau length of 14 to 18 nm (*i.e.*, close to the contour length of the ssDNA aptamer). In the presence of adenosine, instead, the distribution of tip-sample separations clusters between 22 and 30 nm, with a mean value of 25.2 ± 3.4 nm (mostly corresponding to a plateau length of less than 12 nm in the obtained FD curves), as shown in Figure 4.4f. The decrease in tip-sample separation confirms the successful binding of the ssDNA aptamer with adenosine molecules, which leads to the formation of a folded, hairpin-like DNA structure and thus to a statistically reduced length of the adsorbed strand.[49, 162, 174]

The interaction force of the complex with graphite surfaces has never been studied before. For the first time, our SMFS finding indicates that the hairpin-folded DNA structure stabilized by adenosine has a stronger interaction with graphite than the pure ssDNA strand. The behavior of the folded aptamer/adenosine complex is thus different from the one of a fully hybridized dsDNA helix structure, which shows a smaller adsorption force on graphite compared to each individual ssDNA strand.[79] We speculate that the intercalated adenosine molecules within the adsorbed strand hinders a smooth base-after-base detachment upon AFM pulling, effectively increasing the cooperativity of binding of several bases to the surface and therefore leading to a statistically increased adhesion force. Notably, the folded structure does not present perfectly matched double-helical folding, which is a strict prerequisite for a decrease of interaction force to graphite. In fact, we have previously observed that even a single base-pair mismatch in a dsDNA oligonucleotide leads to higher adhesion forces, comparable to the ones of ssDNA.

4.3.3 Sensitivity of the adenosine aptasensor

To evaluate the sensitivity of our sensor architecture, different concentrations of

adenosine from one stock solution were added into the liquid cell before performing the SMFS measurements.

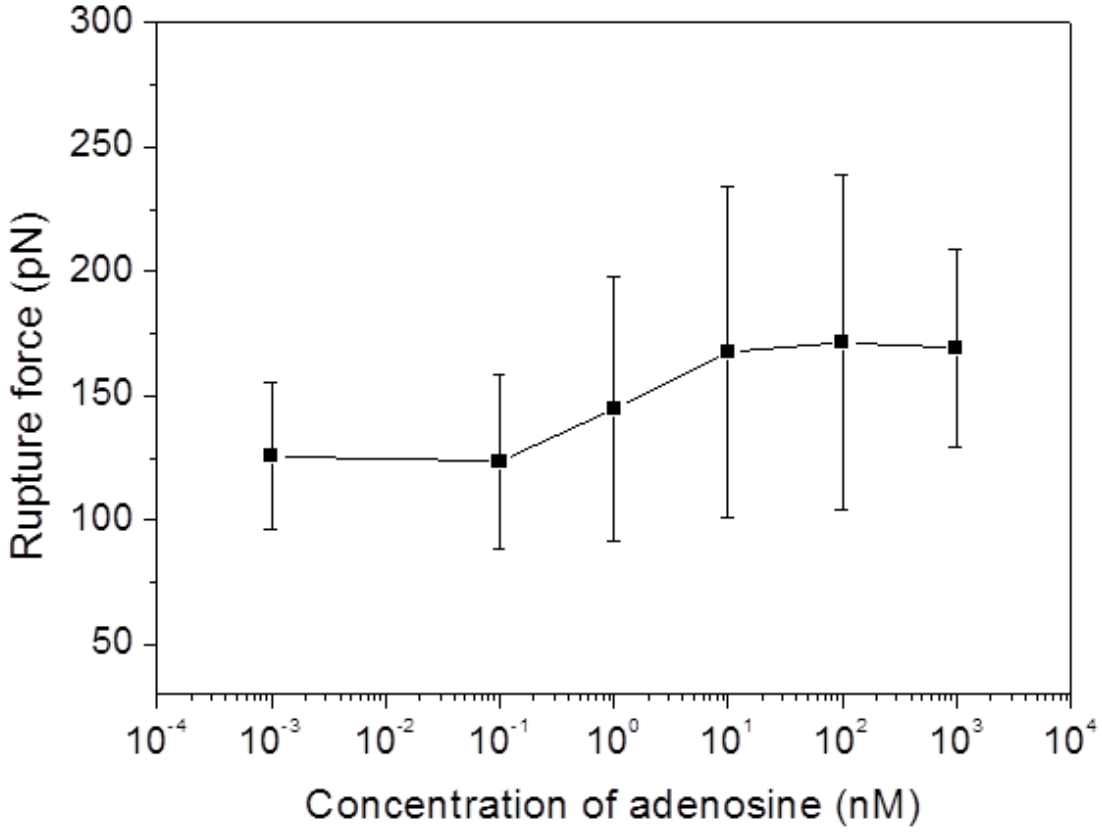

Figure 4.5 Mean desorption forces from SMFS experiments conducted in binding buffer with different concentrations of adenosine (1 pM, 100 pM, 1 nM, 10 nM, 100 nM, and 1 µM).

Figure 4.5 shows the force responses of this SMFS-based sensor to different concentrations of adenosine. It can be seen that at very low adenosine concentration (less than 100 pM) the mean rupture force is around 125 pN (for example, the force is 125.9 ± 29.5 pN in 1 pM adenosine, and 123.3 ± 35.1 pN in 100 pM adenosine), which remains the same level as the rupture force obtained in binding buffer without adenosine (123.9 ± 18.0 pN). After increasing of the adenosine concentration to 1 nM, a first force increase (144.7 ± 52.8 pN) is observed. The further increase of the adenosine concentration to 10 nM caused a further enhancement of the detachment force to 167.5 ± 66.5 pN, after which it remains constant with adenosine concentration at a level around 170 pN. These results confirm the enhancement of the adhesion force between the folded aptamer/adenosine complex and the graphite

surface and suggest a detection limit of our sensor architecture is in the range of 0.1 to 1 nM.

4.3.4 Selectivity of the adenosine aptasensor

To investigate the selectivity of our sensor architecture towards adenosine, we performed additional SMFS measurements after adding to the binding buffer uridine, guanosine, cytidine or adenosine at the same concentration (1 µM).

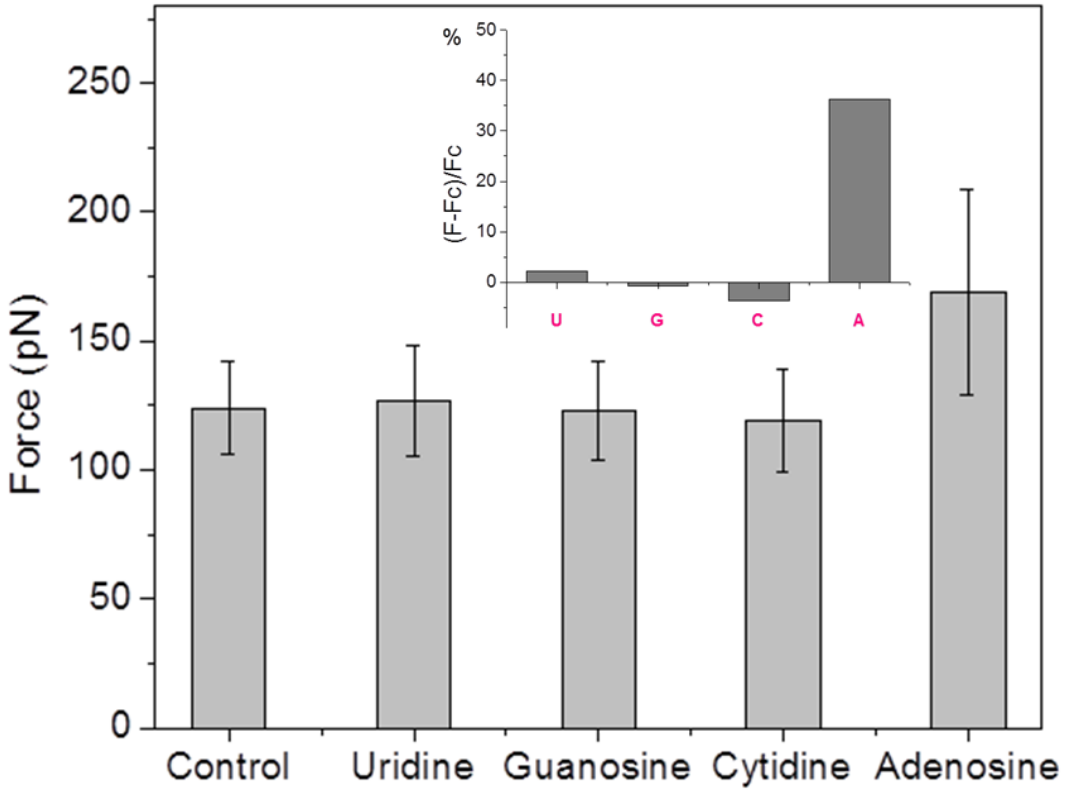

Figure 4.6 Mean desorption force obtained in SMFS measurements performed in pure binding buffer (control), and in the presence of uridine (U), guanosine (G), cytidine (C), or adenosine (A). The inset shows the relative force increase after addition of each analyte to the binding buffer. This experiment was done by Mrs Jingfeng Li.

As before, a SMFS experiment in binding buffer alone was performed as control. All the experiments were conducted at the same condition. Each time after adding the analyte (uridine/guanosine/cytidine/adenosine) to the liquid cell, the AFM probe was kept away from the surface in the bulk solution for 1 h before force measurement, to allow for the aptamer/analyte molecular recognition. The obtained mean desorption forces in the four cases are shown in Figure 4.6.

It can be clearly seen that addition of uridine, guanosine and cytidine does not lead to a change of the desorption force with respect to pure buffer, whereas the adding of adenosine again caused the adsorption forces to increase. The relative force increase $(F-F_c)/F_c$ (here F is the mean desorption force in the presence of analyte and F_c is the control desorption force in pure buffer) is about 36% for the case of adenosine, and negligible for the other nucleosides, as shown in the inset of Figure 4.6.

4.4 Conclusion

In summary, we have demonstrated a novel SMFS-based sensor architecture for highly sensitive and selective detection of adenosine. This sensor takes advantages of the specific molecular recognition between adenosine and an appropriate DNA aptamer, as well as of the intrinsic SMFS sensitivity. We have reached a relatively low adenosine detection limit in the range of 0.1-1 nM and very good selectivity against uridine, guanosine and cytidine. The effect of loading rate and the precise composition of the aqueous solution were also discussed in our published paper (*Biosensors* 2015, **5**, 85-97), both showed negligible effects on the adenosine detection capability. Interestingly, we could show that the folded, hairpin-like structure of the adenosine/aptamer complex has a stronger interaction with graphite than the ssDNA alone. This simple but powerful SMFS-based biosensing technique is very promising for the detection of a wide range of other analytes, since aptamers for numerous molecules have been reported and the methods for discovering new aptamers are also well-established.

5 Mercury ions detection

This chapter aims to introduce single-molecule force spectroscopy methods applied to detect mercury ions, both based on individual force-distance curves and force maps. Parts of this chapter have been published in *Analyst*, 2015, **140**, 5243 (DOI: 10.1039/c5an00708a); other parts of this chapter have been submitted to *Scientific Reports*.

5.1 Introduction

Mercury is one of the most highly toxic and widely spread pollutants in the environment. It originates from natural sources (such as oceanic and volcanic emissions),[175] as well as anthropogenic sources (such as urban and industrial discharges, agricultural materials and mining).[176] Divalent mercury ions (Hg^{2+}), the most stable form of inorganic mercury,[177] can damage the brain, heart, kidneys and nervous system.[178] The maximum allowable level of Hg^{2+} in drinking water ruled by the US Environmental Protection Agency (EPA) is 10 nM (2.0 parts per billion (ppb)). Therefore, it is of high importance to develop effective approaches to detect Hg^{2+} with simple procedures presenting both high sensitivity and high selectivity.

Traditionally, techniques such as cold vapor atomic absorption spectrometry (CVAAS) and inductively coupled plasma mass spectrometry (ICP-MS) have been widely used for the detection of Hg^{2+},[179-183] but these techniques require sophisticated and expensive equipment, which may not be suitable for on-site detection. To overcome this drawback, a number of novel Hg^{2+} biosensors have been developed in the past years. For example, Wegner et al. designed a special fluorescent Hg^{2+} biosensor based on the specific ion binding to MerR proteins.[184] The binding of Hg^{2+} to a labeled MeR/DNA complex causes a distortion of the protein, eventually triggering a fluorescence response. Zhao and co-workers employed a foldable cholate hexapeptide to sense mercury.[185] With the help of fluorescence resonance energy transfer, they found that Hg^{2+} concentrations as low as 20 nM could

be detected. Kim et al. utilized an agglutination assay to detect Hg^{2+}, based on the response of a conjugated polymer on proteins.[186] They found that 20 μM Hg^{2+} could be effectively detected. However, most of these methods have limitations for practical applications, such as complex sample preparation, poor aqueous solubility, or low accuracy.

Recently, a significantly novel method to detect Hg^{2+} by means of oligonucleotides has been introduced.[26, 187] The method is based on the finding by Ono and Togashi that Hg^{2+} can selectively bind between two mutually facing thymine (T) bases to form T-Hg^{2+}-T complexes.[188] These strong complexes can stabilize DNA mismatches in a DNA duplex, and the formed T-Hg^{2+}-T pair is more stable than the Watson-Crick A-T pair.[189] Based on this finding, T-Hg^{2+}-T coordination chemistry has been used for the design of aptamer-based sensors (aptasensors) for the easy and fast detection of Hg^{2+}.[28, 29, 190, 191] A specific ssDNA aptamer forms a hairpin structure in the presence of Hg^{2+}, while it presents a random-coil conformation in the absence of Hg^{2+}. Li et al. developed a colorimetric method using a T-rich DNA aptamer to detect Hg^{2+}.[190] Zhu et al. used an electrochemical method to detect Hg^{2+} by immobilizing another aptamer on Au electrodes to capture free Hg^{2+} in aqueous media, and gold nanoparticles were used to amplify the resulting electrochemical signal.[28] Helwa et al. immobilized a DNA aptamer within a polyacrylamide hydrogel, and detected Hg^{2+} by the visual fluorescence signal produced by adding SYBR Green I.[191] Recently, Zhang and co-workers reported a surface enhanced resonance Raman scattering (SERRS) method for Hg^{2+} detection by using nanoporous gold as a substrate and a Cy5-labeled aptamer as an optical tag.[29] These aptasensor methods are impressive, but most of them require fluorescence labelling, which makes the experiments more complex and expensive. Indeed, many efforts have been carried out to develop label-free methods for detecting small molecules.[79, 192-194]

In this chapter we report a novel highly selective and sensitive aptasensor for detecting low concentrated Hg^{2+} based on SMFS and the formation of T-Hg^{2+}-T complexes. To this aim we have bound an ssDNA aptamer to an AFM probe, and recorded the force-distance (FD) curves between the probe and graphite surfaces in

water solutions with different concentrations of Hg^{2+}, under varying loading rates and ionic strengths. We have found that this SMFS-based aptasensor has a detection limit of approximately 0.1-1 nM and a very high selectivity for Hg^{2+}. To the best of our knowledge, it is the first demonstration of a label-free detection of Hg^{2+} using single-molecule force spectroscopy.

Although the SMFS-based biosensing is very sensitive, it has still problems like time-consumption and existence of subjective statistic error. Usually, hundreds even thousands of force-distance (FD) curves should be obtained and measured to get the mean rupture force within the molecular interactions.[23, 79, 80, 155] Thanks to the development in the AFM-based SMFS techniques, a new function of force mapping has been proposed and utilized to visualize the special molecules or structures on a surface.[195-198] SMFS-based force mapping (SMFM) is constructed by the adhesion force between the tip and substrate measured by point-to-point (16×16 or more) force measurements on the surface,[198] and every point is assigned to a color according to the obtained adhesion force between the tip and this detected point.

It is hypothesized that the addition of a target of small molecules or metallic ions into the system will greatly affect the adhesion force and the color of the obtained force maps due to the specific molecular recognition, and therefore the target can be determinated by the visual distinction of the force maps without and with target recognition. We herein describe a general SMFM technique for the determination of Hg^{2+}. By visualizing the color transition of the obtained force maps, we can compare the change of dark to bright (weak to strong adhesion force), in order to sense mercury ions (Hg^{2+}). In addition, a traditional statistic method is utilized to analyze the obtained FD curves in all force maps and the feasibility of the SMFM-based colorimetric sensing is further identified.

5.2 Experimental section

5.2.1 Reagents and materials

All the ssDNA and ssDNA aptamers were synthesized and provided by IBA GmbH

(Göttingen, Germany). Table 5-1 showed the sequences of mercury ions aptamer. All the aptamers were aliquoted and stored at -20 °C. Non-conductive silicon nitride AFM probes (DNP-S10) coated on the back side with a 45±10 nm thick Ti/Au layer were obtained from Bruker Corporation (France). A highly oriented pyrolytic graphite (HOPG) wafer with ZYB quality (10×10 mm^2) was purchased from NT-MDT Company (Moscow, Russia). Silica wafer (100) coated with highly polycrystalline gold (111) orientation was used as the substrate for the formation of DNA monolayers. Mercury acetate, O-[(N-Succinimidyl)succinyl-aminoethyl]-O'-methylpolyethylene glycol (PEG-NHS), 4,7,10,13,16,19,22,25,32,35,38,41,44,47,50,53-Hexadecaoxa-28,29-dithiahexapentacontanedioic acid di-N-succinimidyl ester (NHS-PEG-NHS), 3-mercapto-1-propanesulfonic sodium (MPS, $HS(CH_2)_3SO_3Na$), (3-Aminopropyl)triethoxysilane (APTES), triethoxy(ethyl)silane (TEES), and phosphate buffered saline (PBS) were purchased from Sigma-Aldrich company (Germany). Aqueous solutions were prepared with ultrapure water after purification with a Mill-Q Integral system (18.0 MΩ).

Table 5-1 Sequences of mercury ions aptamer.

DNA	Sequences
Hg-apta	5'-NH_2-$(CH_2)_6$- TCA TGT TTG TTT GTT GGC CCC CCT TCT TTC TTA -3'
Hg-apta-P1	5'-NH_2-$(CH_2)_6$-TCA TGT TTG TTT GTT GGC C-3'
Hg-apta-P2	5'-SH-$(CH_2)_6$-CCC CTT CTT TCT TA-3'

5.2.2 Functionalization of AFM probes

All silicon nitride AFM probes were cleaned in newly prepared Piranha solution (H_2SO_4: 30% H_2O_2=7:3) for 30 min to remove the organic contaminants on the probes. All AFM probes were washed with large amount of ultrapure water and ethanol (98%) for several times. Then the cleaned probes were functionalized in two procedures. Figure 5.1 shows two procedures for AFM probe functionalization. Generally speaking, the SMFS method followed Procedure 1 (Figure 5.1a), while the SMFM method followed Procedure 2 (Figure 5.1b).

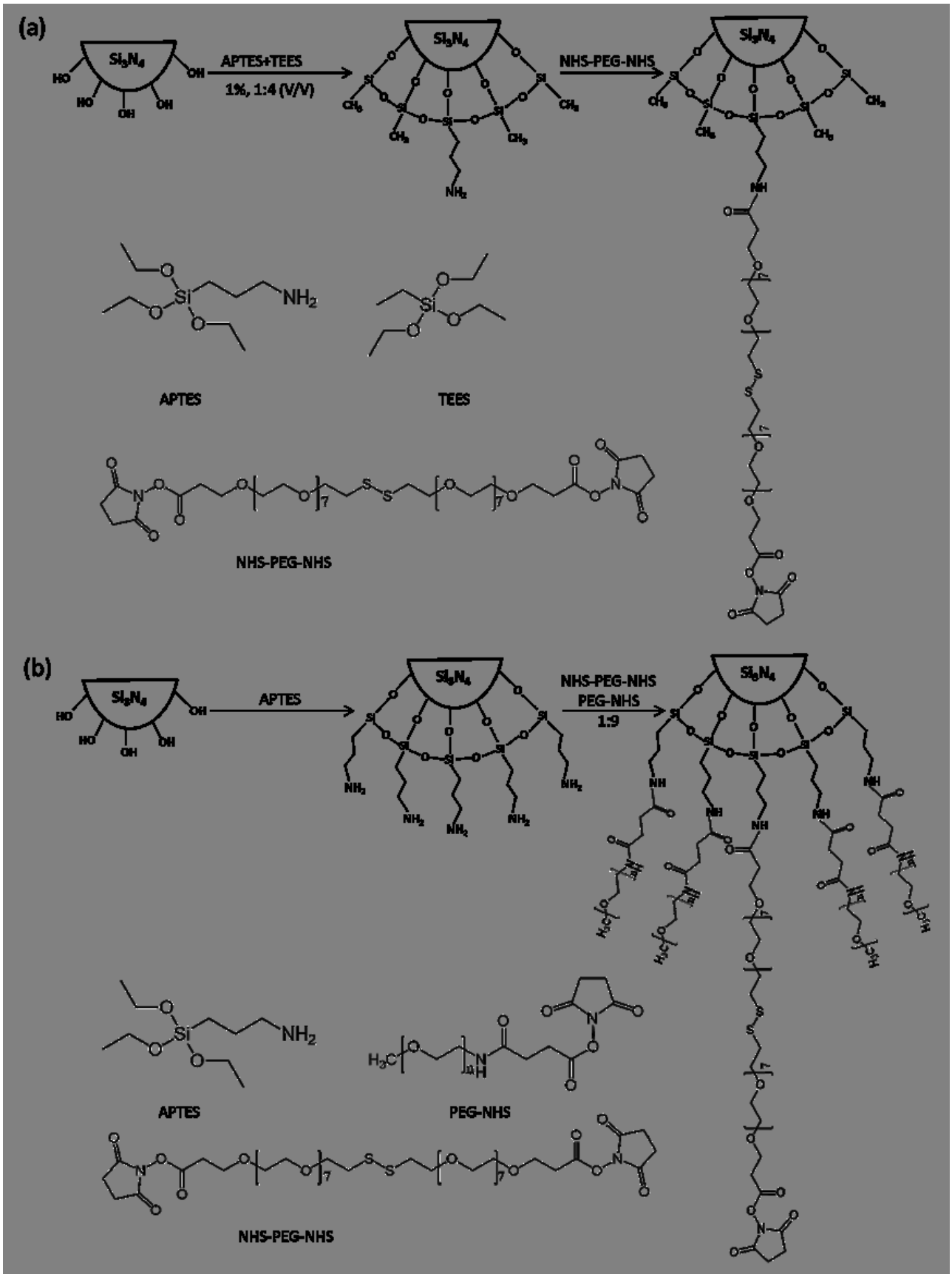
(a)
APTES+TEES
1%, 1:4 (V/V)
NHS-PEG-NHS
APTES
TEES
NHS-PEG-NHS
(b)
APTES
NHS-PEG-NHS
PEG-NHS
1:9
APTES
PEG-NHS
NHS-PEG-NHS

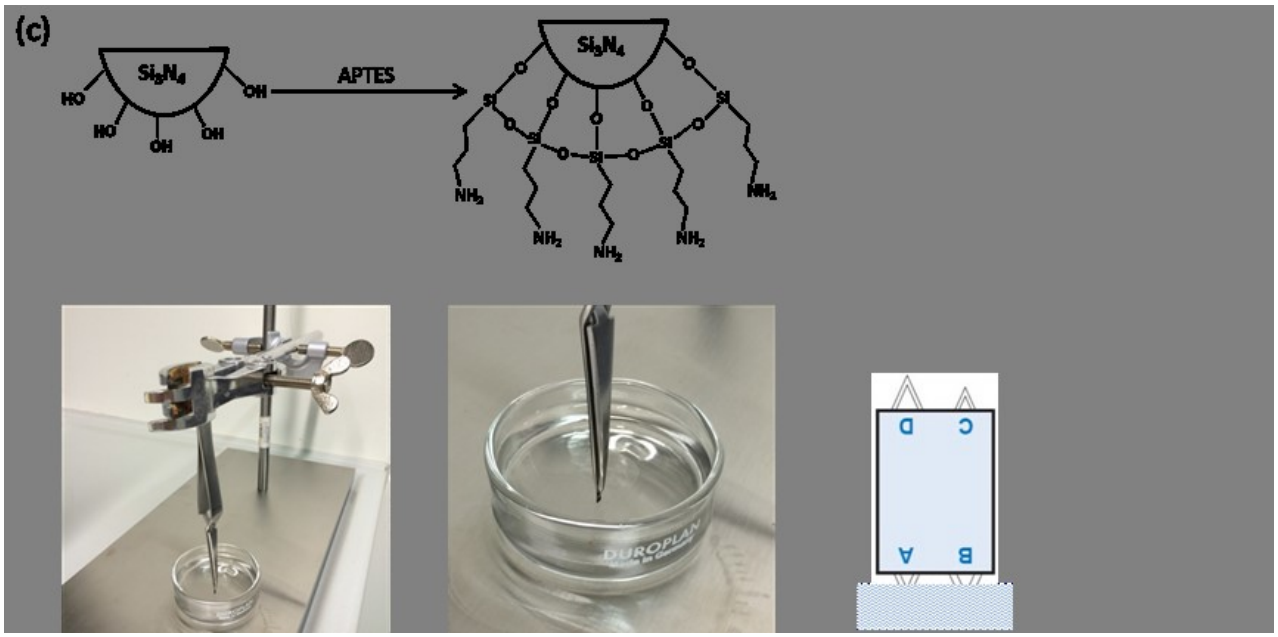

Figure 5.1 (a) Procedure 1 for functionalization of AFM probes; (b) Procedure 2 for functionalization of AFM probes; (c) A special treatment at the step of APTES modification, in which only the cantilever part of the AFM probe was immersed into the APTES solution.

For the SMFS method, the Hg-aptamer was tethered to the AFM probes. For the modification, cleaned probes were immersed into a mixed solution of APTES and TEES (1% in toluene, APTES: TEES, 1:4, v/v) for 15 minutes. After washing with ethanol and ultrapure water for several times, the AFM probes were transferred into NHS-PEG-NHS (0.1 mg/ml) for 1 h to tether the PEG-NHS ester disulfide to the AFM probes by covalent interaction between the NH_2 and NHS groups. Then the probes were washed with ultrapure water and then incubated with ssDNA (100 nM) for 30 minutes to bind the DNA molecules to the probes. Finally, the modified AFM probes were washed with a large amount of ultrapure water to remove non-covalently adsorbed DNA molecules prior to the experiments.

For the SMFM method, the Hg-aptamer-P1 was linked to the AFM probes. For the modification, the cleaned AFM probes (only the cantilever part but not whole probe, Figure 5.1c) were then immersed into APTES solution (5% in toluene) for 30 minutes. After washing with DI water and ethanol, the AFM probes were transferred into a mixed aqueous solution of PEG-NHS and NHS-PEG-NHS (1:9, 0.1 mg/ml) for 1 h to bind the PEG-NHS and NHS-PEG-NHS onto the AFM probe by covalent interaction

between $–NH_2$ and NHS-ester. In the last step, the AFM probes were immersed into Hg-apta-P1 aptamer solution for another 1 h to bind the aptamer onto the probes. The DNA aptamers were connected to the AFM probes through the binding of their terminal $-NH_2$ group with another N-succinimidyl ester of NHS-PEG-NHS linker. Finally, the probes were washed with a large amount of PBS buffer to remove non-covalently adsorbed ssDNA molecules prior to the single-molecule force mapping experiments.

5.2.3 Preparation and characterization of flat graphite surfaces

The preparation of flat graphite surfaces were performed as described in the previous chapter (Section 4.2.2).

5.2.4 Fabrication of self-assembled monolayer of ssDNA on Au surfaces

A gold substrate (1 cm × 1 cm) was cleaned by immersing it into freshly prepared Piranha solution (H_2SO_4:30% H_2O_2, 7:3, v/v) to remove the organic coverings and then washed with larger amount of DI water and ethanol (99%) for several times. The fabrication of a self-assembled monolayer (SAM) of ssDNA on the Au surface was carried out according to the previous report by Nguyen *et al.*[155] A mixed solution of ssDNA and MPS with a molar ratio of 1:20 in PBS buffer (10 mM, pH 7.4) was first prepared, and the concentration of ssDNA and MPS were fixed to 2 and 40 µM, respectively. The cleaned Au substrates were then immersed into this mixed solution and kept at -4 °C for 24 h. This preparation process can not only passivate the uncovered parts of the gold surface to reduce the possibility to get force-distance curves with non-specific binding events, but also provide the suitable space for the DNA hybridization and formation of Hg^{2+}-induced DNA duplex. Finally, the modified Au substrates were thoroughly rinsed with PBS buffer to remove all the unbound molecules from the Au surface.

5.2.5 Force measurements

Cantilevers with a nominal spring constant of 0.35 N m^{-1} were used in the SMFS experiments, which were performed using a NanoScience atomic force microscope (JPK Instruments AG, Berlin, Germany) in liquid cell with the “Force Spectroscopy”

and “Force Mapping” modes. The graphite surface was freshly cleaved with the Scotch® tape prior to each experiment and immediately placed in a fluid cell, which was then filled with water solutions at different concentrations of Hg^{2+}. For the force mapping mode, each data set was comprised of 256 (16 × 16) individual force curves taken over a (2 × 2) μm^2 area. Typical parameters for the SMFS measurements were: (1) Z-length: 0.4 µm, (2) moving speed of the AFM probe: 0.5 µm s^{-1}, (3) extend time: 0.8 s, (4) delay time on the substrate: 1 s. The aim of this 1 s delay is to favor the interaction of the ssDNA attached onto the AFM probe with the flat graphite surfaces. It will take about 20 min to obtain a complete force mapping data set.

SMFM experiments were carried out with the same atomic force microscope in a liquid cell using the “Force Mapping” mode. Cantilevers with spring constant of about 0.32 N/m were calibrated in PBS buffer (10 mM, pH 7.4) at 40 °C before each experiment. Adhesion force maps were recorded on a scan area of 1 µm×1 µm with a resolution of 16 × 16 pixels. The retraction speed was fixed to 0.5 µm/s and a stay time of 1 s was used for all the force mapping experiments. For every sample, at least three scan areas were selected and two force maps were obtained in the same scan area.

5.2.6 Sensitivity test

The sensitivity of the aptasensor was verified by adding different concentrations (1 pM, 10 pM, 100 pM, 1 nM, 10 nM, 50 nM, 100 nM, 500 nM, 1 µM) of Hg^{2+} (obtained upon dilution of the same stock solution) into the liquid cell. The incubation time for each Hg^{2+} concentration was fixed to 20 min for SMFS method, while 1 h for SMFM method.

5.2.7 Selectivity test

To verify the selectivity of the aptasensor for detecting Hg^{2+}, other metal cations such as K^+, Ca^{2+}, Zn^{2+}, Fe^{2+} and Cd^{2+} with the same concentration (1 µM) and also a mixture of all the metal cations were placed in the liquid cell to be tested.

5.2.8 Effect of loading rate

Nominal loading rates r were defined as $r=df/dt=vk_{eff}$, with v being the pulling velocity (from 0.01 to 2 μm/s) and k_{eff} being the effective spring constant of the cantilever, corresponding to loading rates in the range of 3.5×10^3 to 7×10^5 pN s^{-1}.

5.2.9 Effect of the ionic strength

All FD curves were collected in a liquid cell with the same retraction speed of 0.5 μm s^{-1}. The concentration of NaCl in the liquid cell was adjusted to 0, 20, 50, 100 and 150 mM, respectively.

5.2.10 Statistic analysis of force data

All the SMFS data were analyzed with the JPK SPM Data processing software (Version 4.3.11). For the statistical analysis, all data were expressed as means ± standard deviation (SD) for n>80 (n represents the number of data being analyzed). The statistical analysis was conducted with the software Origin 8 (version 8.0724; OriginLab Corp., Northampton, USA, 2007) at a confidence level of 95%.

All the SMFM data were analyzed with the JPK SPM Data Processing software (Version spm-4.3.41). For the statistic of the number of different types of FD curves, a "Filter" function in this software was utilized. For the measurement of unbinding force of the FD curves in all force maps, a self-written AFM force analysis software (afmtool, version 1.1) was used. By this software, the unbinding forces of all the FD curves with specific binding can be easily obtained and transferred to a TXT file.

5.2.11 CV-AFS/AAS test

Cold vapor-atomic fluorescence spectroscopy/atomic adsorption spectroscopy (CV-AFS/AAS) (MLS GmbH, Germany) was used to perform control experiments. The detection limit of this technique is about 10 ng/L. Five samples, MilliQ water, 1 mM Cd^{2+}, 1 pM (0.2 ng/L) Hg^{2+}, 10 pM (20 ng/L) Hg^{2+}, and 10 nM (2000 ng/L) Hg^{2+} were tested. All samples were diluted with MilliQ water. This test and the data analysis were done by Dr. Jens Gröger-Trampe (Landesamt für Bergbau, Energie und Geologie (LBEG)).

5.3 Results and discussion of single-molecule force spectroscopy method

5.3.1 Sensing principle

The strategy for Hg^{2+} detection by our SMFS-based aptasensor is illustrated in Figure 5.2. The idealized cartoon shows the frictionless peeling of an aptamer (ssDNA) conjugated to an AFM probe from a graphite surface. In the absence of Hg^{2+}, the ssDNA molecule lays on the graphite surface as a flexible random-coil, and the adsorbed bases of the ssDNA slide nearly freely on the graphite surface.[55] The interactions between the ssDNA and the graphite surface are mainly of hydrophobic character (including π-stacking and dispersion interactions).[54, 55] When Hg^{2+} is added into the system, a more rigid hairpin-shaped duplex DNA structure will form through formation of T-Hg^{2+}-T complexes and folding of the aptamer.[188, 190, 199] We expect a variation of the average forces required to peel the aptamer off the surface before and after adding Hg^{2+}. These forces can be easily obtained from force-displacement (FD) curves recorded in force-spectroscopy experiments, which are thus employed as a mean of sensing the presence of Hg^{2+}.

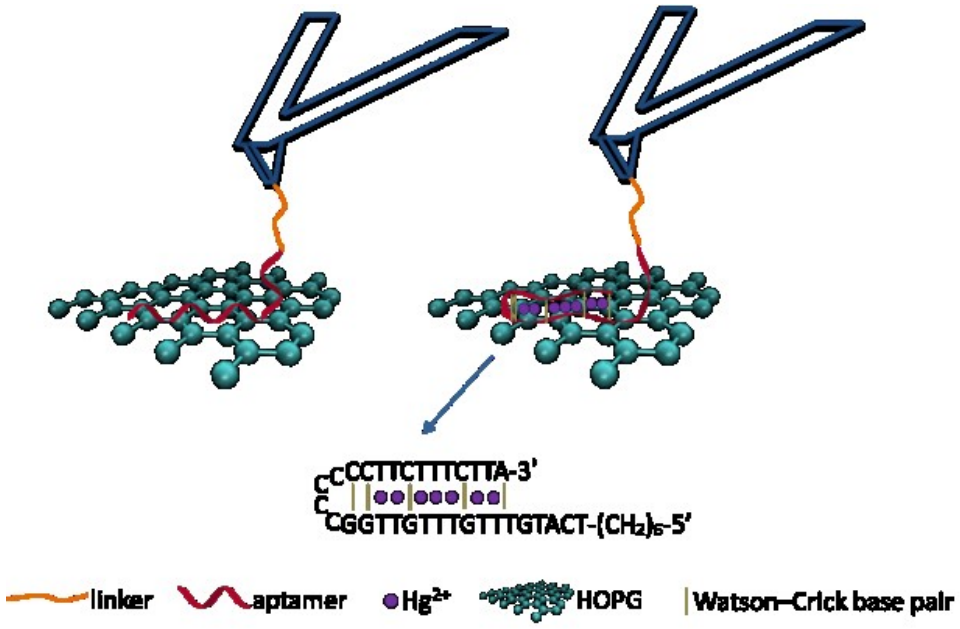

Figure 5.2 Schematic representation of the strategy for Hg^{2+} detection using AFM-based SMFS with an ssDNA aptamer.

5.3.2 Force changes induced by Hg^{2+}

FD curves were then collected peeling the ssDNA aptamer off the prepared flat graphite surface. For each FD curve, we measured the desorption force jumps that corresponded to the complete detachment of one or more molecules from the surface.[28] Two representative FD curves obtained in the absence and in the presence of Hg^{2+} under a loading rate of 1.75×10^5 pN s^{-1} are presented in Figure 5.3. The approaching traces of both curves (Figure 5.3a and c) display a jump-to-contact force at about 6 nm, which agrees with the previous reports.[54, 79] The retraction traces of both FD curves show an initial large and sharp pull-off peak, which is followed by a plateau where the tip-sample separation increases at a roughly constant force. The first large and sharp peak is due to the breaking of the non-specific adhesive junction between the AFM probe's monolayer coating and the hydrophobic surface.[54, 98] The stable plateau force is interpreted as the progressive detachment of the ssDNA aptamer from graphite.[54, 79, 200]

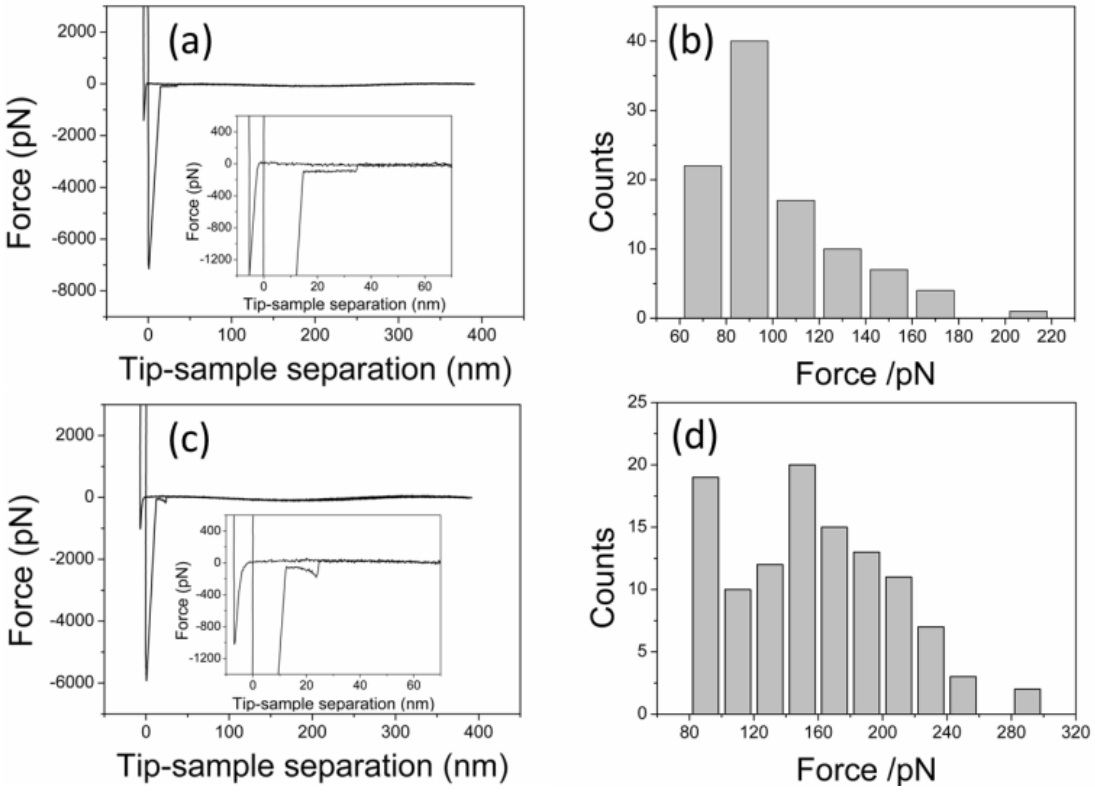

Figure 5.3 Typical FD curves and distribution histograms of the peeling force of aptamer from graphite surface in (a, b) water and (c, d) Hg^{2+} solution (1 μM) with a loading rate of 1.75×10^5 pN s^{-1}. The average force was 99.3 ± 13.4 and 157.7 ± 32.3 pN, respectively.

After analyzing the plateau force jumps, we obtained a mean force of 99.3 ± 13.4 pN (±SD, N=101) before adding Hg^{2+}. This value increased to 157.7 ± 32.3 pN (N=112), i.e. by about 59%, after adding Hg^{2+} at a concentration of 1 µM. Moreover, from the distribution histograms (Figure 5.3b and d), it can be seen that the most probable forces were located around 90 pN in pure water, and around 150 pN when 1 µM Hg^{2+} was present. As we can see from the distribution histograms, the force distributions of our results are relatively broad, which can be explained by the stochastic nature of the unbinding process in the single molecule limit. These broad force distributions are error bars for the force data. We note that, however, that the average forces are well reproducible in different sets of measurements. In addition, we observed a nearly 30% decrease of the tip-sample separation from 36.8 ± 5.8 nm (in water) to 25.9 ± 5.4 nm (in 1 µM Hg^{2+}). We suggest that this decrease can be attributed to the folding of aptamer as a consequence of the formation of duplex T-Hg^{2+}-T complexes.[201]

The behavior of this kind of duplex DNA structure is different from the one of double-strand DNA (dsDNA) reported in our group's previous work.[79] There we found that the adhesion force between dsDNA and graphite is about 40% lower that the adhesion force of corresponding ssDNA sequences.[79] On the contrary, the formation of the mercury-stabilized hairpin results in a clear increase of the adhesion force. This may be due to relatively strong interactions between the Hg^{2+} ions themselves and graphite. In fact, divalent cations are known to form stable intercalates between graphene sheets and may act here as a stabilizing bridge between the surface and the DNA molecule. Alternatively, Hg^{2+} ions may force the basis to detach from the surface in a cooperative manner rather than one-by-one, thus effectively increasing the overall adhesion strength, as also hypothesized in the previous chapter for the case of adenosine sensing.

5.3.3 Sensitivity of the Hg^{2+} aptasensor

To evaluate the sensitivity of our aptasensor, different concentrations of Hg^{2+} from one stock solution were added into the liquid cell before measuring the aptamer/surface FD curves.

Figure 5.4 shows the force and tip-sample separation responses obtained in a wide range of Hg^{2+} concentrations. The mean peeling force remains roughly constant until the Hg^{2+} concentration reaches 0.1 to 1 nM, where the already observed force increase takes place. After that, further increasing of the Hg^{2+} concentration does not have an appreciable effect on the peeling force. Correspondingly, the mean tip-sample separation experiences a decrease from about 35 nm to 25 nm at the same concentration level (0.1-1 nM). When the concentration is higher than 10 nM, the measured force does not change any further, which means that the reaction between aptamer and Hg^{2+} is completed, and a saturated T-Hg^{2+}-T duplex structure is formed at this concentration. This level thus represents the detection limit of our aptasensor, which is compared to that of some previous Hg^{2+} sensors in Table 5-2.

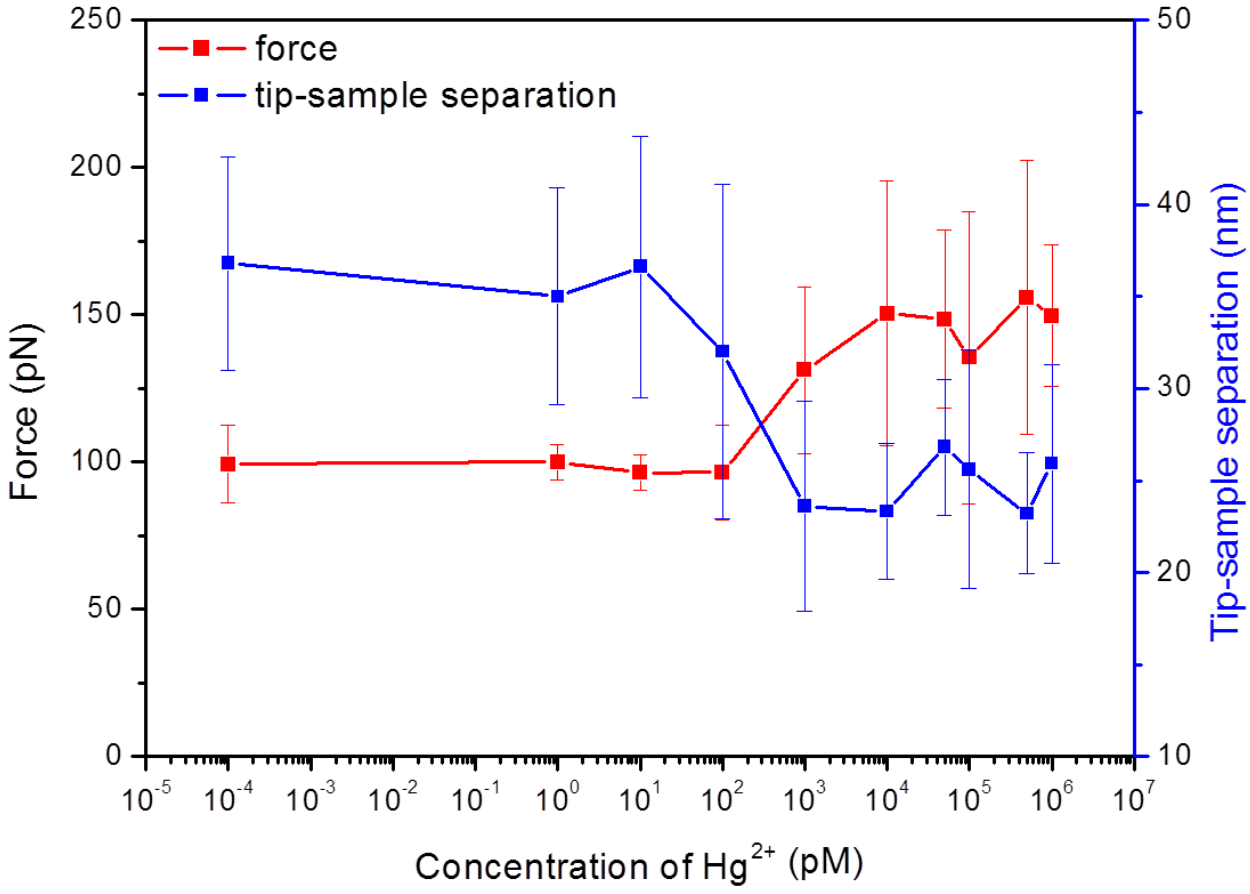

Figure 5.4 Force and tip-sample separation responses of the aptasensor after adding different concentrations of Hg^{2+} with a loading rate of 1.75×10^5 pN s^{-1}. The Hg^{2+} concentration is 0, 1 pM, 10 pM, 100 pM, 1 nM, 10 nM, 50 nM, 100 nM, 500 nM, and 1 µM, respectively.

Table 5-2 Comparison of the detection limit of our Hg^{2+} aptasensor with previously published sensor methods.

Method	Label/Label-free	Detection limit (nM)	Reference
CVAAS	label-free	0.05	179
ICP-MS	label-free	1	180
Colorimetric	label-free	0.6	190
Electrochemistry	label-free	0.5	28
Fluorescence	Label	3.2	199
SERRS	Label	0.001	29
SMFS	label-free	0.1	this work

To identify the advantages of our SMFS-based aptasensor for the detection of Hg^{2+}, five control samples with the control and Hg^{2+} samples with different concentrations were tested by means of CV-AFS/AAS, and the results are shown in Table 5-3.

Table 5-3 Detection of control and Hg^{2+} samples with different concentrations by CV-AFS/AAS. This test was done with the support from Dr Jens Gröger-Trampe (Landesamt für Bergbau, Energie und Geologie (LBEG)).

Sample	Detectable/ Undetectable	Tested value
MilliQ water	Undetectable	<10 ng/L
Cd^{2+} (1 mM)	Undetectable	<10 ng/L
1 pM Hg^{2+} (0.2 ng/L)	Undetectable	<10 ng/L
10 pM Hg^{2+} (20 ng/L)	Undetectable	<10 ng/L
10 nM Hg^{2+} (2000 ng/L)	Detectable	1407 ± 15.2 ng/L

It can be found that the Hg^{2+} concentration in the sample of MilliQ water, Cd^{2+} (1 mM), Hg^{2+} (0.2 ng/L), and Hg^{2+} (20 ng/L) is undetectable, while the Hg^{2+} concentration in the sample of Hg^{2+} (2000 ng/L) was measured to be 1407 ± 15.2 ng/L. It is clear that the measured concentration is smaller than the nominal concentration. This can be explained by the dilution process. Normally the CV-AFS/AAS test of Hg^{2+} should be done in a 1% nitric acid (HNO_3) solution because Hg^{2+} is only stable at low pH, while it becomes unstable and form hydroxide species

such as $HgOH^+$ or $Hg(OH)_2$ when pH value increases. In our system, the experiments are performed in pure water, therefore the test concentrations of Hg^{2+} are slightly smaller than expected.

We interpret the above results according to the following interaction mechanism between the ssDNA aptamer and Hg^{2+} (Figure 5.5). At very low concentration the amount of Hg^{2+} ions is not enough to form stable T-Hg^{2+}-T complexes (Step I). Only when the concentration of mercury reaches the value required to shift the binding equilibrium towards the formation of a saturated DNA·7Hg^{2+} complex (0.1-1 nM) does the formation of a folded hairpin structure take place (Steps II to III). Notably, the here individuated affinity constant of about $5 \cdot 10^9$ M^{-1} is much higher than the affinity constant of single T-Hg^{2+}-T complexes (about $5 \cdot 10^6$ M^{-1}),[202] suggesting a large degree of binding cooperativity in the formation of the hairpin. In fact, cooperative binding has been already suggested for the binding of Hg^{2+} to two consecutive T:T mismatched base pairs in dsDNA.[203] After saturation of the hairpin with 7 cations, further increase of the Hg^{2+} concentration has no significant effect on the measured forces (Step IV). The results reported in Figure 5.4 indicate that the tip-sample separation begins to decrease slightly before the increase of the adhesion force, suggesting a gradual folding of the aptamer before completion of the hairpin, as presented in Figure 5.5.

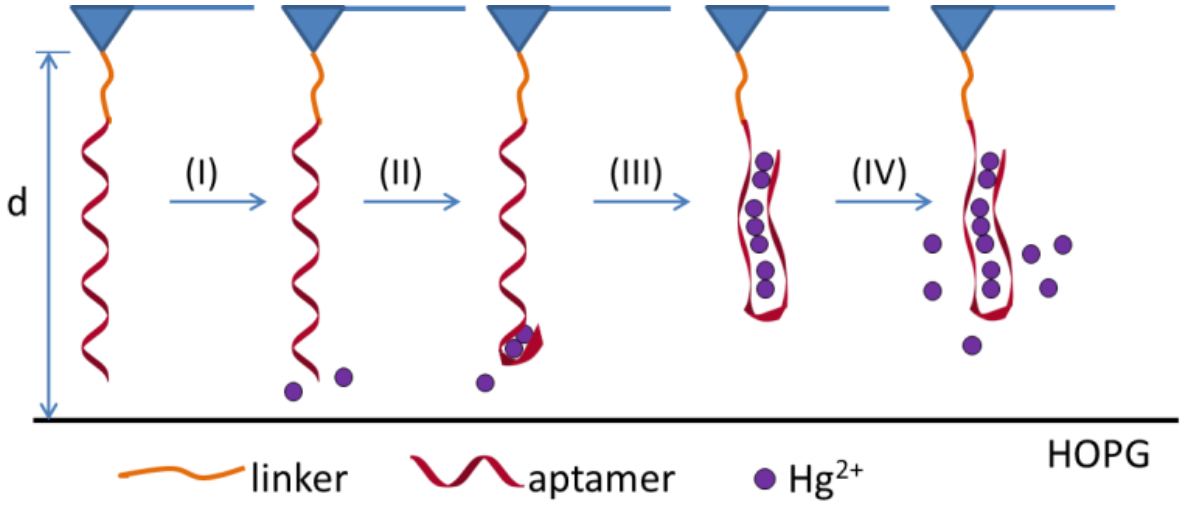

Figure 5.5 Schematic illustration of force and distance change after adding different concentrations of Hg^{2+}.

5.3.4 Selectivity of the Hg^{2+} aptasensor

In order to prove the unique selectivity of our SMFS-based aptasensor for Hg^{2+}, other cations (K^+, Ca^{2+}, Zn^{2+}, Fe^{2+}, Cd^{2+}) and also a mixture of all cations (including Hg^{2+}) were added into the liquid cell at the same concentration (1 µM) and the FD curves were recorded with the same experimental conditions. Defining F as the mean peeling force measured in the presence of a certain cation and F_0 the mean peeling force in pure water, the selectivity can be quantified by the ratio $(F-F_0)/F_0$.

As shown in Figure 5.6, the largest change was observed in the presence of Hg^{2+} and the mixture, while statistically negligible changes corresponded to all other metal cations. An exception may be Cd^{2+} (about 10% of force increase), which is in agreement with previous reports that Cd^{2+} may have some affinity for Hg^{2+} aptamers.[27, 204] However, the high selectivity for Hg^{2+} detection due to the formation of T-Hg^{2+}-T complexes is obvious from this comparative analysis.

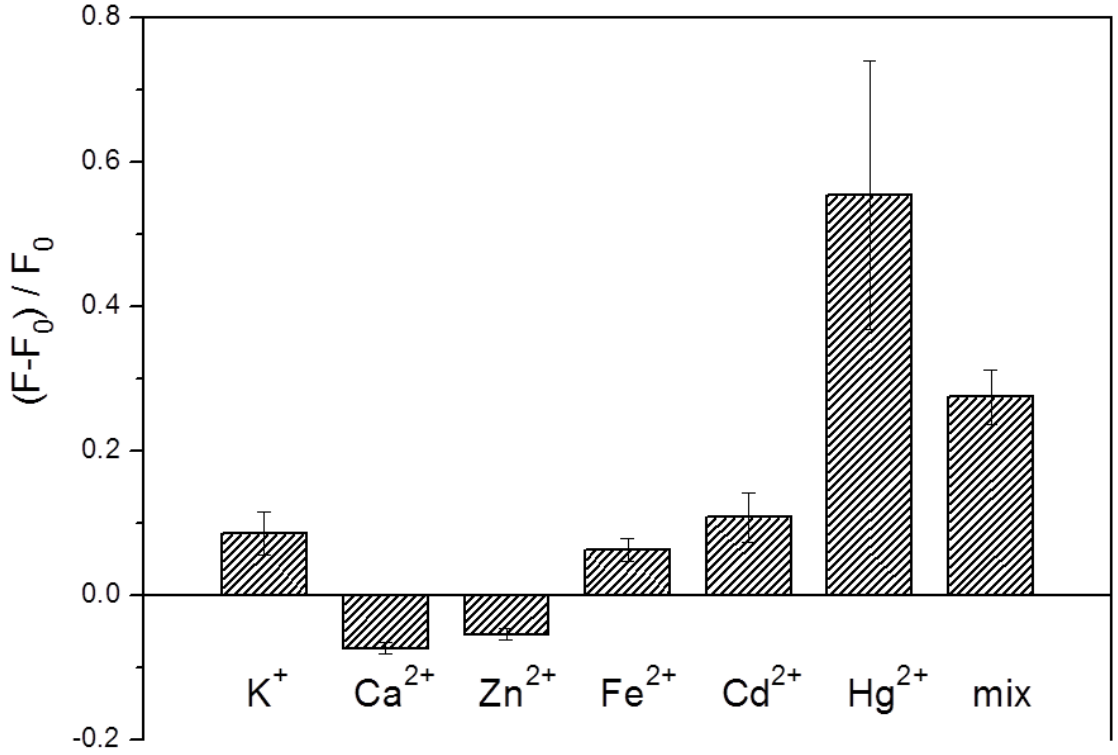

Figure 5.6 Selectivity of the aptasensor for Hg^{2+}. All competing metallic cations were tested at 1 µM and under a loading rate of 1.75×10^5 pN s^{-1}.

5.3.5 Effect of the loading rate

To further explore the physical insight of the interactions between the aptamer molecules and graphite, dynamic force spectroscopy (DFS) was used to measure the adhesion force as a function of the loading rate. According to the classic Bell-Evans model,[205, 206] the measured rupture forces depend on the utilized loading rate for the peeling experiment. Previous studies indicate that the peeling force depend logarithmically on the applied loading rate.[52, 119] The most probable rupture force is:

$$F(r_f) = \frac{k_B T}{x_\beta} \ln r_f + \frac{k_B T}{x_\beta} \ln\left(\frac{x_\beta}{k_B T} \frac{1}{k_{off\,(0)}}\right)$$

where $k_B T$ is the thermal energy, x_β is the distance between the bound and the transition state along the direction of applied force (the width of the energy barrier), $k_{off\,(0)}$ is the dissociation off-rate at zero force, and r_f is the loading rate.

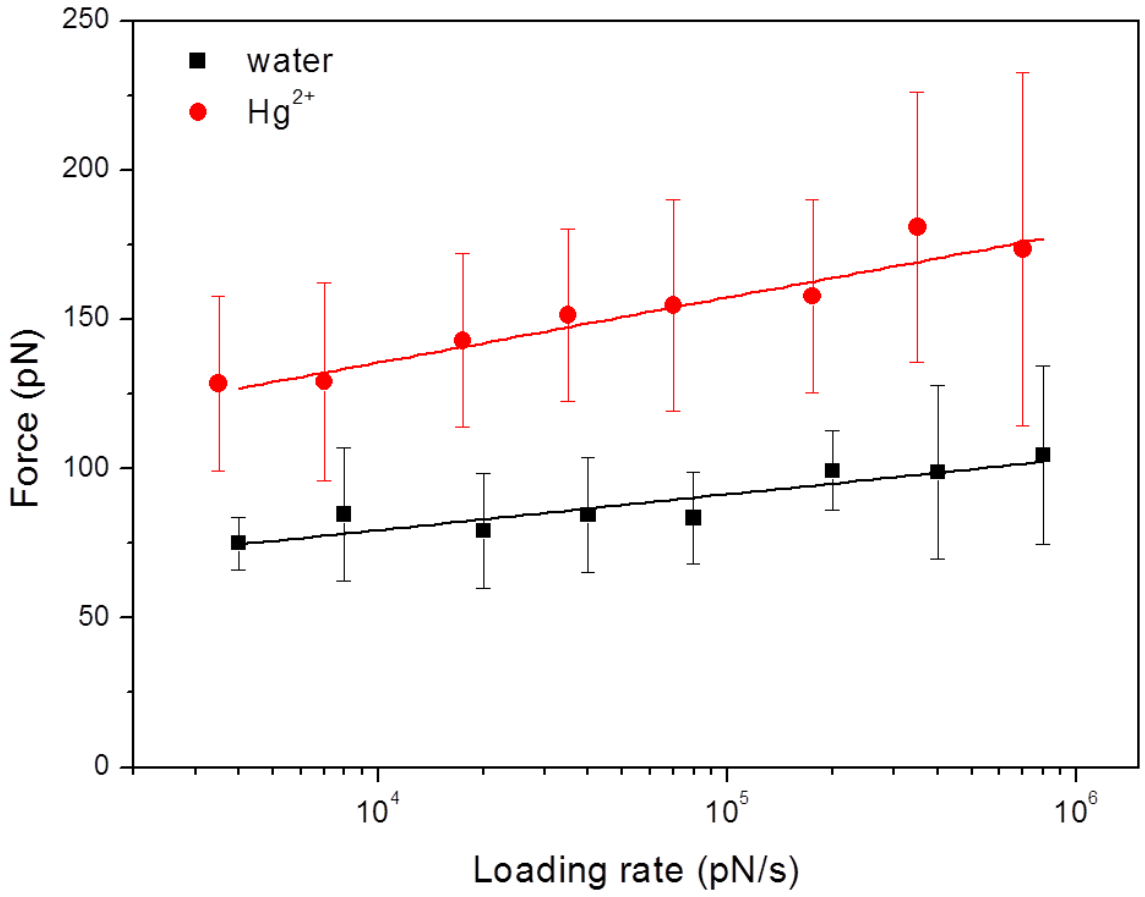

Figure 5.7 The effect of loading rate on the peeling force between the aptamer and graphite in water and 1 μM Hg^{2+}, respectively.

Figure 5.7 shows the dynamic force measurements of the peeling force of aptamer in water and in 1 μM Hg^{2+} solution with different loading rates. In both cases, the mean peeling force increases linearly with the logarithm of the loading with slopes of 11.9 pN and 21.8 pN, respectively. According to the report by Landoulsi *et al.*, the slope represents the ratio between the thermal energy k_BT (~4.1 pN nm at room temperature) to the projected bond displacement, x_β, along the direction of applied force.[119] Correspondingly, x_β amounts to 3.4 Å in pure water and 1.9 Å in Hg^{2+} solution, respectively. These values of x_β are typical of biomolecular systems.[81, 207] The decreased value of x_β after addition of Hg^{2+} implies a decrease of the width of the energy barrier required to detach the folded hairpin from the surface. This corroborates the previously introduced idea that the ions impede a smooth and progressive detachment of single basis (thus also leading to reduced tip-sample separation values) and steepen the barrier for surface desorption. The kinetic off-rate constant of dissociation at zero force is $k_{off(0)} = r_{F=0}x_\beta/k_BT$. In our cases, the $r_{F=0}$ values were estimated to be 0.0024 and 0.006 pN s^{-1}, in the absence and presence of mercury, corresponding to $k_{off(0)}$ values of about 2×10^{-4} and 3×10^{-4} s^{-1} in the two respective cases. Notably, the sensing effect (force increase after addition of Hg^{2+} ions) is clearly evident at all considered loading rates.

5.3.6 Effect of the ionic strength

In this section we present the results concerning the effect of NaCl concentration on the measured peeling forces in the absence and presence of Hg^{2+} (Figure 5.8). The results indicate that the peeling forces are independent on the salt concentration for both cases. In the absence of Hg^{2+}, the peeling forces are at the same level (about 100 pN), which is expected due to the mostly non-polar nature of the DNA/graphite interaction, as mentioned above and pointed out previously by other authors.[54] After adding Hg^{2+} into the system, the peeling force increases but still remains at the same level (about 150 pN), which means that the salt concentration has no significant effect on the Hg^{2+} detection in this system. This finding is similar to the salt effect

observed in the case of adenosine sensing in our published paper.[156]

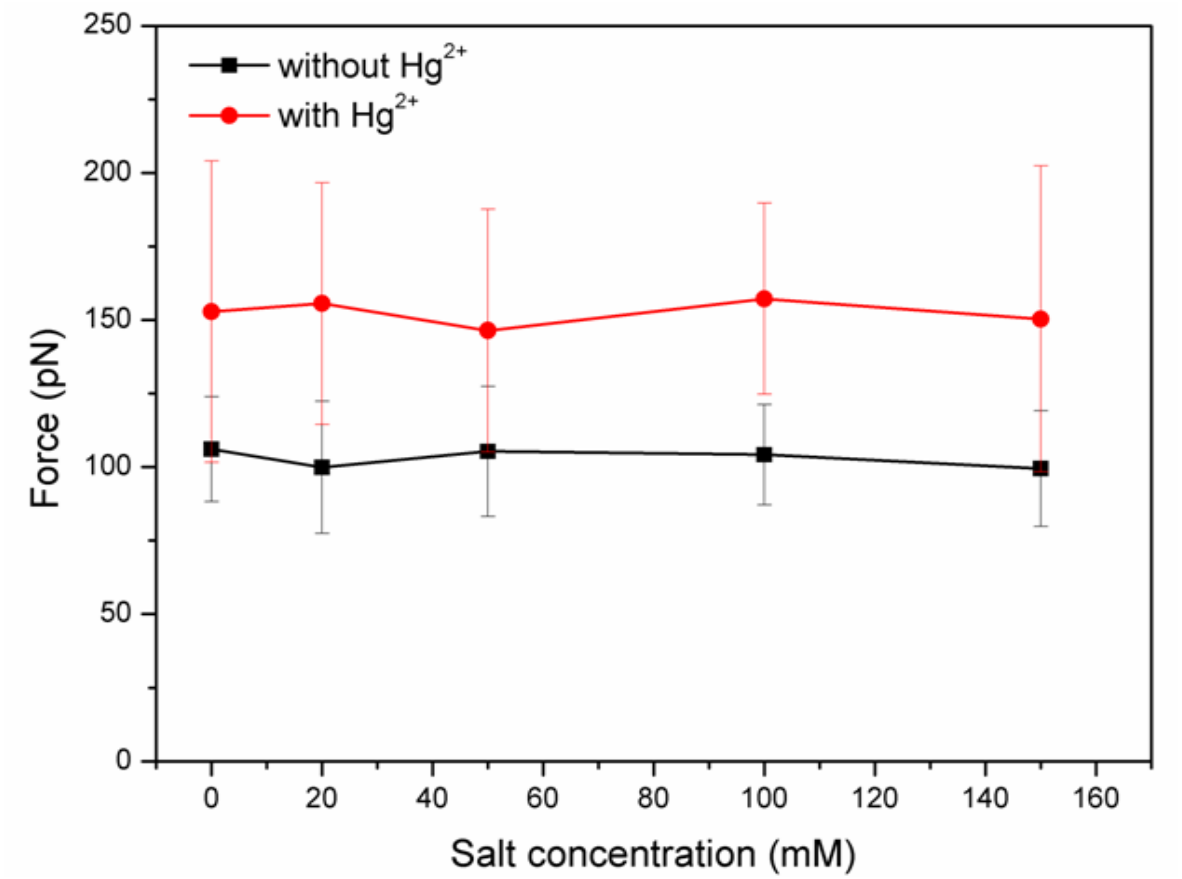

Figure 5.8 The effect of salt concentrations on the peeling force between the aptamer and graphite in water and Hg^{2+} solution with a loading rate of 1.75×10^{5} pN s^{-1}.

5.3.7 Effect of the incubation time

To investigate the effect of the incubation time on the detection of Hg^{2+}, the functionalized probes were incubated for shorter (2 min) and longer (60 min) times than in the standard protocol (20 min). Figure 5.9 shows the force changes vs. different Hg^{2+} concentrations with different incubation periods. While no appreciable force variation takes place after 2 min of incubation up to 10 nM, after 60 min of incubation again a force increase becomes detectable in the concentration range of 10 to 1000 pM. This is of the same order of magnitude or even smaller than after 20 minutes of incubation. Therefore, we conclude that at least 20 minutes of incubation are necessary to reach the equilibrium and form saturated DNA·7Hg^{2+} complexes. This "sensing response" is as quick as the one of similar systems in previous reports.[190, 208]

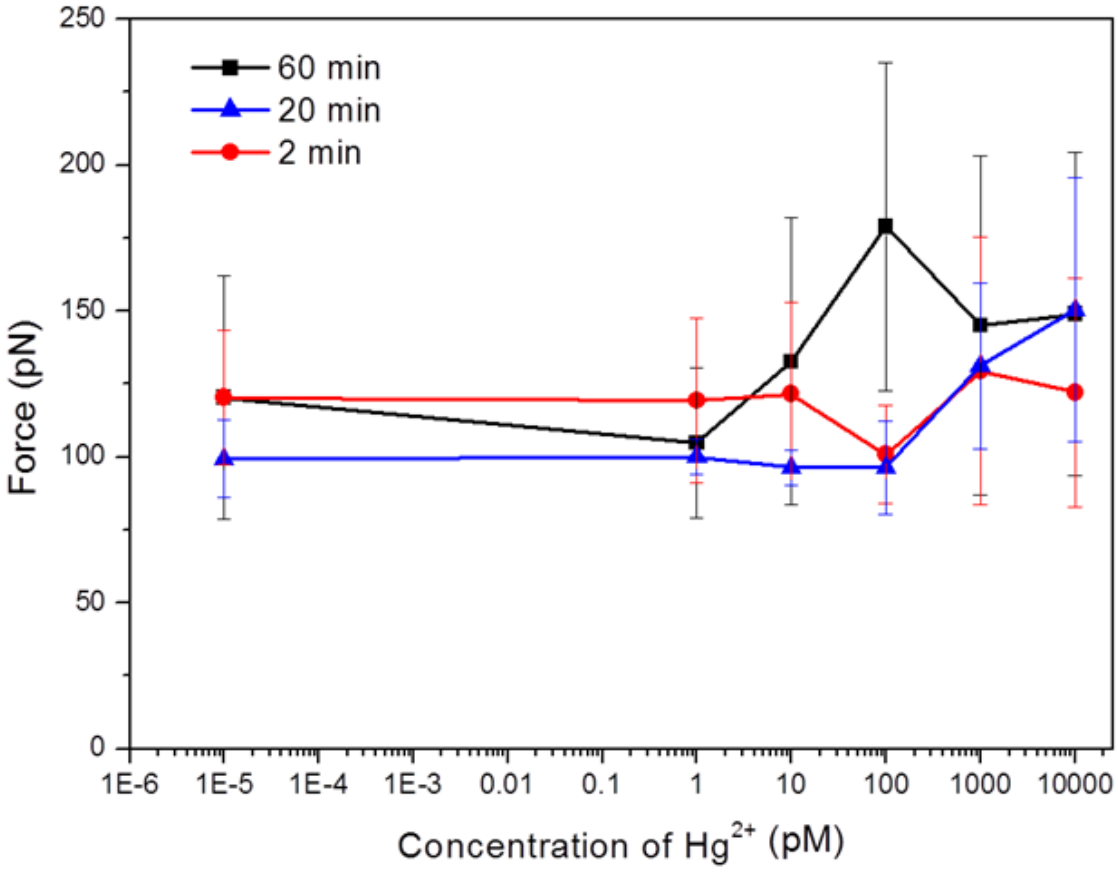

Figure 5.9 The effect of incubation time on the peeling force between the aptamer and graphite in different concentrations of Hg^{2+} solution with a loading rate of 1.75×10^{5} pN s^{-1}.

It should be noted that the total detection time (a few hours) of this label-free aptasensor is much longer than the previously reported labeled methods like fluorescence, electrochemistry, and SERRS.[18-22] Usually, the whole measurement using SMFS for single detection (256 curves) will take about 40 min. After obtaining the data, it will take a few hours to analyze the FD curves and measure the average desorption force. It is expected the automatic data analysis software will reduce the total detection time greatly in the future.

5.4 Results and discussion of single-molecule force mapping method

5.4.1 Sensing principle

Another method based on single-molecule force spectroscopy was also developed to detect mercury ions. In this single-molecule force mapping (SMFM) method, both

tip and substrate need to be modified, with the aim to eliminating non-specific forces.

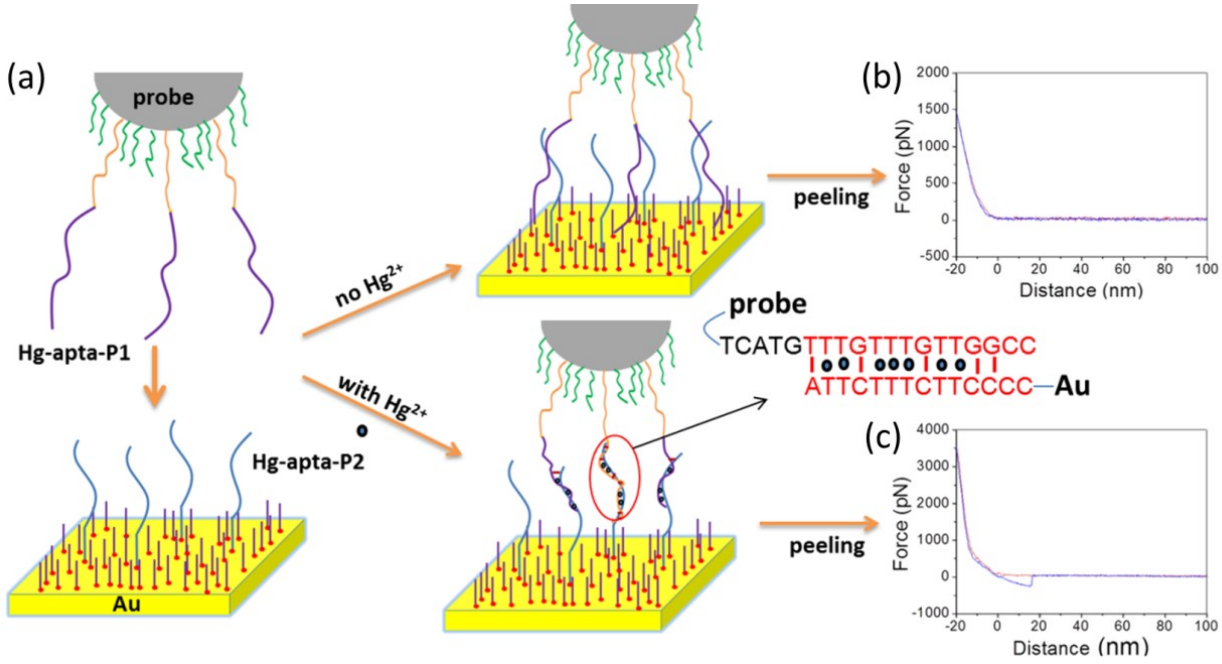

Figure 5.10 Colorimetric determination of Hg^{2+}: (a) Schematic illustration of the detection of Hg^{2+} with SMFM technique; (b) a typical FD curve before adding Hg^{2+} to interact with aptamer; (c) FD curve after adding Hg^{2+}.

The SMFM-based sensor architecture for the detection of Hg^{2+} by visual inspection of force maps from dark to bright is shown schematically in Figure 5.10a. This idea was inspired from previous studies for fabricating Hg^{2+} sensors using the thymine-Hg^{2+}-thymine (T-Hg^{2+}-T) coordination chemistry.[157, 188, 199] Here, we cut the Hg^{2+} aptamer to two fragments, Hg-apta-P1 and Hg-apta-P2, and utilized the Hg-apta-P1 to modify the AFM tip and Hg-apta-P2 to create a SAM on the gold surface. It is assumed that there is no specific binding between the Hg-apta-P1 and Hg-apta-P2 sequences when Hg^{2+} ions are absent (Figure 5.10b), while there are obvious unbinding events when Hg^{2+} ions are present (Figure 5.10c).

5.4.2 Sensitivity test

To test the Hg^{2+} sensitivity of the sensor, we carried out the SMFM experiments by adding Hg^{2+} ions with different concentrations, and the corresponding force maps are shown in Figure 5.11.

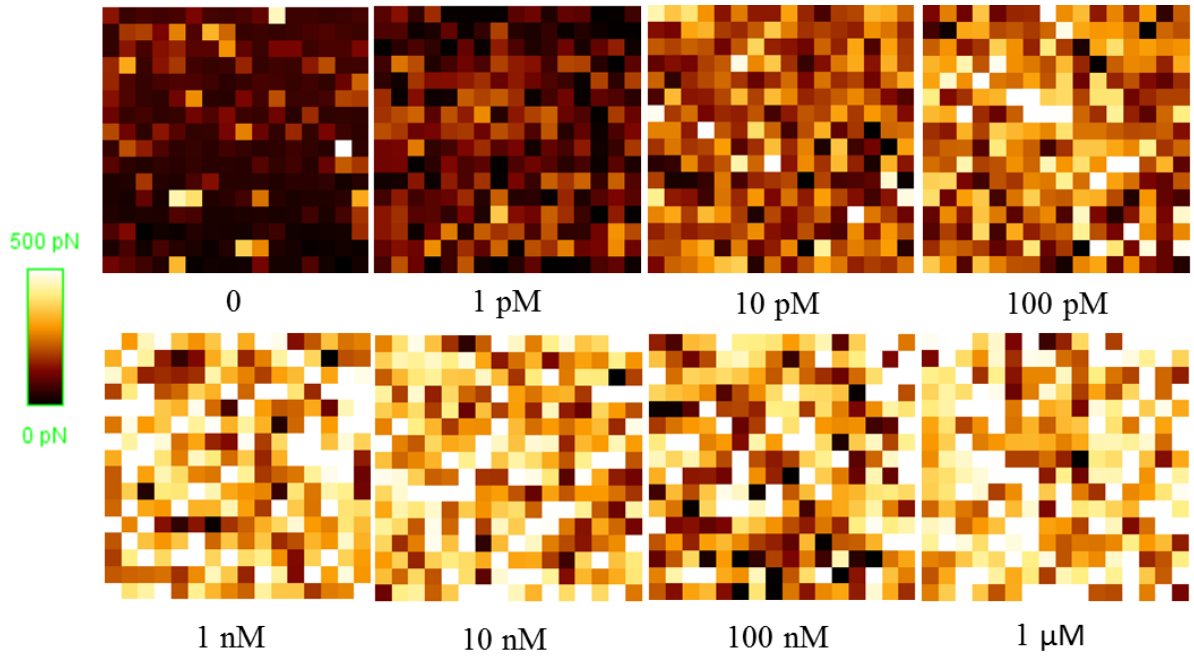

Figure 5.11 SMFM images with different concentrations of Hg^{2+}.

For the control experiment without Hg^{2+}, the force map is dark with few orange points, indicating that in this case the probability to form specific binding is very low and the obtained unbinding forces are weak. The addition of Hg^{2+} induce a structure-switching in the sensor architecture, and the gradual color transition from dark to bright can be seen by the naked eye. When the concentration of Hg^{2+} is larger than 100 pM, further color changes cannot be easily distinguished, indicating that the folded structure of DNA molecules is stable at this concentration of Hg^{2+}.

5.4.3 Analysis of force-distance curves

The statistical analyse of three types of binding events, specific binding, no binding, and non-specific binding are shown in Figure 5.12.

As we can see from the curves, there are several binding events in the individual force-distance curves. Some of the curves have single-binding or double binding events (Figure 5.12a and b), meaning that there are specific binding between the tip and substrate. In the corresponding force maps, the color will be bright depending on the value of the force. Other curves have no binding events or non-specific forces (Figure 5.12d and e). In this case there are no specific interactions between the tip

and substrate, and the corresponding force maps will be dark. All curves in which non-specific binding will affect the specific binding events (Figure 5.12f) are excluded from the results.

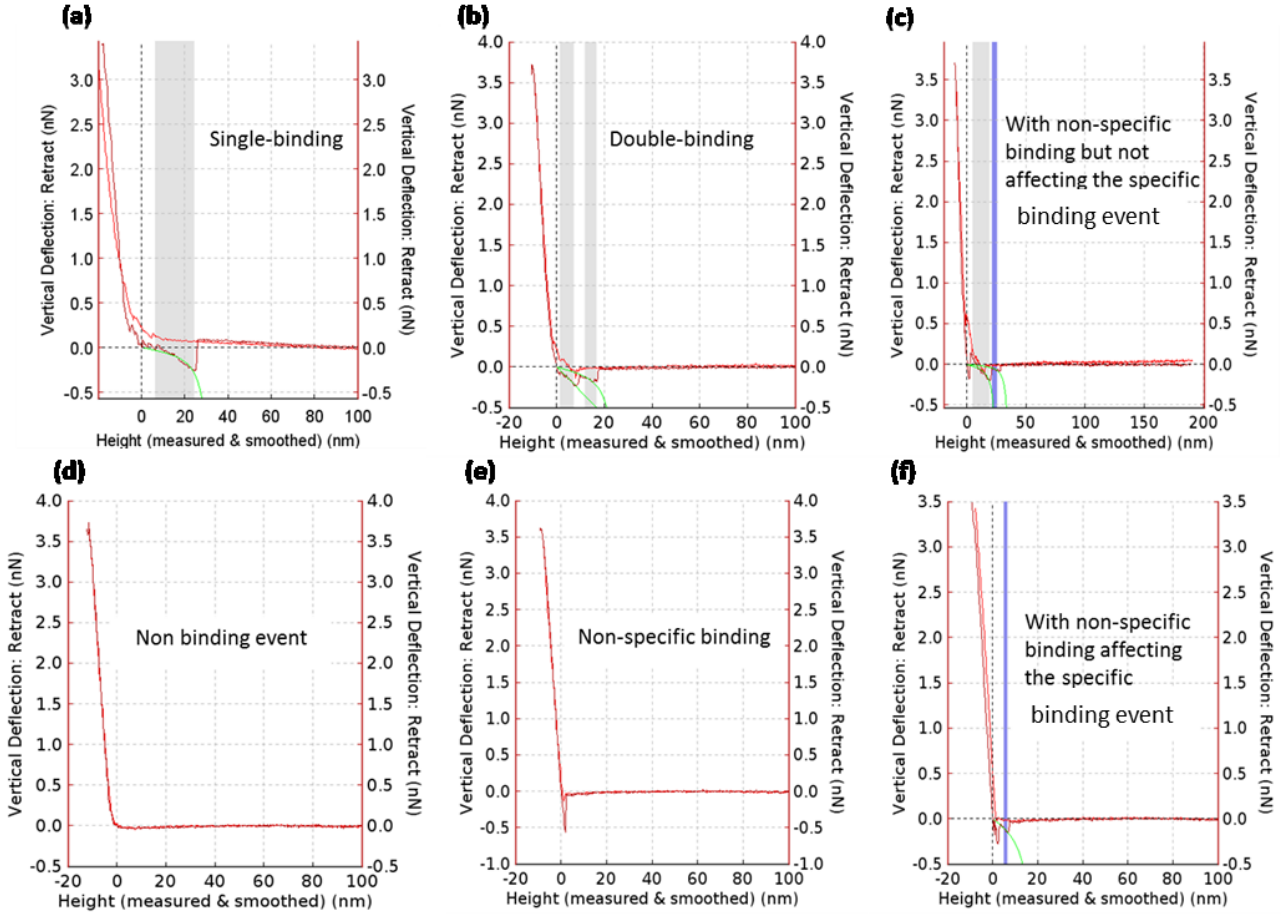

Figure 5.12 Real FD curves of different binding events for detecting Hg^{2+}: (a-c) specific binding, (d) no binding, and (e, f) non-specific binding. It should be noted that the non-specific binding event in FD curve (c) did not affect the specific binding event, and therefore can be counted to as specific binding, but curve (f) is not in this case.

Figure 5.13 shows that the addition of 1 pM Hg^{2+} increases the frequency of specific binding (from 13% to 53%) and decreases that of no binding events (from 76% to 39%) significantly. By increasing the Hg^{2+} concentration to 10 pM, the frequency of specific binding increases further to 68% ± 13% and the frequency of no binding decreases to 21% ± 9%. The further increasing of Hg^{2+} concentration did not change the frequencies of the binding events.

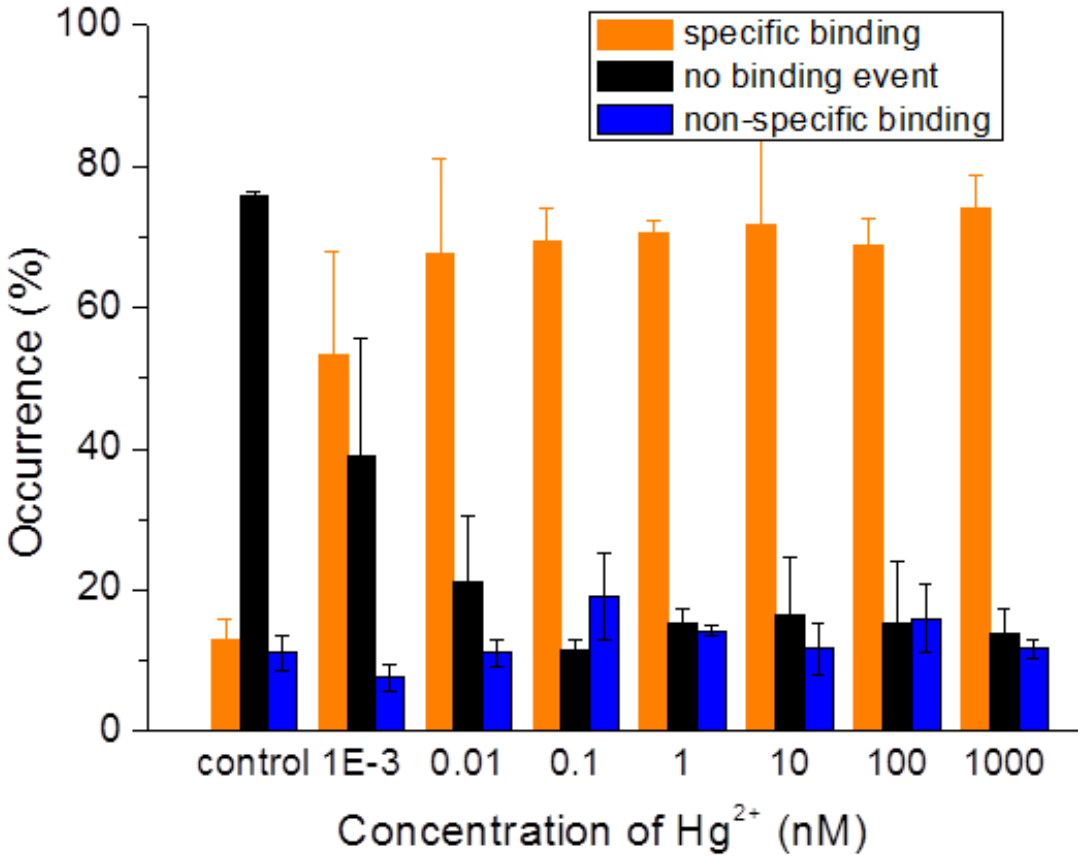

Figure 5.13 Statistic analysis of the frequency (%) of FD curves with specific binding (orange), no binding event (black), and non-specific binding (blue) in about 1000 curves.

The statistical analysis of unbinding forces from all the effective data reveals the same tendency as the frequency of binding events, as shown in Figure 5.14. In the control experiment the unbinding force is 125 ± 38 pN, which is ascribed to the ionic effects of buffer. The addition of 1 and 10 pM Hg^{2+} causes the increased unbinding forces of 146 ± 45 and 233 ± 77 pN, respectively. When the addition of Hg^{2+} is more than 0.1 nM, stable forces are observed, and the force for breaking the stable switched DNA structure is about 250 pN. In summary this statistical analysis of binding frequencies and unbinding forces with specific binding agrees well with the SMFM experiments. Based on the above results, a detection limit of about 10 pM is achieved.

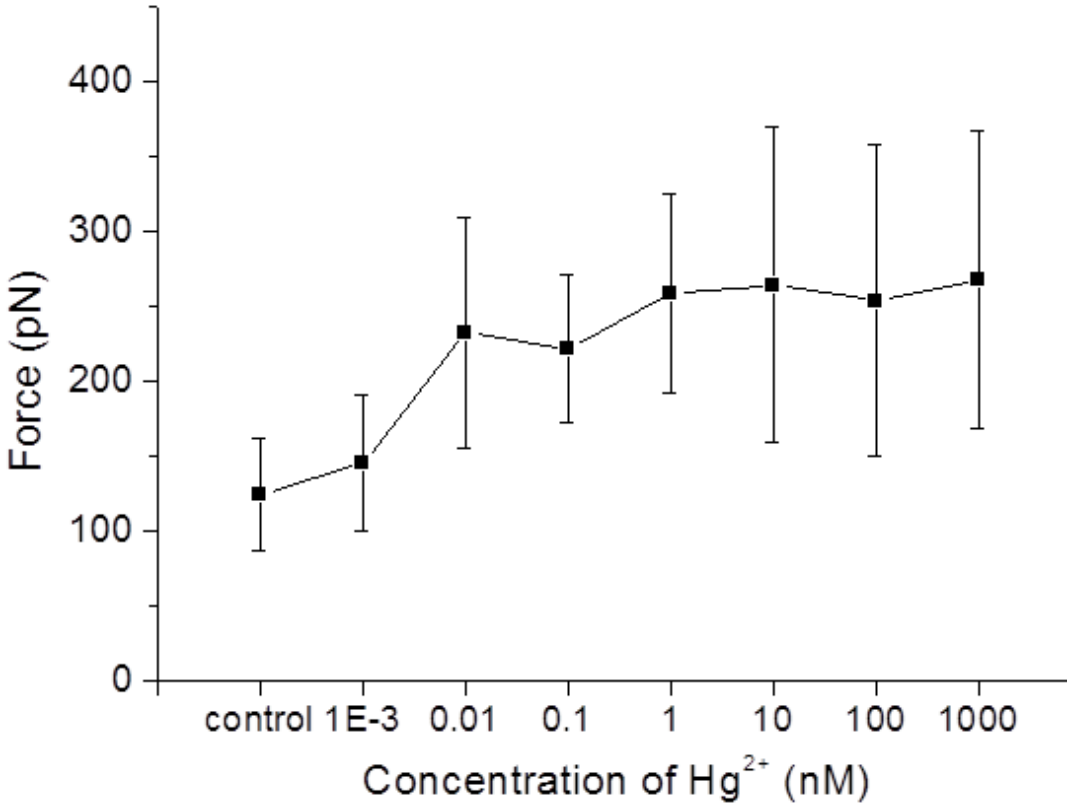

Figure 5.14 Statistic analysis of the rupture force (pN) of the FD curves with specific binding vs. concentration of Hg^{2+}.

5.4.4 Selectivity test

To determine the selectivity of this Hg^{2+} sensor architecture, 1 μM of other metallic ions (Ca^{2+}, Fe^{2+}, K^{+}, Cd^{2+}, Zn^{2+}, Mg^{2+}, Hg^{2+}, and Hg^{2+}+mixed ions) was individually added to the sensor system and the corresponding force maps were obtained. From the force maps in Figure 5.15, it can be seen that the additions of Ca^{2+}, Fe^{2+}, K^{+}, Cd^{2+}, Zn^{2+}, and Mg^{2+} reveal no effects on color transition (as the control experiment), while the additions of Hg^{2+} or Hg^{2+}+mixed ions present an obvious color transition from dark to bright, indicating the high selectivity of this sensor.

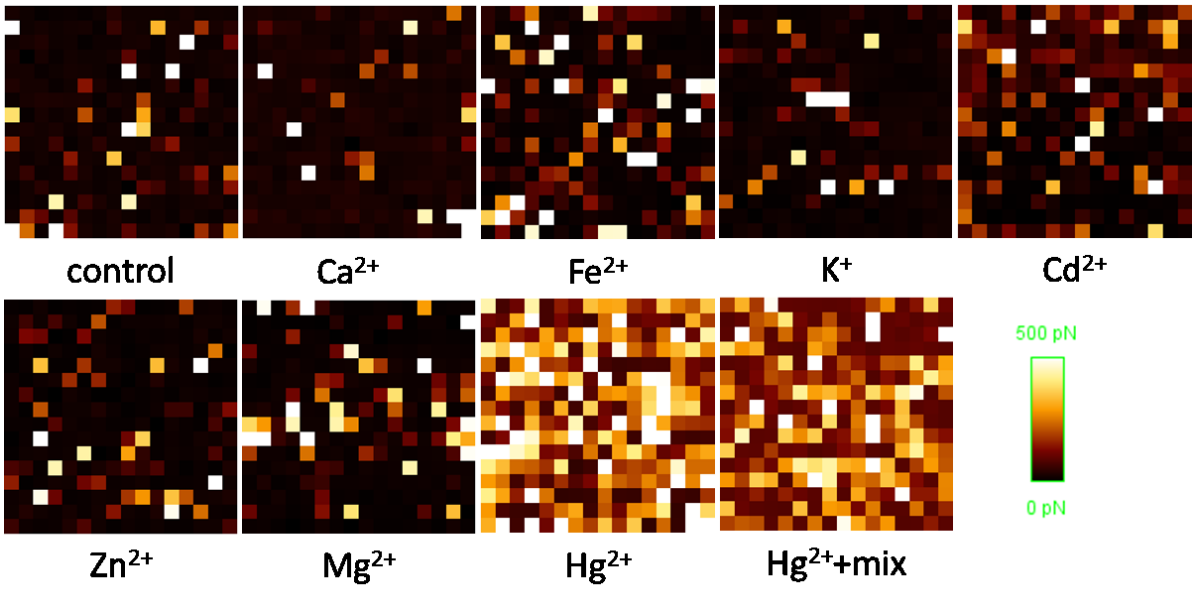

Figure 5.15 Selectivity test of SMFM for detecting Hg^{2+}: SMFM images (16 × 16 pixels) of control and adding 1 μM metallic ions of Ca^{2+}, Fe^{2+}, K^{+}, Cd^{2+}, Zn^{2+}, Mg^{2+}, Hg^{2+}, and Hg^{2+}+mix.

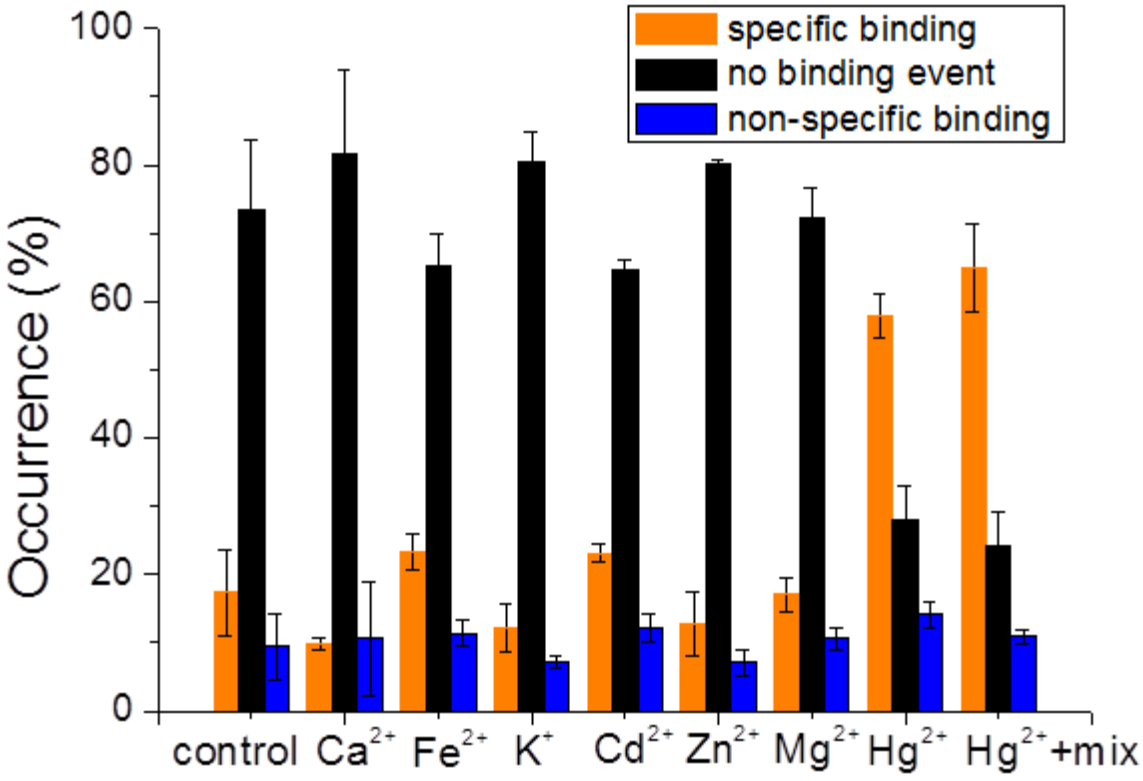

Figure 5.16 Statistic analysis of the frequency (%) of FD curves with specific binding (orange), no binding event (black), and non-specific binding (blue) in about 1000 curves.

The statistical analysis of binding frequencies (Figure 5.16) indicates that only when Hg^{2+} is present, more specific binding events (around 60%) and less no-binding

events (around 24%) than the control experiments are recorded.

Figure 5.17 shows the effect of different ions on the unbinding forces of specific binding events. The selectivity of this force-based sensor can be directly quantified by the relative force change $(F-F_0)/F_0$. The inset figure presents not only the significant effects caused by Hg^{2+} and Hg^{2+}+mix, but also the weak effects of other metallic ions.

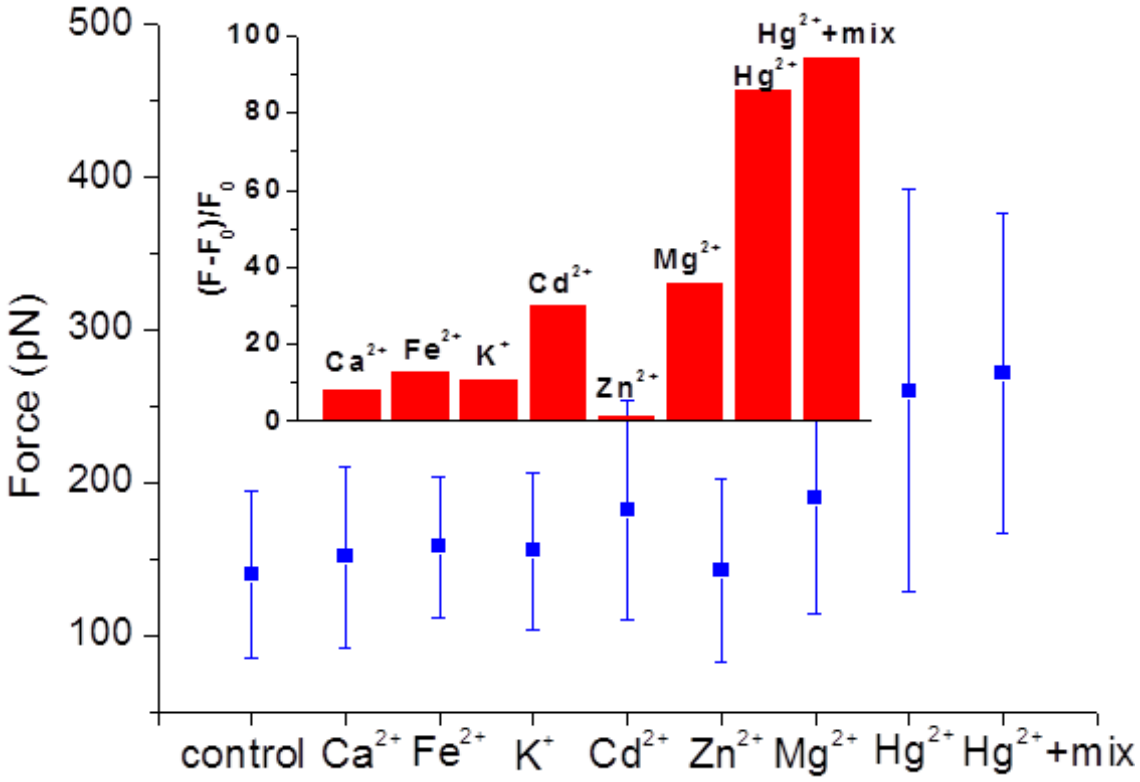

Figure 5.17 Statistic analysis of the rupture force (pN) of the FD curves with specific binding. The difference of the rupture force $[(F-F_0)/F_0]$ by adding different metallic ions is shown in the inset.

5.5 Conclusions

In summary, novel aptasensor strategies based on SMFS and SMFM were developed for the detection of Hg^{2+} with a sensitivity threshold between 0.1 and 1 nM and very good selectivity over other metal ions. Our aptasensor takes advantage of the specific T-Hg^{2+}-T coordination chemistry, which produces a clearly measurable effect on forces measured by means of single-molecule force spectroscopy. In particular, we found that the desorption force of the aptamer from flat graphite surfaces increased by about 60% after addition of an amount of Hg^{2+} larger than the detection limit. The latter is dictated by the affinity constant between Hg^{2+} and the

employed aptamer, and could be potentially lowered by further engineering of aptamer sequences with even larger mercury ion affinity. The kinetics between the aptamer and graphite surface was investigated by dynamic force spectroscopy. It was found that the adding of Hg^{2+} changed the value of x_β and $k_{off(0)}$ parameters of the Bell-Evans model, suggesting different specific interactions of the bare and Hg^{2+}-bound aptamer with the graphite surface. Both the applied loading rate and the solution ionic strength have no significant effects on the Hg^{2+} detection with this novel aptasensor. In addition, an alternative SMFM-based sensor architecture relying on force-mapping color changes was also demonstrated. The obtained SMFM results and corresponding statistic analysis proved the method feasibility, very high sensitivity and selectivity.

Our sensing method has several advantages compared to previous techniques. Firstly, the sensor technique is very universal. In this work, we presented the sensing of Hg^{2+}, but other analytes are also expected to be detected by designing corresponding ssDNA aptamer. Secondly, the detection procedure is relatively simple and quick. One force map can be achieved within 20 minutes and every test can be finished within 1 hour.

6 Thrombin detection

This chapter discusses the SMFS-based biosensing of thrombin enzymes based on ligand-receptor interaction and enzyme cleaving. It contains unpublished results.

6.1 Introduction

Thrombin, an important physiological protease existed in the blood, is composed of two polypeptide strands through crosslinking interaction of disulfide bonds.[209] It plays an essential role in some physiological and pathological processes, such as coagulation cascade, thrombosis and haemostasis.[210] It can selectivity cleave Arginine-Glycine bonds in fibrinogen to form fibrin and platelet activation.[211] Therefore, thrombin detection is very significant in fundamental and clinical research.

Recently, Zhang *et al*. developed a novel graphene oxide (GO) based biosensing platform for thrombin applying a thrombin-recognizing peptide (sequence: KCALNNGSGFPRGRAK) labeled with fluorescein isothiocyanate (FTIC) as the probe biomolecule.[211] The peptide is engineered to that one part of it adsorbs strongly on the GO surface, whereas a second part, namely the one carrying the FTIC labels, remains in solution. Overall, the system remains tightly bound to the surface, which causes strong fluorescence-quenching due to energy transfer between the dye and the GO surface. When thrombin is added into the system, it is able to cleave specifically the peptide in correspondence of the FPR-GR motif. When it does so, the dye-labeled portion of the peptide is released from GO. This can be detected by a fluorescence resonance energy transfer (FRET) signal since desorption no longer permit efficient fluorescence quenching. The system can be thus used for the real-time monitoring of the presence and activity of thrombin.

Based on this previous work, we have envisaged a system in which the same thrombin-recognizing peptide in employed to detect the presence of thrombin in a SMFS experiment. In order to do that, we have attached covalently the thrombin-recognizing peptide to an AFM tip, and modified its free end with biotin.

Biotin, also called vitamin H, is a 32-atoms molecule with a weight of 244.31 g mol^{-1}, is a coenzyme which plays an important role in many carboxylation reactions of metabolism, and is specifically recognized as a ligand by avidin and streptavidin proteins.[212] Both avidin-biotin and streptavidin-biotin are typical ligand-receptor model systems, as they bind together with very high affinity and high specificity. Avidin is a tetrameric glycoprotein consisting of 512 amino acid residues and composed of 8000 atoms, with a molecular weight is 66,000 g mol^{-1}. Streptavidin is a pure protein consisting of 636 amino acid residue, also with a tetrameric structure, and with a molecular weight is 60,000 g mol^{-1}.[213]

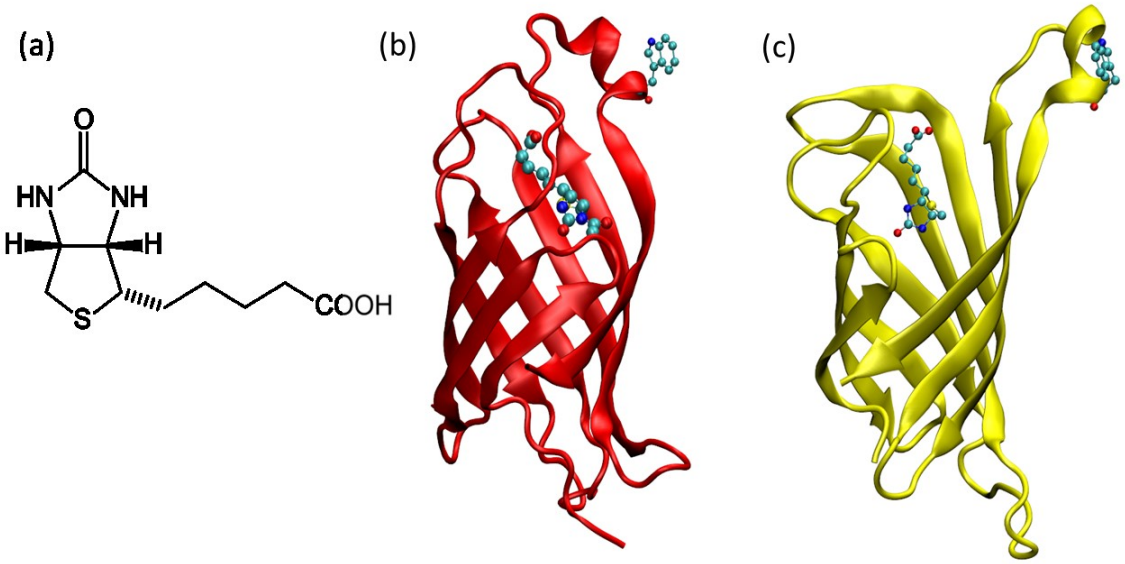

Figure 6.1 Structure of (a) biotin, (b) avidin with biotin (PDB: 3VGW TRP 110), and (c) streptavidin with biotin (PDB: 1SWE TRP 120).

Because of the tetrameric structures, both avidin and streptavidin can bind up to four molecules of biotin. Figure 6.1 shows the structures of biotin, of one chain of avidin with one biotin molecule, and of one chain of streptavidin with one biotin molecule, based on the Protein Data Bank (PDB). The binding affinity of both complexes is extremely high with a dissociation constant K_d=10^{-15} M, which is among the strongest known protein-ligand interactions.[214, 215] This makes the avidin-biotin, streptavidin-biotin systems excellent models for performing SMFS experiments into the nature of the interactions in protein-ligand systems. The strength of

ligand-receptor interactions have been measured with optical tweezer,[216] biomembrane force probe,[217] magnetic torsion device,[218] and atomic force microscopy.[67, 219] Typical unbinding forces for biotin-avidin and biotin-streptavidin complexes range between 20 and 1000 pN, depending on the loading rate and the solution composition.[47, 84, 219-223]

Our AFM tip modified with the biotin-terminated, thrombin-recognizing peptide can be now approached to an inorganic surface with pre-adsorbed or covalently attached avidin or streptavidin. Upon retraction, strong forces due to the breaking of the biotin/protein bonds are expected. In the presence of thrombin, instead, the peptide is cleaved so that we expect only non-specific, weaker forces to be measurable. In this way, collected SMFS curves would be sensitive of the presence of thrombin in concentrations larger than its unbinding constant to the peptide.

6.2 Experimental section

6.2.1 Reagents and materials

Avidin from egg white, streptavidin from streptomyces avidinii, and thrombin from human plasma or bovine plasma were provided by Sigma-Aldrich Company (Germany). The biotin-terminated thrombin-recognizing peptide: KCALNNGSGF PRGRAK(Biotin) was provided by Peptide 2.0 (USA). Aqueous solutions were prepared with ultrapure water after purification with a Mill-Q system. Two kinds of linker were used in the present work (Table 6-1). One is PEG1100, provided by Sigma-Aldrich (Germany), and the other is PEG3400, provided by NOF (Belgium). Phosphate buffered saline solutions (PBS) were used to perform the experiments. PBS tablets, gold-coated silicon wafers, and all the other chemicals were purchased from Sigma-Aldrich (Germany). Mica substrates were provided from Plano (Germany).

Table 6-1 Structures of two linkers.

PEG linker	Structure
PEG1100	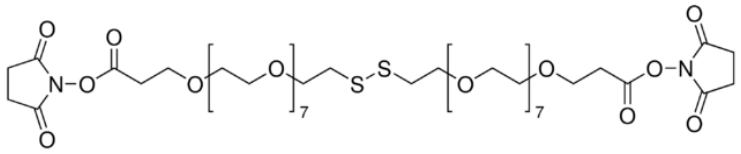
PEG3400	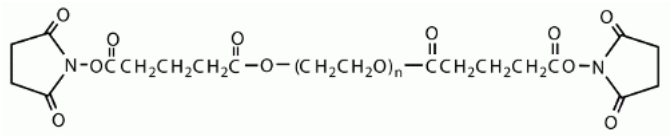

6.2.2 Functionalization of AFM probes

The procedure for AFM probe functionalization was similar to the procedures before, shown for instance in Figure 5.1a. All silicon nitride AFM probes were cleaned in newly prepared Piranha solution (H_2SO_4: 30% H_2O_2=7:3) for 30 min to remove the organic contaminants on the probes. All AFM probes were then washed with large amount of ultrapure water and ethanol (98%) several times. Then the cleaned probes were silanized by a mixed solution of 3-aminopropyl triethoxysilane (APTES) and triethoxy(ethyl)silane (TEES) (1% in toluene, APTES:TEES, 1:4, v/v) for 30 minutes to functionalize the probe with amino groups. After washing with ethanol and ultrapure water for several times, the AFM probes were transferred into 1 mg/ml PEG3400 for 1.5 h to tether the PEG-NHS ester disulfide to the AFM probes by covalent interaction between the NH_2 and NHS groups. Then the probes were washed with ultrapure water and incubated with 1mg/ml peptide solutions for 1.5 h to bind the biotin to the probes. Finally, the biotin-modified AFM probes were washed with a large amount of ultrapure water to remove non-covalently adsorbed peptides prior to the experiments.

6.2.3 Modification of substrates

For the substrates modifications, both covalent and non-covalently binding methods were applied. Both mica and gold were used as substrates.

Silicon AFM probes (NCHV) with a resonant frequency of 320 kHz from Bruker (France) were used as the cantilevers for imaging using tapping mode in air.

Avidin on the substrates

Freshly cleaved mica surfaces are negatively charged, and the avidin proteins, with an Isoelectric Point (IP) of about 10, are positively charged in our PBS buffer with pH 7.4. Therefore, the electrostatic attraction between pure mica and avidin can be exploited to adsorb avidin on the substrate by simply immersing the cleaved surface into avidin solutions.

Streptavidin on the substrates

Streptavidin, instead, presents an IP between 5 and 6, so it presents an overall negative charge in PBS buffer and will not spontaneously adsorb to freshly cleaved mica. To bind streptavidin to mica we follow different methods, as schematically represented in Figure 6.2.

In a first method (Figure 6.2a), the mica substrate is modified with aminopropyltriethoxysilane (APTES) vapor, which lead to surface silanization and results in surface termination with $-NH_2$ groups.[224] These are positively charged in PBS buffer, so that streptavidin can now spontaneously physisorb on the surface thanks to the favorable electrostatic interaction. The silanization reaction was carried out in a small clean desiccator, in which freshly cleaved mica is treated with APTES vapor for 2 h. Immediately after that, the silanized mica is immersed in the streptavidin solutions.

In a second method (Figure 6.2b) the APTES-mica substrate is further modified with the PEG3400, to which streptavidin is tethered covalently. This method is similar to the covalent modification of the AFM probe described above. Namely, the mica substrate is first silanized with APTES and then immersed in a 1 mg/ml solution of PEG3400 for 3 h. This promotes the reaction of the PEG-NHS ester with the surface NH_2 groups. Then the substrate was washed with ultrapure water and incubated with 1 mg/ml streptavidin solutions for 1 h to bind the streptavidin to the second NHS end of the linker. Finally, the substrate was washed with ultrapure water and dried with nitrogen.

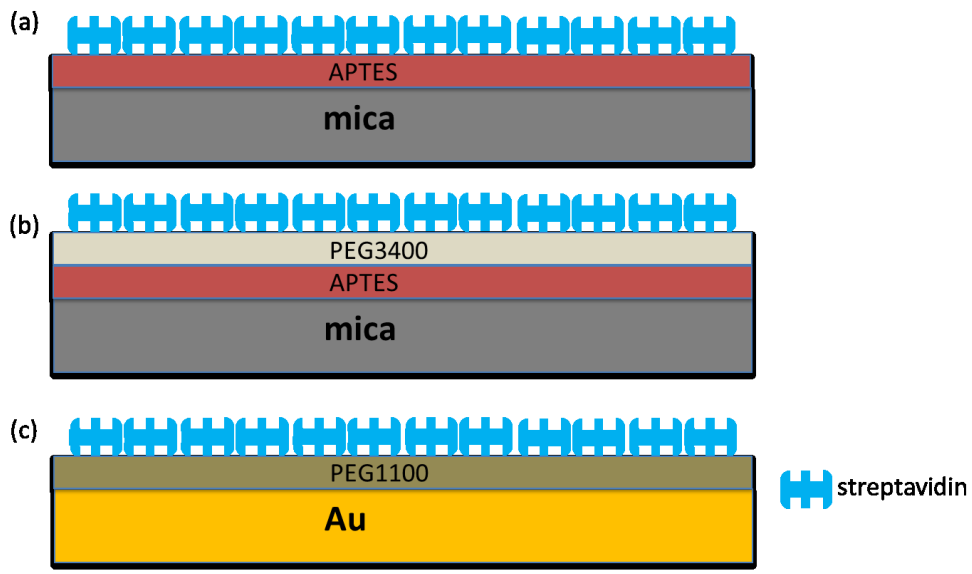

Figure 6.2 Scheme of different ways to adsorb streptavidin on the substrates.

In a third method (Figure 6.2c) we used a gold-coated silicon wafer as the substrate. After cleaning it in ethanol ultrasonic bath for 10 min, it was immersed into a 1 mg/ml PEG1100 solution for 3 h. This leads to reaction between the Au surface and the –S-S- bond in the linker, which dissociate and form a tightly packed layer of half linker molecules bound to the substrate. When immersed in a 100 ng/µl streptavidin solution for 1 h, again the -NHS group of the linker molecules react with free amino groups of streptavidin, binding it to the surface.

6.2.4 Effect of incubation concentrations and time

To investigate the effect of incubation concentrations and time, several pieces of freshly cleaved mica were incubated in different concentrations of avidin, which were 2 ng/µl, 5 ng/µl, 20 ng/µl and 50 ng/µl, respectively. Other pieces of freshly cleaved mica were incubated in 20 ng/µl avidin solution with different incubation times, which were 10 min, 20 min, 40 min, and 60 min, respectively.

6.2.5 Force measurements

Cantilevers with a nominal spring constant of 0.35 N m^{-1} were used in the SMFS experiments, which were performed using a NanoScience atomic force microscope (JPK Instruments AG, Berlin, Germany) in liquid cell with the “Force Spectroscopy” and “Force Mapping” modes. Typical parameters for the SMFS measurements were:

(1) Z-length: 0.2 µm, (2) moving speed of the AFM probe: 0.5 µm s^{-1}, (3) extend time: 0.4 s, (4) delay time on the substrate: 1 s. The aim of this 1 s delay is to favor the interaction of the biotin attached onto the AFM probe with the avidin or streptavidin adsorbed on the surfaces. With these parameters, it took about 20 min to obtain a complete force mapping data set.

6.3 Results and discussion

6.3.1 Sensing principle

The strategy for thrombin detection using AFM-based SMFS is illustrated in Figure 6.3. All the idealized cartoons show the specific interactions between tips and substrates will disappear (or be diminished) after adding thrombin and cleavage of the Arginine-Glycine bonds in the peptide.

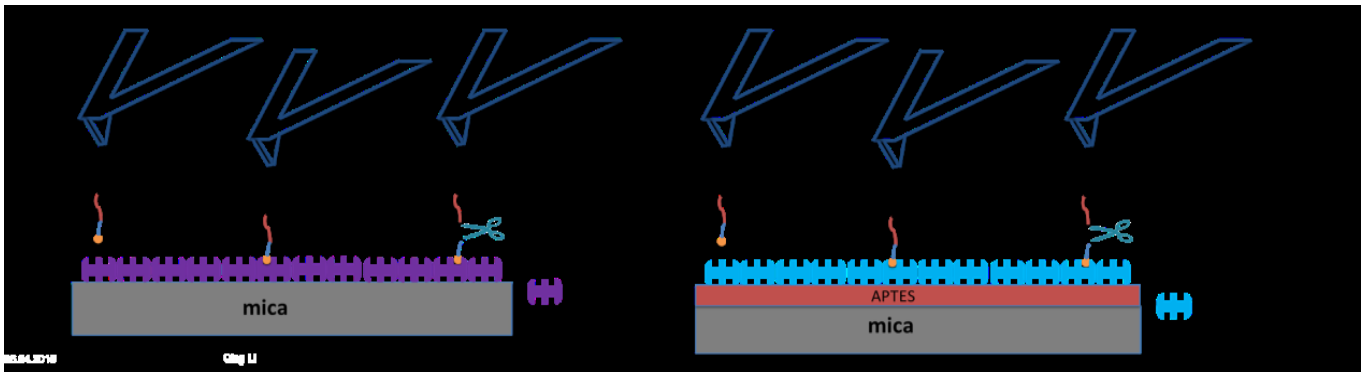

Figure 6.3 Schematic representation of the strategy for thrombin detection using AFM-based SMFS of avidin-biotin and streptavidin-biotin systems.

6.3.2 Results of the avidin-biotin system

Image of avidin adsorbed on the substrates

Figure 6.4 shows the images of mica surface before and after avidin adsorption, collected in air. It is clear that for the avidin-modified surface, particles on the blank mica substrate. From the section analysis in Figure 6.4 (right), we can measure a maximum particle height of around 2.5 nm, which is roughly half the characteristic size of the protein tetramer (~ 5 nm).[225] This reduction of the measured height is typical in AFM imaging of protein adsorbed on flat substrates performed in air, and

can be explained from shrinking of the proteins after drying and under the compressing effect of the AFM probe. The images thus reveal a dense layer of avidin adsorbed on mica, as expected.

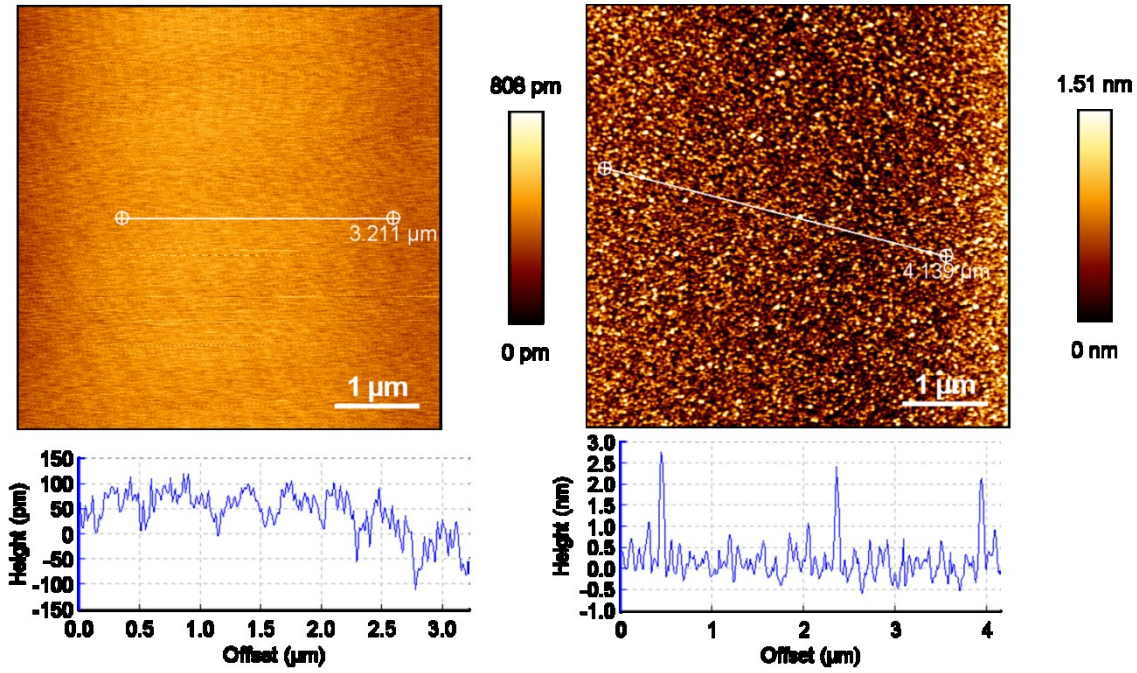

Figure 6.4 AFM topographic images and section analysis of blank mica (left) and 20 ng/µl avidin (right) on mica for 30 min using tapping mode in air.

To study the best conditions to adsorb avidin on the mica substrates, several samples were made with different concentrations of avidin solution. As we can see from the corresponding images in Figure 6.5, the number of protein increased with increasing concentrations of avidin, and when the concentration reaches 50 ng/µl the proteins start to form large agglomerate with characteristic heights between 20 and 30 nm.

To study whether the incubation time will influence the adsorption process, several samples were imaged after different incubation time, as reported in Figure 6.6. In all cases, the concentration of avidin was 20 ng/µl. As we can see from the images, there is no appreciable change of the particle distribution with different incubation times.

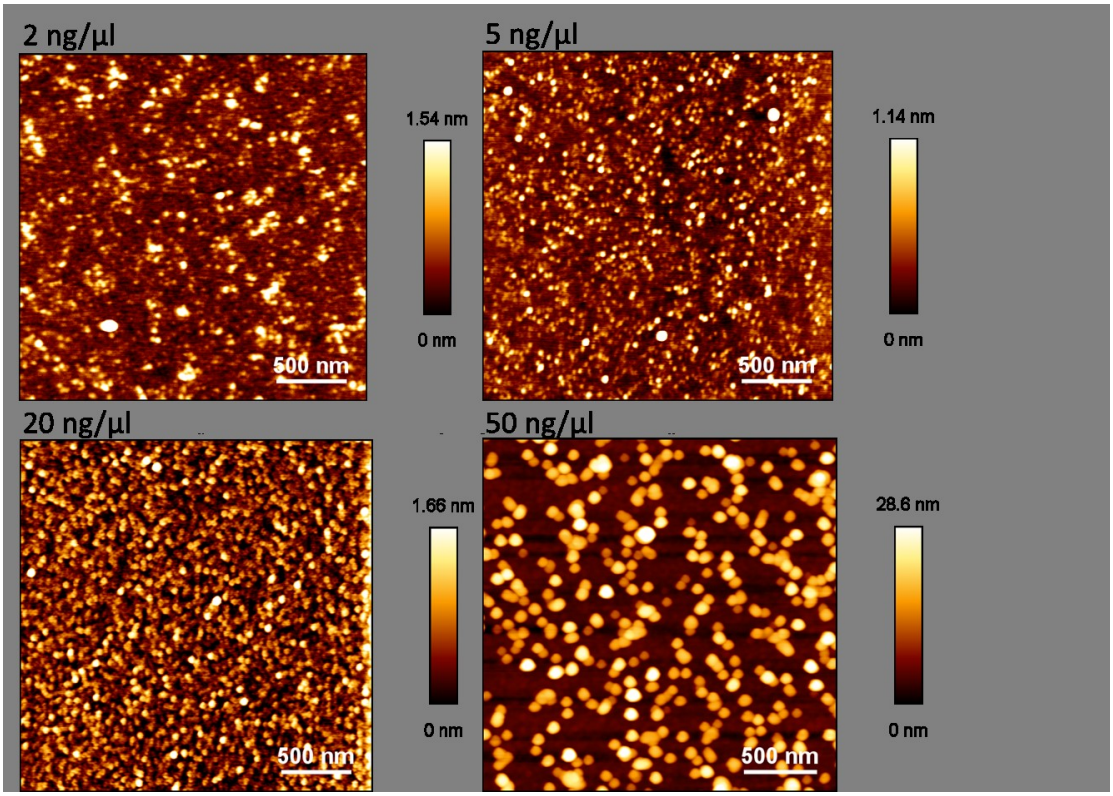

Figure 6.5 AFM topographic images of different concentrations (2 ng/µl, 5 ng/µl, 20 ng/µl, 50 ng/µl, respectively) of avidin on mica substrate using tapping mode in air. The incubation time is 30 min.

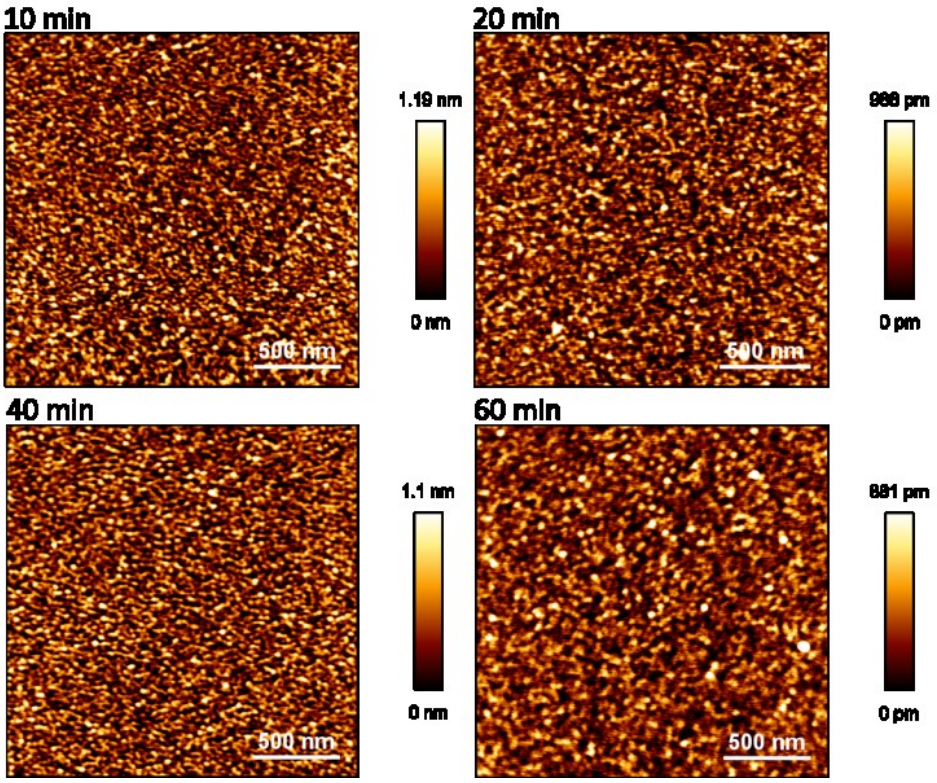

Figure 6.6 AFM topographic images of 20 ng/µl avidin on mica substrate with different incubation times (10 min, 20 min, 40 min, 60 min, respectively) using tapping mode in air.

Based on these combined results, 20 ng/µl avidin and an incubation time of 30 min were chosen as the standard conditions for the substrates to be tested in force-spectroscopy measurements.

Force distributions of avidin-biotin

Figure 6.7 shows exemplary curves presenting no binding interaction (left) and presenting specific signatures of avidin-biotin interactions in PBS. Curves without visible force peaks were often (but not always) obtained upon interaction between the blank mica surface with AFM tips modified with either only the linker, or the linker and the biotin-terminated peptide. Only in the presence of interactions between avidin and biotin clear peaks appear, which can be nicely fitted with theoretical force-distance curves corresponding to a worm-like-chain (WLC) model (Figure 6.7b).

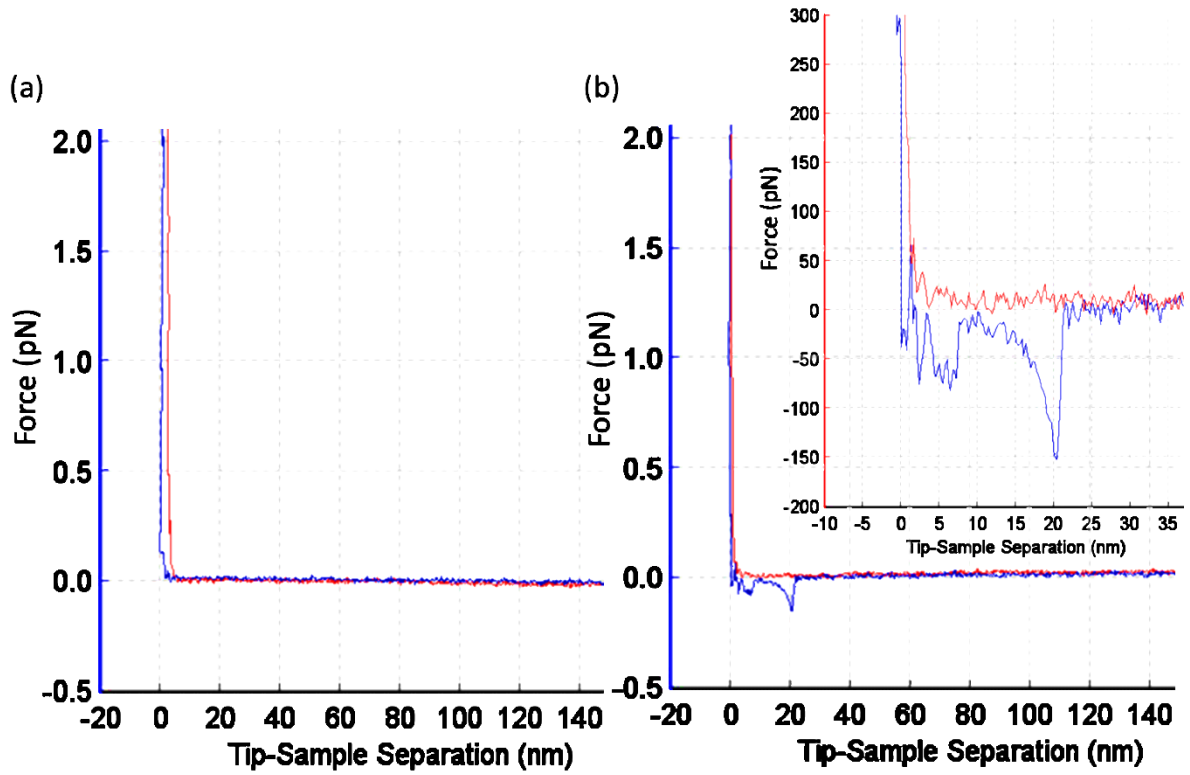

Figure 6.7 Exemplary curves of (a) blank curve, (b) avidin-biotin curve in PBS.

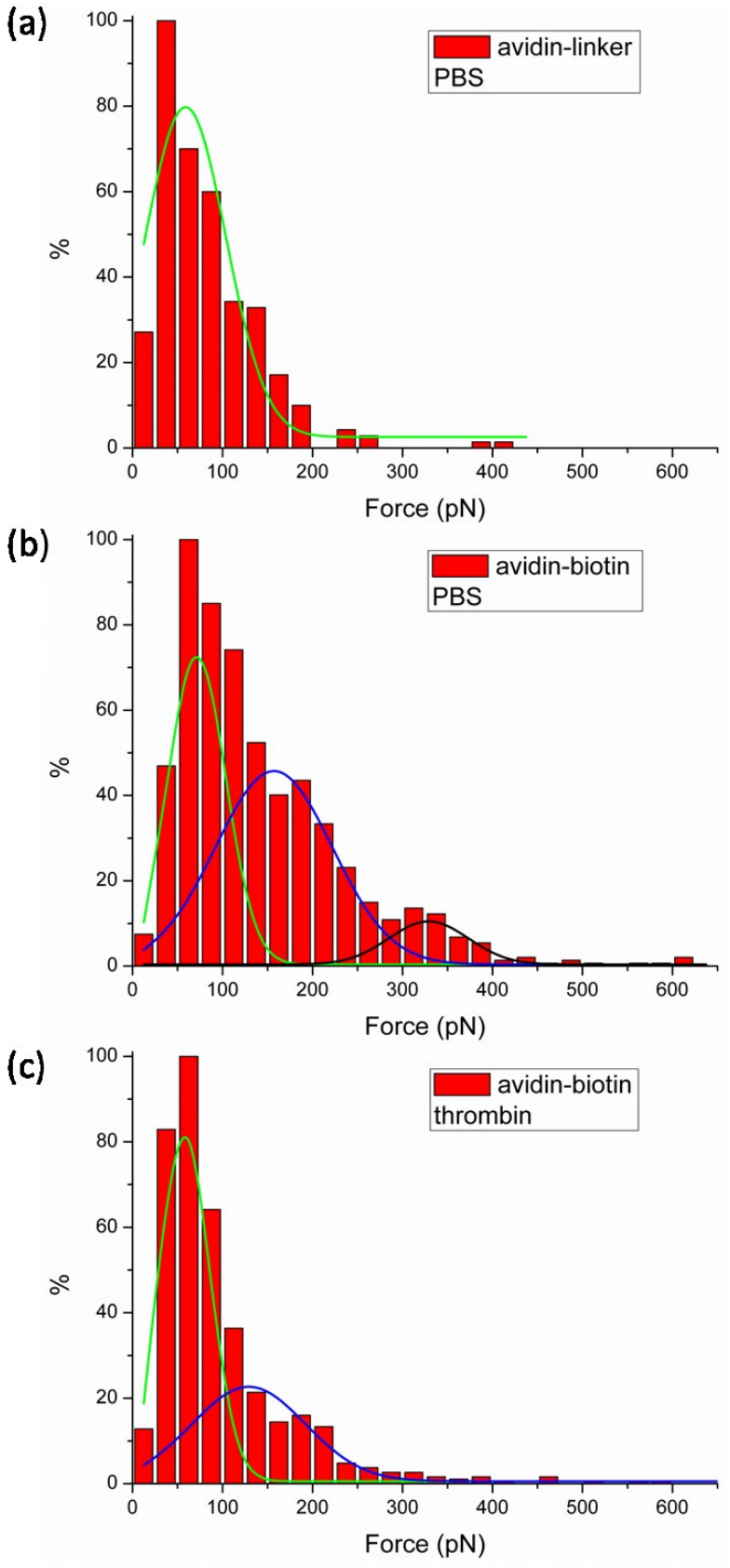

Figure 6.8 Force distributions of the avidin-modified mica with tip modified with (a) PEG3400 linker only; (b) biotin-terminated peptide and collected in pure PBS buffer; and (c) modified with the biotin-terminated peptide and collected in a thrombin solution at the concentration of 5 units/ml.

Figure 6.8 shows the force distributions measured between the avidin-modified mica surface and three different AFM tips, namely (a) modified with the PEG3400 linker only; (b) modified with the biotin-terminated peptide and collected in pure PBS buffer; and (c) modified with the biotin-terminated peptide and collected in a thrombin solution at the concentration of 5 units/ml.

In all cases, we fit Gaussian curves to the distributions. In the first case (Figure 6.8a), the data are reasonably well fitted with a single Gaussian curve, with the maximum in correspondence of about 70 pN. In the second case (Figure 6.8b), the data are best fitted with three Gaussians with maxima at force values of about 70, 160 and 320 pN. In the third case (presence of thrombin), two peaks in correspondence of about 70 and 140 pN were obtained. Although the number of Gaussian used to fit the data is somehow arbitrary, it seems clear that the presence of thrombin results in the disappearance of the third force peak centered at 320 pN and in a shift of the second peak to smaller occurrences values and slightly smaller forces.

Forces between biotin and avidin at a loading rate similar to the one used here have been measured in the work of Moy et al.[226] to be about 160 pN. We could thus interpret the three peaks in Figure 6.8b as arising from (i) non-specific tip-surface interactions (as in the blank control) at 80 pN; (ii) single biotin-avidin binding events at about 160 pN and (iii) double biotin-avidin binding events at about 320 pN. Indeed, it cannot be excluded that more than one molecule is bound to the AFM tip after functionalization. However, an alternative explanation could be that only the smaller peak at larger force values (320 pN) corresponds to specific biotin-avidin interactions, while the intermediate peak at 160 pN could arise from interaction between the peptide and the adsorbed protein. Support of this latter interpretation comes from the presence of a peak in a similar range of forces also in the presence of thrombin (Figure 6.8c) and from the fact that forces of about 300 pN or more are also measured between biotin and streptavidin in the next section.

6.3.3 Results of the streptavidin-biotin system

Image of streptavidin adsorbed on the substrates

To make sure that streptavidin is adsorbed on the mica and gold substrates, AFM images of the functionalized surfaces are collected and reported in Figure 6.9 (a) and (b), respectively. It can be easily seen that the distribution of streptavidin on APTES-silanized mica is not as uniform and clear as for the case of avidin on fresh mica. It can be inferred that the addition of APTES or PEG linkers results in a relatively rough layer with non-uniform distribution of amino groups. In the case of streptavidin on the gold substrates, larger protein agglomerates on top of a rough surface, probably due to the gold particles as the result of the Au coating procedure, are observed.

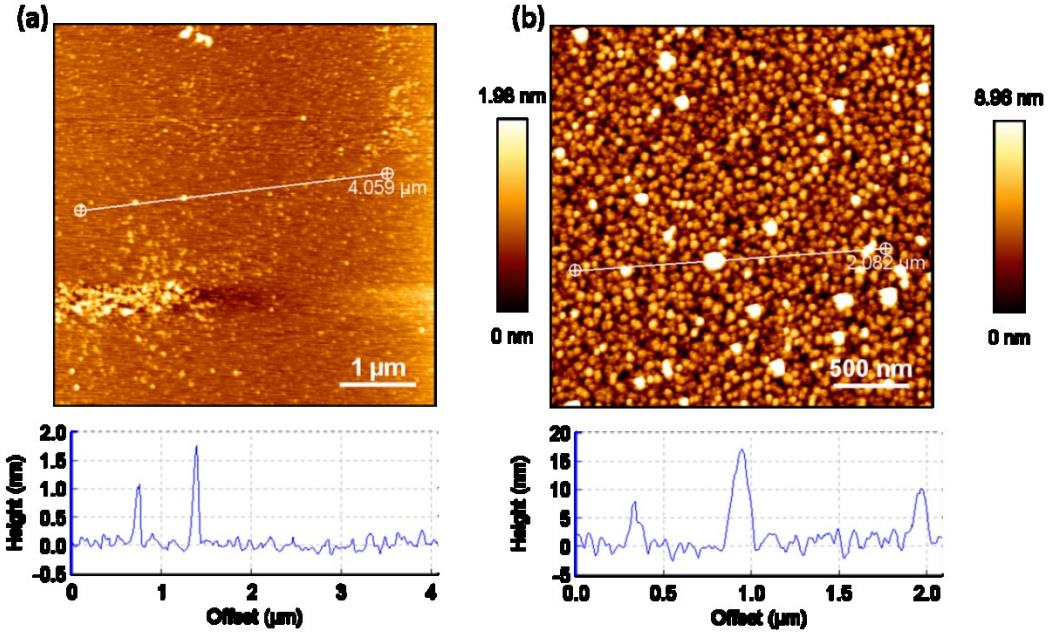

Figure 6.9 AFM topographic images and section analysis of (a) mica under APTES vapor for 2 h and then treated with 5 ng/µl streptavidin for 30 min using tapping mode in air; (b) gold substrate with 1 mg/ml PEG1100 2 h and then treated with 100 ng/ul streptavidin 1 h using tapping mode in air.

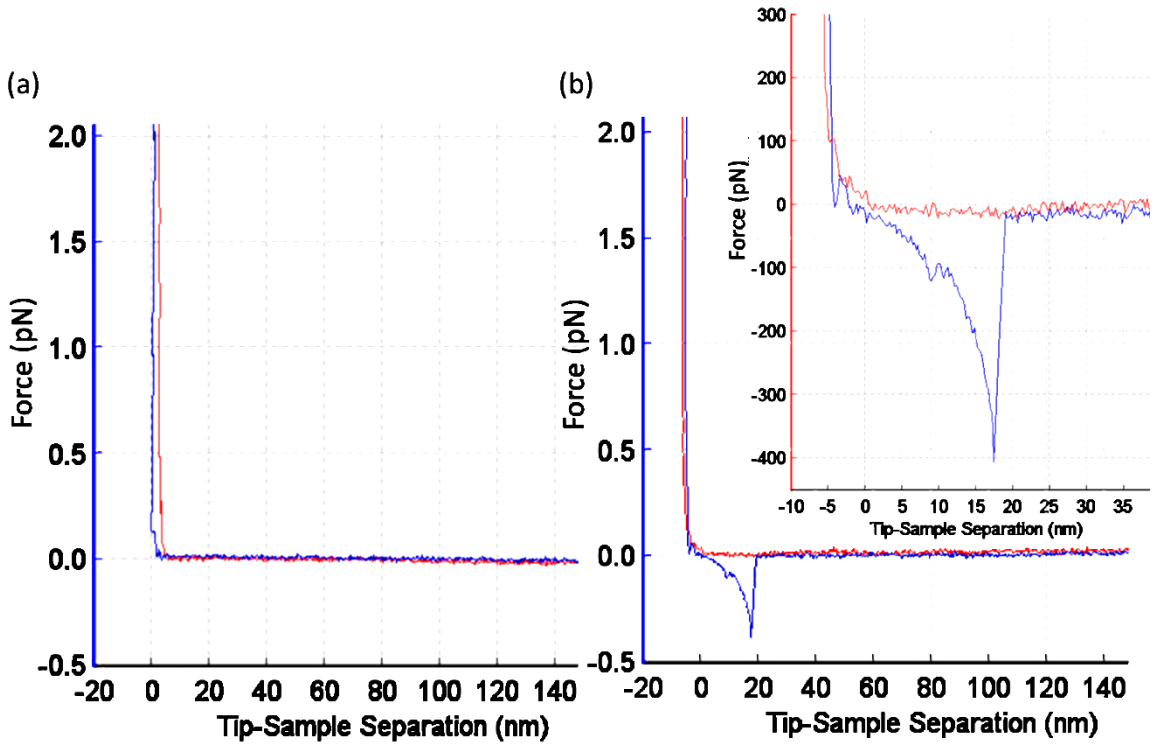

Figure 6.10 Exemplary curves of (a) blank curve, (b) streptavidin-biotin curve in PBS.

Figure 6.10 shows exemplary blank curves presenting no force peak and curves with peak clearly arising from specific streptavidin-biotin interactions in PBS. As in the previous case of avidin-biotin, the peak presents a clear WLC character (Figure 6.10b).

The force distributions collected on the APTES-modified mica in the presence of physisorbed streptavidin are reported in Figure 6.11. Again curves are collected with AFM modified with only the PEG linker (a), or with the linker and the biotin-terminated peptide in the absence (b) or presence (c) of thrombin. The first set of data cannot be fitted with a Gaussian curve, most of the measured forces being smaller than 25 pN and hardly larger than about 100 pN. In the second case, where a biotin-streptavidin interaction is expected, beside a non-specific peak at forces of about 90 pN, a clear peak centered at about 290 pN is present in the force distribution. This peak completely disappears in the presence of thrombin.

Importantly, literature values of streptavidin-biotin forces correspond well to our data. For example in the work of Lee et al.[227] an average value of 350 pN is reported. Therefore, we can safely assume that the presence of thrombin can be inferred by the disappearance of this peak, as visible in Figure 6.11c.

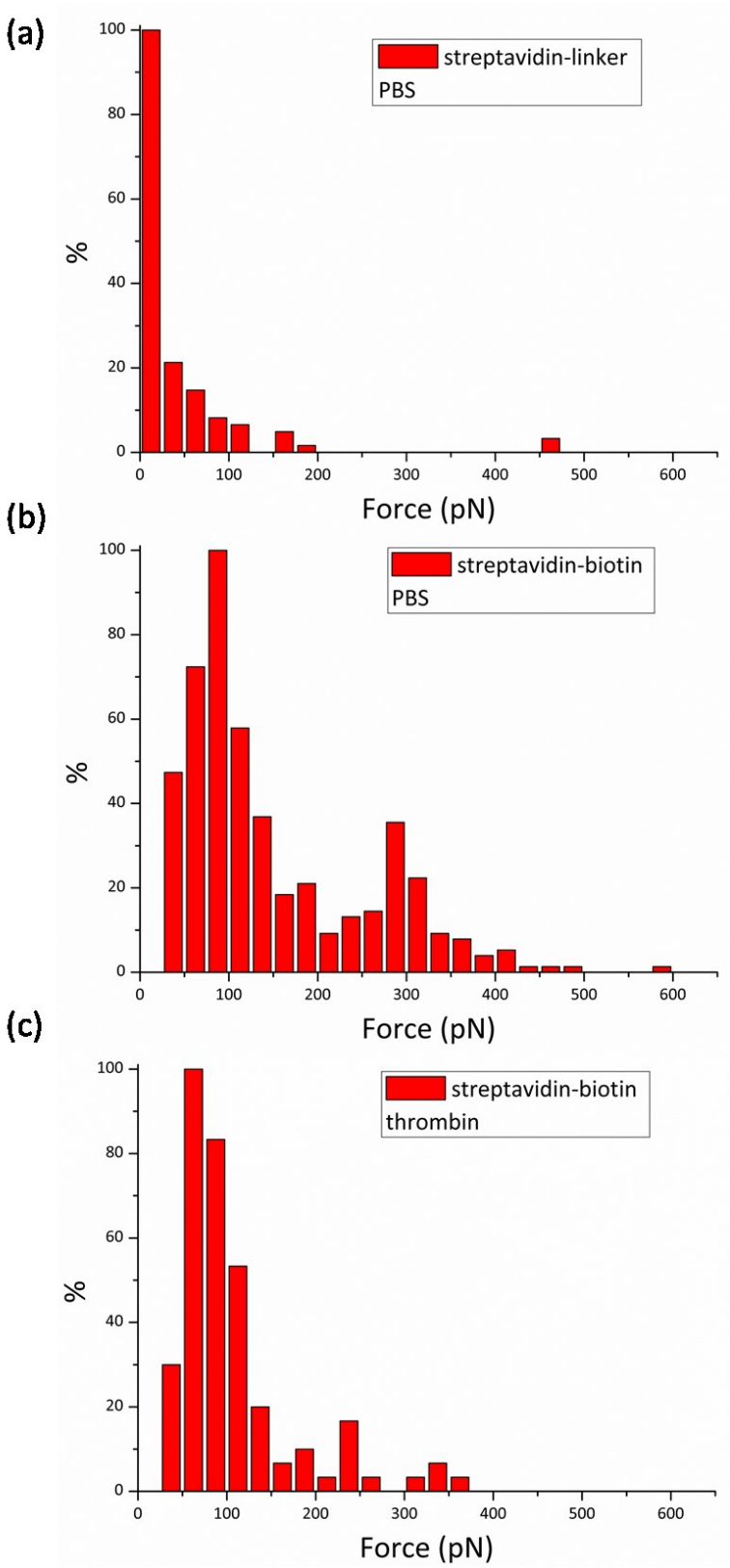

Figure 6.11 Force distributions of (a) streptavidin with PEG3400 linker only in PBS; (b) streptavidin with biotin-terminated peptide in pure PBS; (b) streptavidin with biotin-terminated peptide in 5 units/ml thrombin. 20 ng/µl streptavidin was adsorbed on the APTES-mica substrate for 30 min.

6.3.4 Results of the covalently modified substrates

In contrast with the results presented in the previous two sections, when we try to bind streptavidin covalently either to Au or to silanized mica, no clear force distribution could be obtained. In Figure 6.12 the force distribution collected in the absence (a) or presence (b) of thrombin are reported. In this case, the reduction of the number of force values between 100 and 300 pN could indeed indicate cleavage of the peptide. However, the observed presence of much larger forces (up to 1200 pN) irrespective of the presence or absence of thrombin is not clear, so that it is difficult to make firm conclusion about the interactions present in the system.

The situation is even worse for the case of APTES-silanized mica substrates and streptavidin bound via the PEG linker (Figure 6.13). In this case, only a general reduction of the force peak with WLC-character (which is used to build up the force distributions) is observed after addition of thrombin. However, both in the presence and absence of thrombin the force values are spread between 50 and 1200 pN, so that no sensing principle can be derived from this set of measurements.

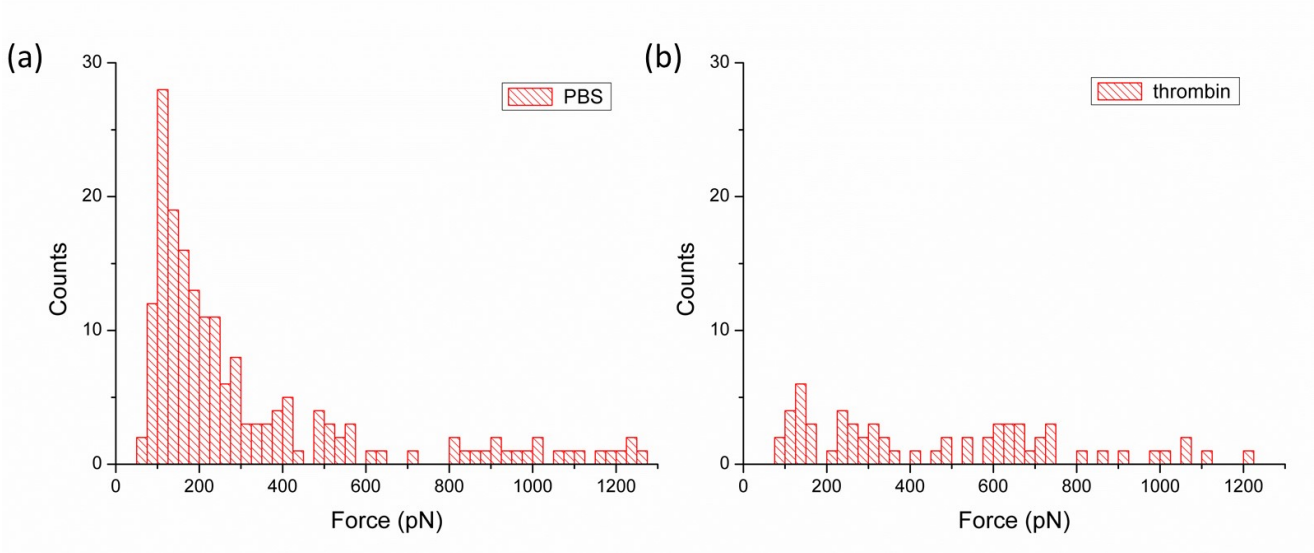

Figure 6.12 Force distributions of streptavidin with biotin in (a) PBS, (b) 8.75 units/ml thrombin. Gold substrate with 1 mg/ml PEG1100 3 h, and then treated with 20 ng/µl streptavidin for 30 min. The results are analyzed from 512 curves.

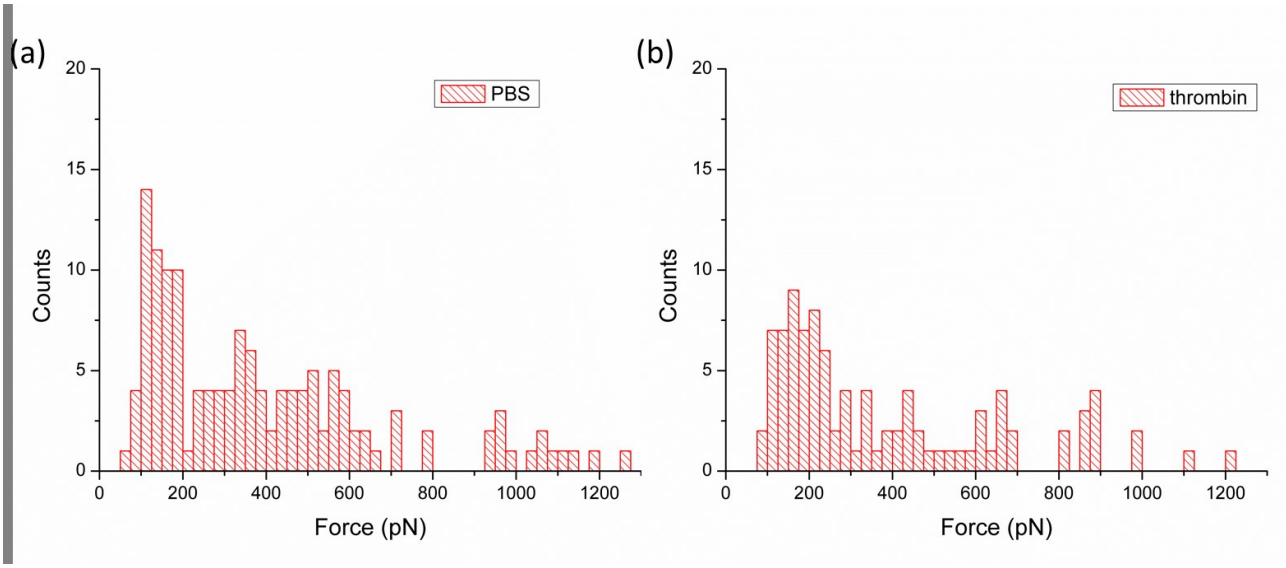

Figure 6.13 Force distributions of streptavidin with biotin in (a) PBS, (b) in 20 units/ml thrombin from bovine plasma. APTES-mica substrate was incubated with 1 mg/ml PEG 3400 3 h, and then with 1 mg/ml streptavidin for 30 min. The results are analyzed from 768 curves.

6.4 Conclusion

In summary, single-molecule force spectroscopy was used to investigate the presence of thrombin in solution exploiting the presence of peaks in force-displacement curves arising from strong avidin-biotin and streptavidin-biotin interactions. Namely, solid substrates were functionalized with the proteins and the biotin ligand was tethered to AFM probes via a PEG linker and a specific peptide sequence which is enzymatically cleaved by thrombin. Different functionalization strategies (non-covalent or covalent) and substrates (fresh mica, APTES-silanized mica, gold-coated silicon wafer) were tested.

We found that non-covalent adsorption of avidin to pristine mica surfaces results in the best uniformity and density of the protein layers on the surfaces, followed by non-covalent adsorption of streptavidin to APTES-silanized mica. When covalent protein binding was attempted, no uniform protein layer could be obtained.

Correspondingly, the expected effect of thrombin cleaving the peptide and leading to a measurable change of the force distributions between tip and substrate could also be clearly proven only for physisorbed protein layers. Some uncertainty remains whether the avidin-biotin specific force is around 160 or 320 pN, but in either case

the presence of thrombin can be unequivocally be detected by disappearance of the large forces in the region between 280 and 350 pN.

Compared with the sensing strategy used in the previous chapter to detect mercury ions or adenosine, the system is more complex, which naturally leads to the simultaneous presence of largely intertwined interaction forces. Further research is needed to test the sensitivity of the system, working with different concentrations of thrombin. To test the selectivity of the biosensor strategy, other enzymes such as lysozyme or several proteases could be used. Finally, it would be interesting to repeat the experiment in the presence of natural thrombin inhibitors and/or activators and try to detect their action in real time by performing force-clamping AFM experiments.

7 Conclusions and outlook

In the thesis, AFM-based single-molecule force spectroscopy has been used to detect the presence of adenosine, mercury ions and thrombin in water solutions at very small concentrations. The used methods rely on the engineering of specific DNA and peptide sequences presenting high affinity and selectivity towards the specific analytes. Also, it requires a fundamental understanding of the interactions taking place between biomolecules and biomolecules and inorganic surfaces. The DNA and peptide binding to AFM probes and the functionalization of substrates against which the force response is collected have been performed comparing several methods.

We have shown that the interaction strengths between heteropolymer ssDNA sequences and graphite surfaces depend on the specific basis sequence and differ, in particular, from the desorption behavior of homopolymer oligonucleotides (Section 2.4). These results have been exploited to develop SMFS-based biosensors for the detection of adenosine (Chapter 4) and Hg^{2+} ions (Chapter 5), in which the sensing elements are an adenosine-binding aptamer and a Hg^{2+}-binding aptamer, respectively, covalently attached to AFM tips. In both cases, the sensing signal is the adhesion force between the aptamer and a clean graphite surface. It must be stressed that sensors of this kind do not allow for a quantitative estimation of the amount of dissolved analytes, but only to detect their presence above a critical concentration value (the detection limit) corresponding to the dissociation constant of the aptamer/analyte system. As the affinities of the aptamers for its specific ligands are generally very high, correspondent low detection limits could be achieved, namely about 0.1-1 nM in both cases. This is low enough to be useful in practical applications, being for instance lower than the legally allowable level of mercury ions in drinking water (10 nM).

Also, given that the aptamer sequence is engineered ad hoc to bind only a certain ligand, the selectivity of the sensors with respect to similar molecules (other nucleosides for the case of adenosine, other metal ions for the case of mercury) has

been found to be excellent. Our simple but powerful SMFS-based biosensing approach is believed to be promising for the detection of a wide range of other analytes, since aptamers for numerous molecules have been reported in the literatures and the protocols for engineering new aptamer sequences are also well established. This inherent transferability is in fact one of the largest advantages of our method with respect to other existing sensing or biosensing principles.

A disadvantage may be represented by the relatively time-consuming procedure of force acquisition, the required discrimination of the force-distance curves bearing signatures of specific interaction curves against non-specific ones, and large error bars intrinsic in the averaging of the collected data, which are in the same order of magnitude than the forces themselves (100 pN). To partially overcome these limitations, we have tried to exploit the current automatization capability of modern AFM instruments and software by analyzing, rather than individual curves, whole force maps. This has been done for the case of Hg^{2+} ions in the second part of Chapter 5 (SMFM method). We have shown that even without filtering of the as-collected force-map data, visual inspection of the color intensity of the maps already gives a qualitative but very sound indication about the presence of the analytes above a low detection limit. We expect that further progress in the automatization of force map collection and analysis could result in biosensing architectures capable of delivering very quick information free from any bias due to the AFM operating scientist.

As an alternative of measuring the force between an aptamer and a passive inorganic surface, we have explored the possibility of splitting the aptamer sequence in two separate parts, one bound to an AFM tip and one bound to a surface. The SMFM Hg^{2+} biosensing has been performed exploiting this principle, using gold substrates to which thiol-modified aptamers can be easily bound. This approach presents the advantage of reducing the number of individual force-distance curves presenting non-specific binding peaks. For this reason, we have attempted to extend it to a more complex system designed to sense the presence of thrombin molecules (Chapter 6).

In this last approach, the sensing principle can be generally applied to enzymes

with the ability of cleaving via hydrolysis the peptide bonds at specific sites in a polypeptide sequence. In this thesis, we have chosen thrombin as a representative example. The force signal to be measured arises from specific interactions between a surface-immobilized protein (avidin or streptavidin, in our case) and its specific ligand (biotin) tethered to an AFM tip via a PEG linker and an oligopeptide sequence containing the motif which is recognized and cleaved by the enzyme. When the latter is present in sufficient concentration, the expected measured forces should dramatically decrease.

Although we could demonstrate the general functionality of such a system, we found that the detection of thrombin is not as obvious as we hoped for. In particular, the protein-functionalization of the surface play a very important role and its uniformity and density are crucial to obtain clear results. Non-covalent and covalent methods have been both tested, and we found that non-covalent modifications (especially in the case of avidin) led to the clearest information. However, these results are still preliminary and we have not yet determined the detection limit and the sensitivity of the system towards thrombin.

Comparing the three biosensor architectures, it can be seen that the synthetic DNA-based sensors (for adenosine and mercury ions) show better performance than the synthetic peptide-based sensor (for thrombin). However, there are still some drawbacks and limits in the current study of AFM-based SMFS biosensing.

First of all, data analyzing may still require human intervention, which easily can become very time-consuming. Problems arise when the force-distance curves of the same measurement set present very different features and many interaction peaks, not all of which are indicative of the sought-for specific interactions. In some cases, especially when the functionalization of the tips or the surface is not extremely homogeneous, only a small portion of the binding events can be used to discriminate between presence or absence of the analyte. This was especially visible when trying to detect thrombin with covalently-functionalized mica or gold substrates (Chapter 6, Figure 6.12 and Figure 6.13).

Moreover, in our preliminary investigations we have carefully selected a testing

environment to enhance the sensitivity and selectivity of the analyte/probe binding. In particular we have explored different pH or salt concentrations. It remains to be seen whether our technique is robust enough to be used in on-field investigations using either biological fluids (urine, blood) or soil suspensions (for the detection of polluting heavy metal ions).

A possibility to solve the drawbacks and limits mentioned above, it could be a viable strategy to integrate AFM with other techniques, even if in this case the simplicity of the measurement principle could be reduced. For example, AFM can be integrated with fluorescence microscopy,[228] total internal reflection fluorescence (TIRF) microscopy,[229] and fluorescence resonance energy transfer (FRET) microscopy.[230] Combing the fluorescence techniques with AFM would help to address with great specificity the desired binding sites between the employed biomolecules. In addition, to make sure that both probes and substrates are correctly modified with specific aptamers or proteins, it could be necessary to use other technique such as X-ray photoelectron spectroscopy (XPS). Multi-parametric surface plasmon resonance (MP-SPR) can also be employed to test the thickness of functional biomolecular layers.

Combining single-molecule AFM with genetic manipulations is also a powerful tool in cell biology. Some research showed that the AFM force-spectroscopy can not only probe surface-associated proteins, but proteins which are embedded within the cell wall or beneath the surface as well.[231] The combined technique opens a new way to measure the thickness of microbial cell walls under different environmental conditions. On the basis of these findings we envisage that extension of the methods that we have presented in this thesis could thus open the way to force-based detection of substances within living cells.

The combination of AFM experiments with the computer modeling will also be an interesting direction to go, as molecular simulation would help to reveal the nature of the fundamental interactions and the mechanisms of molecular recognition.[115]

Although biosensors are widely used in many applications, most efforts are still at the level of research interest in universities or institutes. Only a few biosensors have

been successfully developed into commercial products, while the majority of them still have to overcome some barriers before being commercialized. First of all, biosensors need to be at least as sensitive as conventional techniques, and this can be improved by the development of specific interactions between biomolecules and analytes. Secondly, biosensors need to be reproducible and stable, as the performance of the biosensor might be influenced in the development and manufacturing processes because of mass production. To overcome this obstacle, it is important to keep their chemical and physical design characteristics as simple as possible. Next, biosensors need to be easy to operate. This might be solved by the development of compact and robust equipment, which might be portable in the future. Finally, biosensors should be cheap so that the market size can be expanded. Because of the complexity of devices and the cost of biomolecules, this seems to be a goal that is difficult to reach. Private companies will be motivated to adopt biosensor technologies in their products only when profitable marketplaces are grown. This might be achieved thanks to future development of synthetic biology principles and device miniaturization. I believe that with the rapid development of synthetic biology, chemistry and manufacturing technology, biosensors will have a bright future in the analytical industry and society.

References

[1] A. S. Khalil and J. J. Collins, *Nat. Rev. Genet.*, 2010, **11**, 367-379.

[2] E. Andrianantoandro, S. Basu, D. K. Karig and R. Weiss, *Mol. Syst. Biol.*, 2006, **2**, 1-14.

[3] F. S. Collins, E. S. Lander, J. Rogers, R. H. Waterston and I. H. G. S. Conso, *Nature*, 2004, **431**, 931-945.

[4] S. A. Benner and A. M. Sismour, *Nat. Rev. Genet.*, 2005, **6**, 533-543.

[5] D. B. Wilson, D. Weisburd and D. McClure, *Campbell Systematic Reviews*, 2011, **7**, 1-52.

[6] J. H. Luong, K. B. Male and J. D. Glennon, *Biotechnol. Adv.*, 2008, **26**, 492-500.

[7] C. R. Lowe, *Trends Biotechnol.*, 1984, **2**, 59-65.

[8] A. Reeve, *Control and Instrumentation*, 1991, **23**, 50-51.

[9] S. S. Kim, *The Journal of Supercomputing*, 2015, **72**, 177-184.

[10] X. Q. Wu, J. G. Ma, H. Li, D. M. Chen, W. Gu, G. M. Yang and P. Cheng, *Chem. Commun.*, 2015, **51**, 9161-9164.

[11] M. Li, X. Zhou, W. Ding, S. Guo and N. Wu, *Biosens. Bioelectron.*, 2013, **41**, 889-893.

[12] M. Q. Yuan, E. C. Alocilja and S. Chakrabartty, *Ieee Sensors Journal*, 2014, **14**, 941-942.

[13] M. J. Dennison and A. P. F. Turner, *Biotechnol. Adv.*, 1995, **13**, 1-12.

[14] D. A. Rathbone, P. J. Holt, C. R. Lowe and N. C. Bruce, *Enzyme Engineering Xiii*, 1996, **799**, 90-96.

[15] Y. Li, H. Qi, Y. Peng, J. Yang and C. Zhang, *Electrochem. Commun.*, 2007, **9**, 2571-2575.

[16] M. E. Davidson, S. V. Harbaugh, Y. G. Chushak, M. O. Stone and N. Kelley-Loughnane, *ACS Chem. Biol.*, 2013, **8**, 234-241.

[17] Y. Yu, Q. Cao, M. Zhou and H. Cui, *Biosens. Bioelectron.*, 2013, **43**, 137-142.

[18] M. Y. Ho, N. D'Souza and P. Migliorato, *Anal. Chem.*, 2012, **84**, 4245-4247.

[19] S. Fields and O.-k. Song, *Nature*, 1989, **340**, 245-246.

[20] S. Frokjaer and D. E. Otzen, *Nat. Rev. Drug Discov.*, 2005, **4**, 298-306.

[21] D. S. Johnson, A. Mortazavi, R. M. Myers and B. Wold, *Science*, 2007, **316**, 1497-1502.

[22] C. Albrecht, K. Blank, M. Lalic-Multhaler, S. Hirler, T. Mai, I. Gilbert, S. Schiffmann, T. Bayer, H. Clausen-Schaumann and H. E. Gaub, *Science*, 2003, **301**, 367-370.

[23] Y. J. Jung, J. A. Albrecht, J. W. Kwak and J. W. Park, *Nucleic Acids Res.*, 2012, **40**, 11728-11736.

[24] H. Dietz and M. Rief, *Japanese Journal of Applied Physics*, 2007, **46**, 5540-5542.

[25] E. A. Placzek, M. P. Plebanek, A. M. Lipchik, S. R. Kidd and L. L. Parker, *Anal. Biochem.*, 2010, **397**, 73-78.

[26] C. K. Chiang, C. C. Huang, C. W. Liu and H. T. Chang, *Anal. Chem.*, 2008, **80**, 3716-3721.

[27] X. Xu, J. Wang, K. Jiao and X. Yang, *Biosens. Bioelectron.*, 2009, **24**, 3153-3158.

[28] Z. Zhu, Y. Su, J. Li, D. Li, J. Zhang, S. Song, Y. Zhao, G. Li and C. Fan, *Anal. Chem.*, 2009, **81**, 7660-7666.

[29] L. Zhang, H. Chang, A. Hirata, H. Wu, Q. K. Xue and M. Chen, *ACS Nano*, 2013, **7**, 4595-4600.

[30] Z. Zhang, E. Sharon, R. Freeman, X. Liu and I. Willner, *Anal. Chem.*, 2012, **84**, 4789-4797.

[31] W. G. Cox and V. L. Singer, *Biotechniques*, 2004, **36**, 114-122.

[32] J. S. Lee, M. S. Han and C. A. Mirkin, *Angew. Chem. Int. Ed. Engl.*, 2007, **46**, 4093-4096.

[33] R. C. Jin, G. S. Wu, Z. Li, C. A. Mirkin and G. C. Schatz, *J. Am. Chem. Soc.*, 2003, **125**, 1643-1654.

[34] M. S. Han, A. K. R. Lytton-Jean and C. A. Mirkin, *J. Am. Chem. Soc.*, 2006, **128**, 4954-4955.

[35] J. Liu and Y. Lu, *J. Am. Chem. Soc.*, 2004, **126**, 12298-12305.

[36] J. M. Nam, C. S. Thaxton and C. A. Mirkin, *Science*, 2003, **301**, 1884-1886.

[37] C. A. Mirkin, R. L. Letsinger, R. C. Mucic and J. J. Storhoff, *Nature*, 1996, **382**, 607-609.

[38] S. S. Babkina and N. A. Ulakhovich, *Bioelectrochemistry*, 2004, **63**, 261-265.

[39] S. Zhang, J. Xia and X. Li, *Anal. Chem.*, 2008, **80**, 8382-8388.

[40] E. J. Blackie, E. C. Le Ru and P. G. Etchegoin, *J. Am. Chem. Soc.*, 2009, **131**, 14466-14472.

[41] X. Xu, H. Li, D. Hasan, R. S. Ruoff, A. X. Wang and D. L. Fan, *Adv. Funct. Mater.*, 2013, **23**, 4332-4338.

[42] X. Fan, I. M. White, S. I. Shopova, H. Zhu, J. D. Suter and Y. Sun, *Anal. Chim. Acta*, 2008, **620**, 8-26.

[43] R. W. Carpick and M. Salmeron, *Chem. Rev.*, 1997, **97**, 1163-1194.

[44] A. Weisenhorn, P. Maivald, H. J. Butt and P. Hansma, *Physical Review B*, 1992, **45**, 11226-11232.

[45] E. M. Puchner and H. E. Gaub, *Curr. Opin. Struct. Biol.*, 2009, **19**, 605-614.

[46] K. Liu, Y. Song, W. Feng, N. Liu, W. Zhang and X. Zhang, *J. Am. Chem. Soc.*, 2011, **133**, 3226-3229.

[47] R. De Paris, T. Strunz, K. Oroszlan, H.-J. Güntherodt and M. Hegner, *Single Molecules*, 2000, **1**, 285-290.

[48] Y. F. Dufrene, *J. Bacteriol.*, 2002, **184**, 5205-5213.

[49] F. Schwesinger, R. Ros, T. Strunz, D. Anselmetti, H. J. Guntherodt, A. Honegger, L. Jermutus, L. Tiefenauer and A. Pluckthun, *Proc. Natl. Acad. Sci. U. S. A.*, 2000, **97**, 9972-9977.

[50] Y. Jiang, C. Zhu, L. Ling, L. Wan, X. Fang and C. Bai, *Anal. Chem.*, 2003, **75**, 2112-2116.

[51] J. Wang and A. J. Bard, *Anal. Chem.*, 2001, **73**, 2207-2212.

[52] R. Merkel, P. Nassoy, A. Leung, K. Ritchie and E. Evans, *Nature*, 1999, **397**, 50-53.

[53] G. Wei, Q. Li, S. Steckbeck and C. Ciacchi Lucio, *Phys. Chem. Chem. Phys.*, 2014, **16**, 3995-4001.

[54] S. Manohar, A. R. Mantz, K. E. Bancroft, C. Y. Hui, A. Jagota and D. V. Vezenov, *Nano Lett.*, 2008, **8**, 4365-4372.

[55] S. Iliafar, K. Wagner, S. Manohar, A. Jagota and D. Vezenov, *J. Phys. Chem. C*, 2012, **116**, 13896-13903.

[56] S. V. Patwardhan, G. Patwardhan and C. C. Perry, *J. Mater. Chem.*, 2007, **17**, 2875-2884.

[57] D. Ho, K. Falter, P. Severin and H. E. Gaub, *Anal. Chem.*, 2009, **81**, 3159-3164.

[58] X. Liu, L. Shi, W. Niu, H. Li and G. Xu, *Biosens. Bioelectron.*, 2008, **23**, 1887-1890.

[59] R. Singh, D. Pantarotto, D. McCarthy, O. Chaloin, J. Hoebeke, C. D. Partidos, J.-P. Briand, M. Prato, A. Bianco and K. Kostarelos, *J. Am. Chem. Soc.*, 2005, **127**, 4388-4396.

[60] A. A. Bhirde, V. Patel, J. Gavard, G. Zhang, A. A. Sousa, A. Masedunskas, R. D. Leapman, R. Weigert, J. S. Gutkind and J. F. Rusling, *ACS Nano*, 2009, **3**, 307-316.

[61] K. Maehashi, T. Katsura, K. Kerman, Y. Takamura, K. Matsumoto and E. Tamiya, *Anal. Chem.*, 2007, **79**, 782-787.

[62] K. A. Drouvalakis, S. Bangsaruntip, W. Hueber, L. G. Kozar, P. J. Utz and H. Dai, *Biosens. Bioelectron.*, 2008, **23**, 1413-1421.

[63] C. K. O'Sullivan, *Anal. Bioanal. Chem.*, 2002, **372**, 44-48.

[64] A. D. Ellington and J. W. Szostak, *Nature*, 1990, **346**, 818-822.

[65] J. Katoch, S. N. Kim, Z. Kuang, B. L. Farmer, R. R. Naik, S. A. Tatulian and M. Ishigami, *Nano Lett.*, 2012, **12**, 2342-2346.

[66] T. J. Park, S. Y. Lee, S. J. Lee, J. P. Park, K. S. Yang, K. B. Lee, S. Ko, J. B. Park, T. Kim, S. K. Kim, Y. B. Shin, B. H. Chung, S. J. Ku, D. H. Kim and I. S. Choi, *Anal. Chem.*, 2006, **78**, 7197-7205.

[67] G. Binnig and C. F. Quate, *Phys. Rev. Lett.*, 1986, **56**, 930-933.

[68] H.-J. Butt, B. Cappella and M. Kappl, *Surf. Sci. Rep.*, 2005, **59**, 1-152.

[69] B. Drake, C. B. Prater, A. L. Weisenhorn, S. A. Gould, T. R. Albrecht, C. F. Quate, D. S. Cannell, H. G. Hansma and P. K. Hansma, *Science*, 1989, **243**, 1586-1589.

[70] P. W. PETER EATON, *Oxford university press* 2010.

[71] E. Meyer, R. Overney, D. Brodbeck, L. Howald, R. Luthi, J. Frommer and H. Guntherodt, *Phys. Rev. Lett.*, 1992, **69**, 1777-1780.

[72] H. G. Hansma and J. H. Hoh, *Annu. Rev. Biophys. Biomol. Struct.*, 1994, **23**, 115-139.

[73] N. A. Geisse, *Materials Today*, 2009, **12**, 40-45.

[74] P. Zhang, H. Wang, X. Zhang, W. Xu, Y. Li, Q. Li, G. Wei and Z. Su, *Biomater Sci*, 2015, **3**, 852-860.

[75] S. Stankovich, D. A. Dikin, R. D. Piner, K. A. Kohlhaas, A. Kleinhammes, Y. Jia, Y. Wu, S. T. Nguyen and R. S. Ruoff, *Carbon*, 2007, **45**, 1558-1565.

[76] P. Eaton and P. West, *Atomic force microscopy*, Oxford University Press, 2010.

[77] J. E. Sader, J. A. Sanelli, B. D. Adamson, J. P. Monty, X. Wei, S. A. Crawford, J. R. Friend, I. Marusic, P. Mulvaney and E. J. Bieske, *Rev. Sci. Instrum.*, 2012, **83**, 103705-103716.

[78] D. Roy, S. H. Kwon, J. W. Kwak and J. W. Park, *Anal. Chem.*, 2010, **82**, 5189-5194.

[79] G. Wei, S. Steckbeck, S. Koppen and L. Colombi Ciacchi, *Chem. Commun.*, 2013, **49**, 3239-3241.

[80] Z. Jiang, Y. Zhang, Y. Yu, Z. Wang, X. Zhang, X. Duan and S. Wang, *Langmuir*, 2010, **26**, 13773-13777.

[81] Y. Razvag, V. Gutkin and M. Reches, *Langmuir*, 2013, **29**, 10102-10109.

[82] M. Strackharn, S. W. Stahl, E. M. Puchner and H. E. Gaub, *Nano Lett.*, 2012, **12**, 2425-2428.

[83] Q. Wang, B. Luo, X. Yang, K. Wang, L. Liu, S. Du and Z. Li, *J. Mol. Recognit.*, 2016, **29**, 151-158.

[84] S. S. Wong, E. Joselevich, A. T. Woolley, C. L. Cheung and C. M. Lieber, *Nature*, 1998, **394**, 52-55.

[85] F. A. Carvalho and N. C. Santos, *IUBMB Life*, 2012, **64**, 465-472.

[86] S. Krysiak, S. Liese, R. R. Netz and T. Hugel, *J. Am. Chem. Soc.*, 2014, **136**, 688-697.

[87] C. K. Riener, C. M. Stroh, A. Ebner, C. Klampfl, A. A. Gall, C. Romanin, Y. L. Lyubchenko, P. Hinterdorfer and H. J. Gruber, *Anal. Chim. Acta*, 2003, **479**, 59-75.

[88] P. Hinterdorfer and Y. F. Dufrene, *Nat. Methods*, 2006, **3**, 347-355.

[89] T. Strunz, K. Oroszlan, R. Schafer and H. J. Guntherodt, *Proc. Natl. Acad. Sci. U. S. A.*, 1999, **96**, 11277-11282.

[90] Z. H. Wang and G. Jin, *Colloids Surf. B Biointerfaces*, 2004, **34**, 173-177.

[91] Y. H. Zhang, C. J. Liu, W. Q. Shi, Z. Q. Wang, L. M. Dai and X. Zhang, *Langmuir*, 2007, **23**, 7911-7915.

[92] A. R. Bizzarri and S. Cannistraro, *Chem. Soc. Rev.*, 2010, **39**, 734-749.

[93] U. Dammer, M. Hegner, D. Anselmetti, P. Wagner, M. Dreier, W. Huber and H. J. Guntherodt, *Biophys. J.*, 1996, **70**, 2437-2441.

[94] J. Zhang, H. Liu, R. Zhu, P. Hinterdorfer, B. Zhang and J. Tang, *Analyst*, 2013, **138**, 5325-5331.

[95] R. Barattin and N. Voyer, *Chem. Commun.*, 2008, 1513-1532.

[96] P. Hinterdorfer, W. Baumgartner, H. J. Gruber, K. Schilcher and H. Schindler, *Proc. Natl. Acad. Sci. U. S. A.*, 1996, **93**, 3477-3481.

[97] S. Iliafar, D. Vezenov and A. Jagota, *Langmuir*, 2013, **29**, 1435-1445.

[98] V. Lulevich, S. Kim, C. P. Grigoropoulos and A. Noy, *Nano Lett.*, 2011, **11**, 1171-1176.

[99] T. Sun, G. Qing, B. Su and L. Jiang, *Chem. Soc. Rev.*, 2011, **40**, 2909-2921.

[100] E. Botello, N. C. Harris, J. Sargent, W. H. Chen, K. J. Lin and C. H. Kiang, *J. Phys. Chem. B*, 2009, **113**, 10845-10848.

[101] A. V. Krasnoslobodtsev, I. L. Volkov, J. M. Asiago, J. Hindupur, J. C. Rochet and Y. L. Lyubchenko, *Biochemistry*, 2013, **52**, 7377-7386.

[102] M. R. Arkin and J. A. Wells, *Nat. Rev. Drug Discovery*, 2004, **3**, 301-317.

[103] X. Hu and H. Li, *FEBS Lett.*, 2014, **588**, 3613-3620.

[104] C. Schoeler, K. H. Malinowska, R. C. Bernardi, L. F. Milles, M. A. Jobst, E. Durner, W. Ott, D. B. Fried, E. A. Bayer, K. Schulten, H. E. Gaub and M. A. Nash, *Nat. Commun.*, 2014, **5**, 5635.

[105] I. A. Andreev, S. Hyon Kim, N. O. Kalinina, D. V. Rakitina, A. G. Fitzgerald, P. Palukaitis and M. E. Taliansky, *J. Mol. Biol.*, 2004, **339**, 1041-1047.

[106] N. Liu, B. Peng, Y. Lin, Z. Su, Z. Niu, Q. Wang, W. Zhang, H. Li and J. Shen, *J. Am. Chem. Soc.*, 2010, **132**, 11036-11038.

[107] N. Liu, Y. Chen, B. Peng, Y. Lin, Q. Wang, Z. Su, W. Zhang, H. Li and J. Shen, *Biophys. J.*, 2013, **105**, 2790-2800.

[108] L. Zhang, F. Yang, J. Y. Cai, P. H. Yang and Z. H. Liang, *Biosens. Bioelectron.*, 2014, **56**, 271-277.

[109] W. Zhao, M. Cai, H. Xu, J. Jiang and H. Wang, *Nanoscale*, 2013, **5**, 3226-3229.

[110] S. Kang and M. Elimelech, *Langmuir*, 2009, **25**, 9656-9659.

[111] M. Carrion-Vazquez, A. F. Oberhauser, T. E. Fisher, P. E. Marszalek, H. Li and J. M. Fernandez, *Prog. Biophys. Mol. Biol.*, 2000, **74**, 63-91.

[112] X. Zhang, E. Wojcikiewicz and V. T. Moy, *Biophys. J.*, 2002, **83**, 2270-2279.

[113] F. T. Hane, B. Y. Lee, A. Petoyan, A. Rauk and Z. Leonenko, *Biosens. Bioelectron.*, 2014, **54**, 492-498.

[114] Y. Shan, J. Huang, J. Tan, G. Gao, S. Liu, H. Wang and Y. Chen, *Nanoscale*, 2012, **4**, 1283-1286.

[115] D. Horinek, A. Serr, M. Geisler, T. Pirzer, U. Slotta, S. Q. Lud, J. A. Garrido, T. Scheibel, T. Hugel and R. R. Netz, *Proc. Natl. Acad. Sci. U. S. A.*, 2008, **105**, 2842-2847.

[116] P. Das and M. Reches, *Biopolymers*, 2015, **104**, 480-494.

[117] Y. Li, M. Qin, Y. Cao and W. Wang, *Langmuir*, 2014, **30**, 4358-4366.

[118] H. Lee, N. F. Scherer and P. B. Messersmith, *Proc. Natl. Acad. Sci. U. S. A.*, 2006, **103**, 12999-13003.

[119] J. Landoulsi and V. Dupres, *ChemPhysChem*, 2011, **12**, 1310-1316.

[120] R. H. Meissner, G. Wei and L. C. Ciacchi, *Soft Matter*, 2015, **11**, 6254-6265.

[121] J. Schneider and L. C. Ciacchi, *J. Am. Chem. Soc.*, 2012, **134**, 2407-2413.

[122] C. U. Murade, V. Subramaniam, C. Otto and M. L. Bennink, *ChemPhysChem*, 2011, **12**, 2545-2548.

[123] N. Sewald, S. D. Wilking, R. Eckel, S. Albu, K. Wollschlager, K. Gaus, A. Becker, F. W. Bartels, R. Ros and D. Anselmetti, *J. Pept. Sci.*, 2006, **12**, 836-842.

[124] J. Camunas-Soler, S. Frutos, C. V. Bizarro, S. de Lorenzo, M. E. Fuentes-Perez, R. Ramsch, S. Vilchez, C. Solans, F. Moreno-Herrero, F. Albericio, R. Eritja, E. Giralt, S. B. Dev and F. Ritort, *ACS Nano*, 2013, **7**, 5102-5113.

[125] J. W. Chung, D. Shin, J. M. Kwak and J. Seog, *J. Mol. Recognit.*, 2013, **26**, 268-275.

[126] K. Okumura, A. Itoh, E. Isogai, K. Hirose, Y. Hosokawa, Y. Abiko, T. Shibata, M. Hirata and H. Isogai, *Cancer Lett.*, 2004, **212**, 185-194.

[127] Y. Shan and H. Wang, *Chem. Soc. Rev.*, 2015, **44**, 3617-3638.

[128] P. H. Puech, K. Poole, D. Knebel and D. J. Muller, *Ultramicroscopy*, 2006, **106**, 637-644.

[129] D. J. Muller and Y. F. Dufrene, *Trends Cell Biol.*, 2011, **21**, 461-469.

[130] Y. Shan, S. Ma, L. Nie, X. Shang, X. Hao, Z. Tang and H. Wang, *Chem. Commun.*, 2011, **47**, 8091-8093.

[131] Z. G. Wang and B. Ding, *Adv. Mater.*, 2013, **25**, 3905-3914.

[132] J. Wang and A. J. Bard, *Anal. Chem.*, 2001, **73**, 2207-2212.

[133] B. D. Sattin, A. E. Pelling and M. C. Goh, *Nucleic Acids Res.*, 2004, **32**, 4876-4883.

[134] P. E. Nielsen, M. Egholm, R. H. Berg and O. Buchardt, *Science*, 1991, **254**, 1497-1500.

[135] M. Cao, L. Deng and H. Xu, *Colloids and Surfaces A: Physicochemical and Engineering Aspects*, 2015, **470**, 46-51.

[136] R. Zhu, S. Howorka, J. Proll, F. Kienberger, J. Preiner, J. Hesse, A. Ebner, V. P. Pastushenko, H. J. Gruber and P. Hinterdorfer, *Nat. Nanotechnol.*, 2010, **5**, 788-791.

[137] J. Zlatanova, S. M. Lindsay and S. H. Leuba, *Prog. Biophys. Mol. Biol.*, 2000, **74**, 37-61.

[138] S. J. Sowerby, M. Edelwirth and W. M. Heckl, *J. Phys. Chem. B*, 1998, **102**, 5914-5922.

[139] A. Noy and R. W. Friddle, *Methods*, 2013, **60**, 142-150.

[140] D. A. Yarotski, S. V. Kilina, A. A. Talin, S. Tretiak, O. V. Prezhdo, A. V. Balatsky and A. J. Taylor, *Nano Lett.*, 2009, **9**, 12-17.

[141] S. Iliafar, J. Mittal, D. Vezenov and A. Jagota, *J. Am. Chem. Soc.*, 2014, **136**, 12947-12957.

[142] D. Roxbury, A. Jagota and J. Mittal, *J. Am. Chem. Soc.*, 2011, **133**, 13545-13550.

[143] M. Rief, F. Oesterhelt, B. Heymann and H. E. Gaub, *Science*, 1997, **275**, 1295-1297.

[144] P. E. Marszalek, H. Li and J. M. Fernandez, *Nat. Biotechnol.*, 2001, **19**, 258-262.

[145] G. Francius, D. Alsteens, V. Dupres, S. Lebeer, S. De Keersmaecker, J. Vanderleyden, H. J. Gruber and Y. F. Dufrene, *Nat. Protoc.*, 2009, **4**, 939-946.

[146] C. K. Lee, Y. M. Wang, L. S. Huang and S. Lin, *Micron*, 2007, **38**, 446-461.

[147] Y. Harada, M. Kuroda and A. Ishida, *Langmuir*, 2000, **16**, 708-715.

[148] J. K. Stuart and V. Hlady, *Langmuir*, 1995, **11**, 1368-1374.

[149] K. Blank, T. Mai, I. Gilbert, S. Schiffmann, J. Rankl, R. Zivin, C. Tackney, T. Nicolaus, K. Spinnler, F. Oesterhelt, M. Benoit, H. Clausen-Schaumann and H. E. Gaub, *Proc. Natl. Acad. Sci. U. S. A.*, 2003, **100**, 11356-11360.

[150] F. Kienberger, A. Ebner, H. J. Gruber and P. Hinterdorfer, *Acc. Chem. Res.*, 2006, **39**, 29-36.

[151] S. Casalini, A. C. Dumitru, F. Leonardi, C. A. Bortolotti, E. T. Herruzo, A. Campana, R. F. de Oliveira, T. Cramer, R. Garcia and F. Biscarini, *ACS Nano*, 2015, **9**, 5051-5062.

[152] L. R. Ditzler, A. Sen, M. J. Gannon, A. Kohen and A. V. Tivanski, *J. Am. Chem. Soc.*, 2011, **133**, 13284-13287.

[153] T. Mori, M. Asakura and Y. Okahata, *J. Am. Chem. Soc.*, 2011, **133**, 5701-5703.

[154] I. Neundlinger, A. Poturnayova, I. Karpisova, C. Rankl, P. Hinterdorfer, M. Snejdarkova, T. Hianik and A. Ebner, *Biophys. J.*, 2011, **101**, 1781-1787.

[155] T. H. Nguyen, L. J. Steinbock, H. J. Butt, M. Helm and R. Berger, *J. Am. Chem. Soc.*, 2011, **133**, 2025-2027.

[156] J. Li, Q. Li, L. Ciacchi and G. Wei, *Biosensors*, 2015, **5**, 85-97.

[157] Q. Li, M. Michaelis, G. Wei and L. Colombi Ciacchi, *Analyst*, 2015, **140**, 5243-5250.

[158] T. Y. Kuo, W. H. Tseng and C. H. Chen, *Angew. Chem. Int. Ed. Engl.*, 2015, **54**, 9213-9217.

[159] G. Hasko, J. Linden, B. Cronstein and P. Pacher, *Nat. Rev. Drug Discov.*, 2008, **7**, 759-770.

[160] J. Liu and Y. Lu, *Angew. Chem.*, 2006, **118**, 96-100.

[161] G. Hasko, J. Linden, B. Cronstein and P. Pacher, *Nat. Rev. Drug Discov.*, 2008, **7**, 759-770.

[162] H. Liu, Y. Xiang, Y. Lu and R. M. Crooks, *Angew. Chem. Int. Ed. Engl.*, 2012, **51**, 6925-6928.

[163] X. Yan, Z. Cao, M. Kai and J. Lu, *Talanta*, 2009, **79**, 383-387.

[164] L. Rimai, T. Cole, J. L. Parsons, J. T. Hickmott and E. B. Carew, *Biophys. J.*, 1969, **9**, 320-329.

[165] J. H. Lin and W. L. Tseng, *Biosens. Bioelectron.*, 2013, **41**, 379-385.

[166] X. F. Xue, J. H. Zhou, L. M. Wu, L. H. Fu and J. Zhao, *Food Chem.*, 2009, **115**, 715-719.

[167] S. Y. Hung, Y. C. Shih and W. L. Tseng, *Anal. Chim. Acta*, 2015, **857**, 64-70.

[168] R. M. Bock, N.-S. Ling, S. A. Morell and S. H. Lipton, *Arch. Biochem. Biophys.*, 1956, **62**, 253-264.

[169] M. Li, J. Zhang, S. Suri, L. J. Sooter, D. Ma and N. Wu, *Anal. Chem.*, 2012, **84**, 2837-2842.

[170] K. Feng, C. Sun, Y. Kang, J. Chen, J.-H. Jiang, G.-L. Shen and R.-Q. Yu, *Electrochem. Commun.*, 2008, **10**, 531-535.

[171] E. Llaudet, N. P. Botting, J. A. Crayston and N. Dale, *Biosens. Bioelectron.*, 2003, **18**, 43-52.

[172] K. S. Novoselov, A. K. Geim, S. V. Morozov, D. Jiang, Y. Zhang, S. V. Dubonos, I. V. Grigorieva and A. A. Firsov, *Science*, 2004, **306**, 666-669.

[173] C. H. Lin and D. J. Patei, *Chem. Biol.*, 1997, **4**, 817-832.

[174] D. E. Huizenga and J. W. Szostak, *Biochemistry*, 1995, **34**, 656-665.

[175] A. Renzoni, F. Zino and E. Franchi, *Environ. Res.*, 1998, **77**, 68-72.

[176] O. Malm, *Environ. Res.*, 1998, **77**, 73-78.

[177] N. T. Loux, *Chem. Speciation Bioavailability*, 1998, **10**, 127-136.

[178] P. B. Tchounwou, W. K. Ayensu, N. Ninashvili and D. Sutton, *Environ. Toxicol.*, 2003, **18**, 149-175.

[179] M. Ghaedi, M. Reza Fathi, A. Shokrollahi and F. Shajarat, *Anal. Lett.*, 2006, **39**, 1171-1185.

[180] M. Wang, W. Feng, J. Shi, F. Zhang, B. Wang, M. Zhu, B. Li, Y. Zhao and Z. Chai, *Talanta*, 2007, **71**, 2034-2039.

[181] J. Qvarnstrom, L. Lambertsson, S. Havarinasab, P. Hultman and W. Frech, *Anal. Chem.*, 2003, **75**, 4120-4124.

[182] O. T. Butler, J. M. Cook, C. F. Harrington, S. J. Hill, J. Rieuwerts and D. L. Miles, *J. Anal. At. Spectrom.*, 2006, **21**, 217-243.

[183] N. H. Bings, A. Bogaerts and J. A. Broekaert, *Anal. Chem.*, 2006, **78**, 3917-3946.

[184] S. V. Wegner, A. Okesli, P. Chen and C. He, *J. Am. Chem. Soc.*, 2007, **129**, 3474-3475.

[185] Y. Zhao and Z. Zhong, *J. Am. Chem. Soc.*, 2006, **128**, 9988-9989.

[186] I. B. Kim and U. H. Bunz, *J. Am. Chem. Soc.*, 2006, **128**, 2818-2819.

[187] B. Liu, *Biosens. Bioelectron.*, 2008, **24**, 762-766.

[188] A. Ono and H. Togashi, *Angew. Chem. Int. Ed. Engl.*, 2004, **43**, 4300-4302.

[189] Y. Miyake, H. Togashi, M. Tashiro, H. Yamaguchi, S. Oda, M. Kudo, Y. Tanaka, Y. Kondo, R. Sawa, T. Fujimoto, T. Machinami and A. Ono, *J. Am. Chem. Soc.*, 2006, **128**, 2172-2173.

[190] L. Li, B. Li, Y. Qi and Y. Jin, *Anal. Bioanal. Chem.*, 2009, **393**, 2051-2057.

[191] Y. Helwa, N. Dave, R. Froidevaux, A. Samadi and J. Liu, *ACS Appl. Mater. Interfaces*, 2012, **4**, 2228-2233.

[192] T. Li, S. Dong and E. Wang, *Anal. Chem.*, 2009, **81**, 2144-2149.

[193] E. Sharon, X. Liu, R. Freeman, O. Yehezkeli and I. Willner, *Electroanalysis*, 2013, **25**, 851-856.

[194] W. P. Zhu, Z. W. Zhao, Z. Li, H. Li, J. H. Jiang, G. L. Shen and R. Q. Yu, *New J. Chem.*, 2013, **37**, 927-932.

[195] V. Dupres, F. D. Menozzi, C. Locht, B. H. Clare, N. L. Abbott, S. Cuenot, C. Bompard, D. Raze and Y. F. Dufrene, *Nat. Meth.*, 2005, **2**, 515-520.

[196] D. J. Muller, J. Helenius, D. Alsteens and Y. F. Dufrene, *Nat. Chem. Biol.*, 2009, **5**, 383-390.

[197] Y. Zhang, D. Zhao, X. Tan, T. Cao and X. Zhang, *Langmuir*, 2010, **26**, 11958-11962.

[198] A. Touhami, B. Nysten and Y. F. Dufrene, *Langmuir*, 2003, **19**, 4539-4543.

[199] Z. Wang, J. Heon Lee and Y. Lu, *Chem. Commun.*, 2008, **45**, 6005-6007.

[200] G. Wei, Q. Li, S. Steckbeck and L. C. Ciacchi, *Phys. Chem. Chem. Phys.*, 2014, **16**, 3995-4001.

[201] M. Li, X. Zhou, W. Ding, S. Guo and N. Wu, *Biosens. Bioelectron.*, 2013, **41**, 889-893.

[202] H. Torigoe, A. Ono and T. Kozasa, *Chemistry*, 2010, **16**, 13218-13225.

[203] H. Torigoe, Y. Miyakawa, A. Ono and T. Kozasa, *Thermochim. Acta*, 2012, **532**, 28-35.

[204] C. C. Huang, Z. Yang, K. H. Lee and H. T. Chang, *Angew. Chem. Int. Ed. Engl.*, 2007, **46**, 6824-6828.

[205] G. I. Bell, *Science*, 1978, **200**, 618-627.

[206] E. Evans, *Annu. Rev. Biophys. Biomol. Struct.*, 2001, **30**, 105-128.

[207] Y. F. Dufrene and P. Hinterdorfer, *Pflugers Arch.*, 2008, **456**, 237-245.

[208] D. Li, A. Wieckowska and I. Willner, *Angew. Chem.*, 2008, **120**, 3991-3995.

[209] X. Wang, J. Zhou, W. Yun, S. Xiao, Z. Chang, P. He and Y. Fang, *Anal. Chim. Acta*, 2007, **598**, 242-248.

[210] H. Yang, J. Ji, Y. Liu, J. Kong and B. Liu, *Electrochem. Commun.*, 2009, **11**, 38-40.

[211] M. Zhang, B. C. Yin, X. F. Wang and B. C. Ye, *Chem. Commun.*, 2011, **47**, 2399-2401.

[212] Y. S. Lo, N. D. Huefner, W. S. Chan, F. Stevens, J. M. Harris and T. P. Beebe, *Langmuir*, 1999, **15**, 1373-1382.

[213] L. Pugliese, A. Coda, M. Malcovati and M. Bolognesi, *J. Mol. Biol.*, 1993, **231**, 698-710.

[214] H. Sakahara, *Adv. Drug Delivery. Rev.*, 1999, **37**, 89-101.

[215] P. C. Weber, D. H. Ohlendorf, J. J. Wendoloski and F. R. Salemme, *Science*, 1989, **243**, 85-88.

[216] A. Ashkin and J. Dziedzic, *Science*, 1987, **235**, 1517-1520.

[217] E. Evans, K. Ritchie and R. Merkel, *Biophys. J.*, 1995, **68**, 2580-2587.

[218] Z. Guttenberg, A. R. Bausch, B. Hu, R. Bruinsma, L. Moroder and E. Sackmann, *Langmuir*, 2000, **16**, 8984-8993.

[219] E. L. Florin, V. T. Moy and H. E. Gaub, *Science*, 1994, **264**, 415-417.

[220] V. T. Moy, E.-L. Florin and H. E. Gaub, *Colloids and Surfaces A: Physicochemical and Engineering Aspects*, 1994, **93**, 343-348.

[221] M. Ludwig, W. Dettmann and H. E. Gaub, *Biophys. J.*, 1997, **72**, 445-448.

[222] M. D. Piramowicz, P. Czuba, M. Targosz, K. Burda and M. Szymonski, *Acta Biochim. Pol.*, 2006, **53**, 93-100.

[223] C. Yuan, A. Chen, P. Kolb and V. T. Moy, *Biochemistry*, 2000, **39**, 10219-10223.

[224] Y. L. Lyubchenko and L. S. Shlyakhtenko, *Proc. Natl. Acad. Sci. U. S. A.*, 1997, **94**, 496-501.

[225] N. M. Green and M. A. Joynson, *Biochem. J.*, 1970, **118**, 71-72.

[226] V. T. Moy, E. L. Florin and H. E. Gaub, *Science*, 1994, **266**, 257-259.

[227] G. U. Lee, D. A. Kidwell and R. J. Colton, *Langmuir*, 1994, **10**, 354-357.

[228] W.-C. Lin, C. D. Blanchette, T. V. Ratto and M. L. Longo, *Biophys. J.*, **90**, 228-237.

[229] H. Gumpp, S. W. Stahl, M. Strackharn, E. M. Puchner and H. E. Gaub, *Rev. Sci. Instrum.*, 2009, **80**, 0637041-0637045.

[230] S. A. Vickery and R. C. Dunn, *J. Microsc.*, 2001, **202**, 408-412.

[231] Y. F. Dufrene, *Yeast*, 2010, **27**, 465-471.

References

Acknowledgements

I am grateful to China Scholarship Council for giving me the financial support to study abroad.

I would like to thank Prof. Lucio Colombi Ciacchi for providing me the opportunity to spend my PhD study in Hybrid Materials Interfaces Group (HMI) at University of Bremen. His suggestions helped me to improve both my experiments and thesis; his enthusiasm in science inspired me a lot. I thank Dr. Gang Wei to be co-supervisor.

I would like to thank all the support from HMI working groups, consisting of Sascha, Julen, Tatjana, Julian, Susi, Nils, Jens, Steffen, Feng, Sabastian, Nina, Lena, Robert, Massimo, and Stefan for not only a relaxed and pleasant working atmosphere, but also kindly discussions about my work whenever needed.

Special thanks to Monika for fruitful discussions of my thesis, and translating the abstract into German. Many thanks to Meike for encouraging me all the time.

I would like to thank my parents and my boyfriend for their support, trust and patience for me.

Finally, I would like to thank all my friends, their motivation and emotional supports ensured my PhD life more interesting and pleasant.

Acknowledgements

Publications

Papers

[1] G. Wei, Q. Li, S. Steckbeck, L. Colombi Ciacchi

Direct force measurements on peeling heteropolymer ssDNA from a graphite surface using single-molecule force spectroscopy

Physical Chemistry Chemical Physics **16**, 3995-4001 (2014)

[2] J. Li*, Q. Li*, L. Colombi Ciacchi, G. Wei

Label-free sensing of adenosine based on force variations induced by molecular recognition

Biosensors **5**, 85-97 (2015)

* shared first authorship

[3] Q. Li, M. Michaelis, G. Wei, L. Colombi Ciacchi

A novel aptasensor based on single-molecule force spectroscopy for highly sensitive detection of mercury ions

Analyst **140**, 5243-5250 (2015)

[4] Q. Li*, T. Zhang*, Y. Pan, L. Colombi Ciacchi, B. Xu, G. Wei

AFM-based force spectroscopy for bioimaging and biosensing

RSC Advances, **6**, 12893-12912 (2016)

* shared first authorship

[5] J. Li, Q. Li, L. Colombi Ciacchi, G. Wei

Single molecule force mapping-based colorimetric detection of adenosine, cocaine, and mercury ions

submitted manuscript

Posters

[1] N. Hildebrand, L. Derr, Q. Li, S. Köppen, L. Treccani, R. Dringen, K. Rezwan, L. Colombi Ciacchi

Molecular Dynamics simulations of the adsorption of chymotrypsin and lysozyme on amorphous silica in aqueous solutions

CECAM Workshop "Liquid/Solid interfaces: Structure and dynamics

from spectroscopy and simulations", Lausanne, Switzerland, June 2013

[2] Q. Li, J. Li, L. Colombi Ciacchi, G. Wei

Label-free Determination of DNA, Protein and Mercury ions with Single-molecule Force Spectroscopy

Conference: Materials Science and Engineering, Darmstadt, Germany, September 2014

[3] J. Li, Q. Li, L. Colombi Ciacchi, G. Wei

Atomic force microscopy force spectroscopy (AFM-FS) based biosensing

UFT flashlight in University of Bremen, Bremen, Germany, March 2016

Declaration/Erklärung

Hiermit erkläre ich, die vorliegende Arbeit selbständig und ausschließlich unter Verwendung der angegebenen Quellen und Hilfsmittel angefertigt zu haben. Alle wörtlich oder inhaltlich übernommenen Stellen habe ich als solche gekennzeichnet.

Bremen, den 27.04.2016

_____

Qing Li